OUKA
Osaka University Knowledge Archive

Title	Role of Hydrophobic Microenvironment at the Active Site of Molybdenum Oxidoreductases
Author(s)	長谷中, 祐輝
Citation	大阪大学, 2015, 博士論文
Version Type	VoR
URL	https://doi.org/10.18910/52299
rights	
Note	

Osaka University Knowledge Archive : OUKA

https://ir.library.osaka-u.ac.jp/

Osaka University

Role of Hydrophobic Microenvironment at the Active Site of Molybdenum Oxidoreductases

A Doctoral Thesis

by

Yuki Hasenaka

Submitted to the Graduate School

of Science, Osaka University

February, 2015

Acknowledgements

This work has been performed under the direction of Associate Professor Taka-aki Okamura and Professor Kiyotaka Onitsuka at Department of Macromolecular Science, Graduate School of Science, Osaka University. The author is greatly indebted to Associate Professor Taka-aki Okamura for his continuous guidance, helpful suggestions, and fruitful discussions. The author wishes his sincere gratitude to Professor Kiyotaka Onitsuka for his cordial encouragement and helpful suggestions. The author also wishes to express his gratitude to Dr. Naoya Kanbayashi for his heartfelt friendship and exciting discussions.

The author is deeply grateful to Dr. Naoya Inazumi for NMR spectral measurements. The author acknowledges Mr. Mitsuo Ohama and Mr. Kazushi Kawamura for IR and Raman spectral measurements. The author wishes to thank Mr. Tetsuo Yamamoto for X-ray measurements. The author would like to thank Mr. Ken-ichi Iijima and Ms. Tomomi Hirai for elemental measurements. The author also thanks Dr. Akihiro Ito for assistance of mass spectral measurements.

The author wishes to thank all the members of Onitsuka laboratory for their heartfelt friendship and productive discussions.

Finally, the author expresses his special thanks to his parents, Teruo and Kumi Hasenaka, for their understanding and continuous support.

February, 2015

長谷中 祐輝

Yuki Hasenaka

Contents

Chapter I General Introduction····· 1

Chapter II Behavior of Anionic Molybdenum(IV, VI) and Tungsten(IV, VI) Complexes Containing Bulky Hydrophobic Dithiolate Ligands and Intramolecular NH···S Hydrogen Bonds in Nonpolar Solvents ····· 15

Chapter III Efficient Uptake of Dimethyl Sulfoxide by Desoxomolybdenum(IV) Dithiolate Complex Containing Bulky Hydrophobic Groups····· 57

Chapter IV Modeling of Hydrophobic Microenvironment of Water-Soluble Molybdoenzymes in Aqueous Micellar Solution ····· 85

Chapter V Summary····· 103

List of Publications ····· 105

Chapter I

General Introduction

The active site of a metalloenzyme can be regarded as a metal complex, which is surrounded by a huge protein. Even if the active site is precisely reconstructed by an artificial metal complex, the activity of the model is far from that of the enzyme. There is no room to doubt that the protein is essential for the enzyme activity.

Understanding how the protein realize the high reactivity and substrate specificity of the metalloenzyme under physiological condition is one object of bioinorganic chemistry. A metalloenzyme is a monodisperse macromolecule having specific folding, and catalyzes a variety of biological reactions in aqueous media at ambient temperature.[1] In the field of theoretical chemistry, Warshel proposed that the ionic and/or polar residues around the active site of enzymes can be regarded as "supersolvent" surrounded by a hydrophobic protein, which can increase rates of reactions by providing optimal solvation to the ionic resonance forms at the transition state.[2] The polar active site is considered to be isolated from bulk water by hydrophobic surroundings even if the enzyme is soluble in aqueous media owing to a hydrophilic shell (Figure 1).

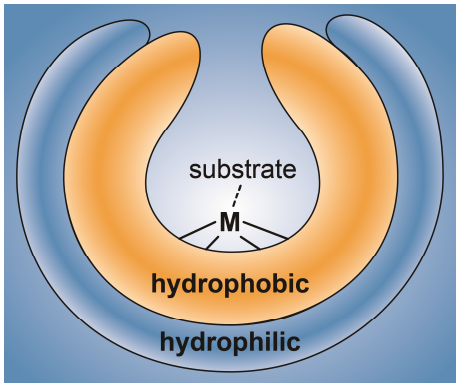

Figure 1. The schematic drawing of metalloenzyme with tri-layered architecture.

Molybdenum, the most abundant transition metal in seawater, has been incorporated widely into biological systems including carbon, nitrogen, and sulfur metabolism.[3] The metal is redox-active under physiological conditions between Mo(IV) and Mo(VI) oxidation states, and a number of molecular structures of molybdenum-containing oxidoreductases in both reduced (Mo(IV)) and oxidized (Mo(VI)) states have been reported.[4-10] Dimethyl sulfoxide reductase (DMSOR) is a principal molybdoenzyme and catalyzes oxygen-atom-transfer (OAT) reaction of DMSO and amine *N*-oxides, and the molecular structures in the reduced, oxidized, and substrate-bound states have been reported. As illustrated in Figure 2, the molybdenum site with two unique dithiolene ligands, MGD, is located at the base of a large funnel-shaped depression (~ 15 Å),[11,12] and the ligands are not exposed to the surface.[13] Aromatic residues at the base of the funnel provides a binding site for the methyl groups of DMSO,[4] which can be regard as a hydrophobic pocket denoted by orange color. In the catalytic cycle of DMSOR, a molybdenum(IV) center reductively eliminates an oxygen atom from the substrates, such as sulfoxides and amine *N*-oxides, to form a Mo^{VI}=O bond (Figure 2b). The Mo(IV) species is regenerated by two successive processes including protonation and one-electron reduction.[4]

The specificity constant (k_{cat}/K_m) is used to describe the catalytic efficiency of the enzyme where the inverse of the Michaelis constant, K_m^{-1}, represents the affinity for the substrate of the enzyme. In the case of well-known metalloenzyme, catalase, a very efficient disproportionation of H_2O_2 proceeds ($k_{cat}/K_m = 4 \times 10^8$ $M^{-1}s^{-1}$) with large k_{cat} (4×10^7 s^{-1}) and large K_m (0.11 M) values. On the contrary, DMSOR has very high affinity for the substrate with small K_m (7 μM), which results in the efficient reduction of DMSO ($k_{cat}/K_m = 7.1 \times 10^6$ $M^{-1}s^{-1}$), while the reaction is apparently slow ($k_{cat} = 50$ s^{-1}).[14] As listed in Table 1, almost all the molybdoenzymes tend to have high affinity for the substrates resulting in the high efficiency, and some of them are referred to contain a hydrophobic pocket or channel.[4,14-21] The result indicates that the efficient binding of the substrates to the active center is accomplished by weak interactions such as

hydrogen bonds and electrostatic interactions in the hydrophobic microenvironment. A hydrophobic environment around the active site should support such weak interactions; however, it is difficult to investigate how the hydrophobicity affects the catalytic reactivity of metalloenzymes in an aqueous media, because numerous interactions by folded polypeptides are complicated. Modeling of the active site is one solution, which gives us the information about the specific characteristics of the enzymes.

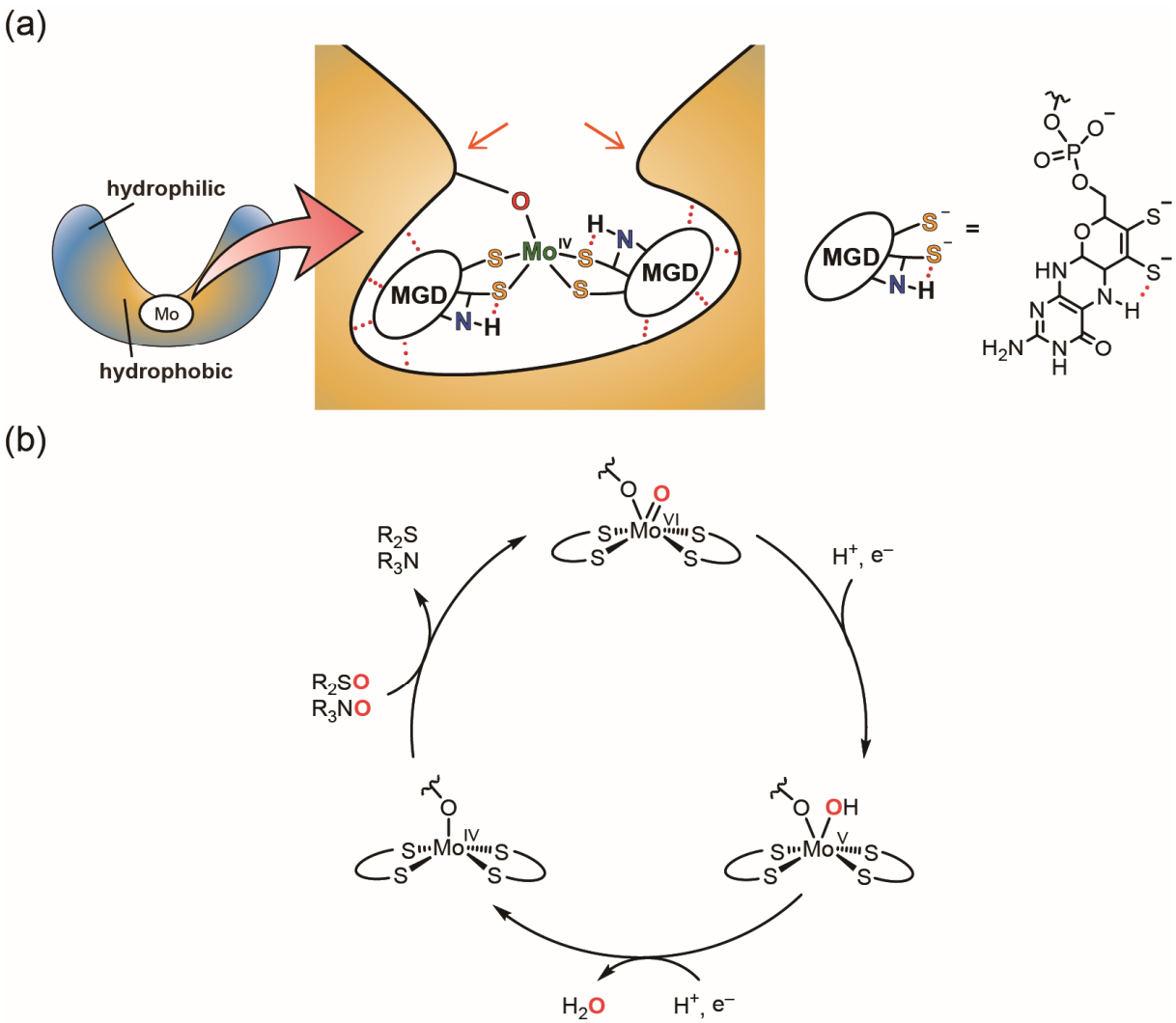

Figure 2. (a) The structure of the active site. Red dot lines denote hydrogen bonds, and orange arrows denote the aromatic residues providing the substrate binding site. (b) The catalytic cycle of dimethyl sulfoxide reductase.

Table 1. Catalytic Properties of Typical Molybdoenzymes

enzyme	PDB ID	hydrophobic pocket[a]	reaction	active site (Mo^{VI})[b]	k_{cat}/s^{-1}	$K_m/\mu M$	k_{cat}/K_m / $M^{-1}s^{-1}$	ref
aldehyde oxidoreductase	1HLR	y	$RCHO \rightarrow RCOOH$	$Mo^{VI}O(OH)S(MCD)$	0.15	0.25	6.0×10^5	15
ethylbenzene dehydrogenase	2IVF	y	$PhCH_2CH_3 \rightarrow PhCH(OH)CH_3$	$Mo^{VI}O(OAsp)(MGD)_2$	1.3	0.45	2.8×10^6	16
CO dehydrogenase	1N5W	y	$CO \rightarrow CO_2$	$Mo^{VI}O_2(S–Cu–SCys)(MGD)$	107	1	1.1×10^8	17
arsenite oxidase	1G8K	n	$AsO_3^{3-} \rightarrow AsO_4^{3-}$	$Mo^{VI}O(OH)(MGD)_2$	27	3	9.0×10^6	4
dimethyl sulfoxide reductase	1EU1	y	$Me_2SO \rightarrow Me_2S$	$Mo^{VI}O(OSer)(MGD)_2$	50	7	7.1×10^6	14
xanthine oxidoreductase	3AM9	n	xanthine → uric acid	$Mo^{VI}O(OH)S(MPT)$	15	8	1.9×10^6	18
biotin sulfoxide reductase	n. d.	n. d.	biotin *S*-oxide → biotin	$Mo^{VI}O(OSer)(MGD)_2$	18	18	1.0×10^6	19
sulfite oxidase	1SOX	n	$SO_3^{2-} \rightarrow SO_4^{2-}$	$Mo^{VI}O_2(SCys)(MPT)$	345	27	1.3×10^7	20
nitrate reductase (dissimilatory)	1Q16	y	$NO_3^- \rightarrow NO_2^-$	$Mo^{VI}O(OAsp)(MGD)_2$	80	50	1.6×10^6	4
nitrate reductase (assimilatory)	2BII	n	$NO_3^- \rightarrow NO_2^-$	$Mo^{VI}O_2(SCys)(MPT)$	210	90	2.3×10^6	4
trimethylamine *N*-oxide reductase	1TMO	y	$Me_3NO \rightarrow Me_3N$	$Mo^{VI}O(OSer)(MGD)_2$	2500	210	1.2×10^7	14
formate dehydrogenase	1AA6	n	$HCOO^- \rightarrow CO_2$	$Mo^{VI}O(SeCys)(MGD)_2$	2800	26000	1.1×10^5	21

[a]Whether or not the presence of a hydrophobic pocket or substrate access channel. [b]MCD: molybdopterin cytosine dinucleotide; MGD: molybdopterin guanine dinucleotide; MPT: molybdopterin.

A number of model complexes of DMSOR have been synthesized.[22-27] For example, desoxomolybdenum(IV) complexes with ene-1,2-dithiolate ligands have been reported to reduce the biological substrate, DMSO (Chart 1a).[28,29] On the other hand, Basu et al. focused on the bulkiness and hydrophobicity of protein matrix, and monooxomolybdenum(V) complexes having dendritic benzenethiolate ligands were synthesized (Chart 1b). The electrochemical investigation revealed that the sterically encumbering ligands regulated the rate of redox process, indicating that the bulky ligands can mimic the protein matrix.[13,30] However, although the OAT reaction has been not examined, the access of the substrate is considered to be restricted due to highly-encumbered dendritic ligands.

As functional models, it has been revealed that a monooxomolybdenum(IV) benzene-1,2-dithiolate (bdt) complexes can catalytically reduce amine *N*-oxide (Chart 1c).[31,32] When NH···S hydrogen bonds were introduced to the bdt ligands, the OAT reaction of Me_3NO were accelerated.[33-36] Moreover, the introduction of bulky CPh_3 groups into the complex resulted in a dramatic acceleration of the OAT reaction; therefore, a "*cis*-attack" mechanism via a distorted intermediate stabilized by congested bulky substituents was proposed (Scheme 1).[33,35,37] In the proposed mechanism, the substrate approaches the polar molybdenum center from the upper side, i.e., *cis* to the oxo ligand, and spontaneously a Mo=O bond is formed. Similarly, DMSO is proposed to attack the active center at the *cis* position to apical serinate ligand in of DMSOR. However, the complex were only slightly soluble in nonpolar solvents due to the strong intermolecular ionic interactions.

Chart 1. The Structures of Model Complexes[a]

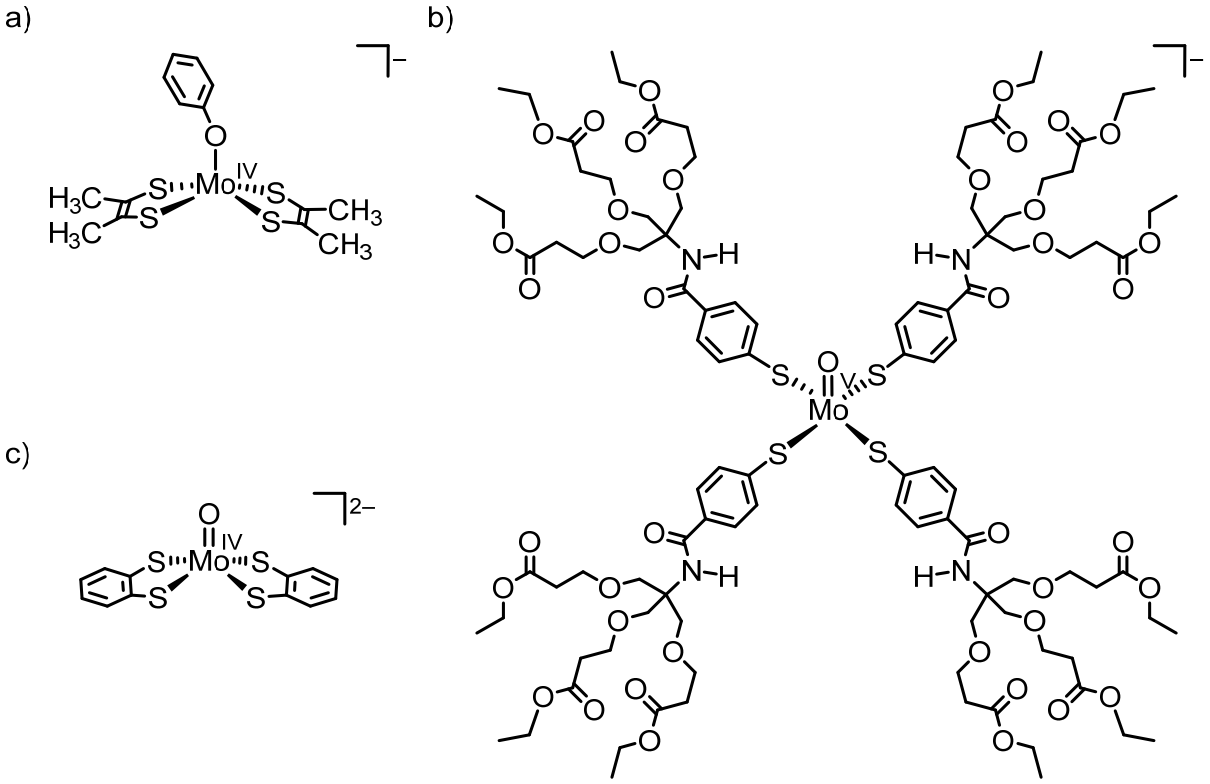

[a]a) Refs. 15,16. b) Refs. 17,18. c) Refs. 19, 20.

Scheme 1. Proposed Reaction Mechanism via the *cis*-Attack of Me_3NO to the Complex

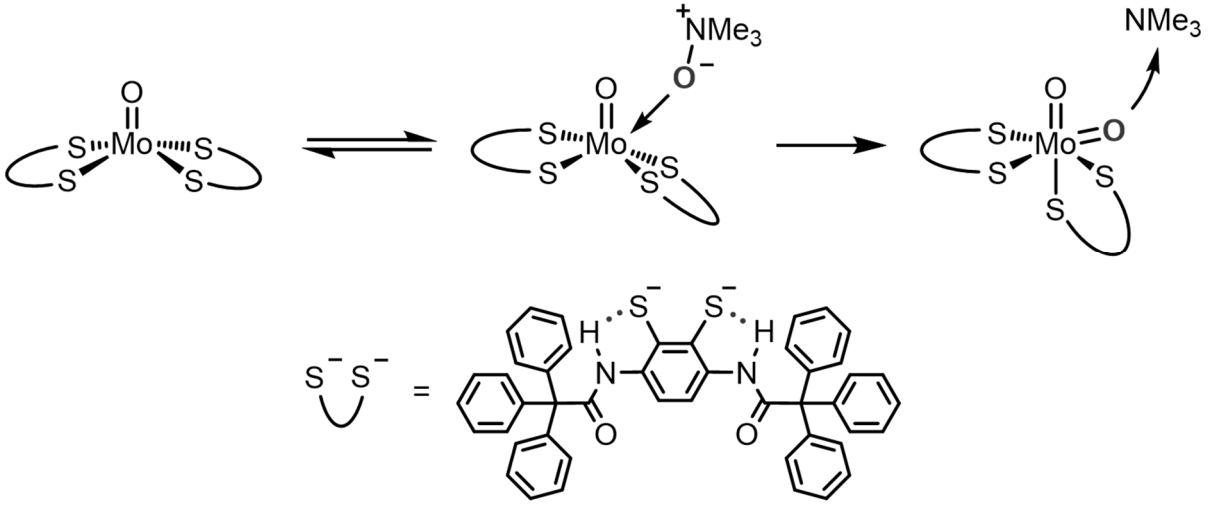

If the reactive site is surrounded by large hydrophobic groups enough to encapsulate the polar Mo=O group and counterions, the complex in nonpolar medium probably simulates the hydrophobic pocket of the active site in molybdoenzymes; therefore, molybdenum(IV, VI) complexes containing bulky hydrophobic $(4\text{-}^{t}BuC_6H_4)_3C$ groups was synthesized, which completely covered the polar Mo=O group as illustrated in Figure 3. The complexes were soluble in nonpolar solvents like toluene, and the approach of Me_3NO was found more efficient in the hydrophobic environment supported by nonpolar media.

"Desoxo"-molybdenum(IV) complexes are known to have the enhanced reactivity with sulfoxides such as DMSO, the biological substrate.[29] A desoxomolybdenum(IV) complex with a siloxo ligand instead of the oxo ligand is synthesized to model the reactivity of DMSOR (Figure 5). The OAT reaction of DMSO in toluene was found as fast as in polar media, which ensured the construction of hydrophobic surroundings at the active center.

In addition, the entire catalytic cycle of trimethylamine *N*-oxide reductase (TMAOR), a molybdoenzyme catalyzing the reduction of Me_3NO by NADH, was modeled. The catalytic reduction of amine *N*-oxide by an NADH analog was achieved even in aqueous micellar solution.

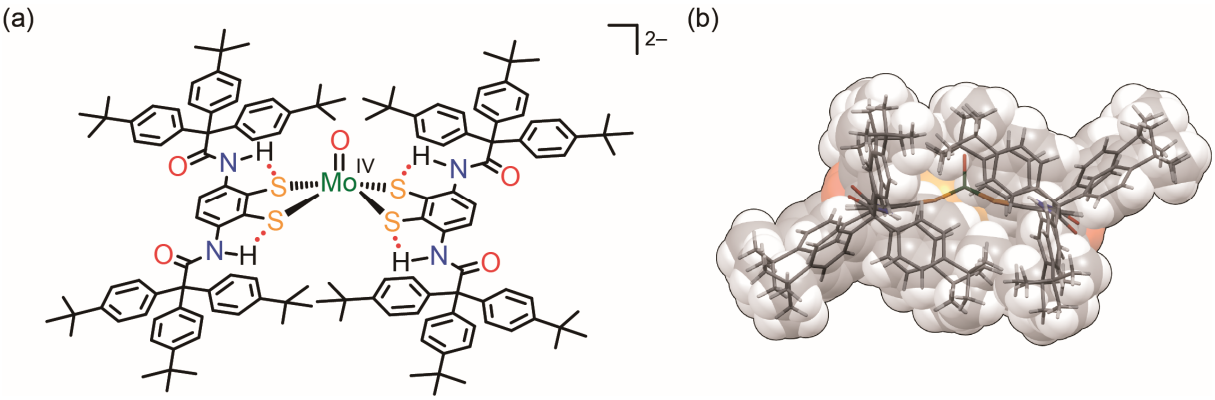

Figure 3. (a) Schematic and (b) side-view structure in the crystal of the anion part of the monooxomolybdenum(IV) complex having bulky hydrophobic groups.

Scope of This Thesis

In order to model the active site of molybdoenzymes in the hydrophobic microenvironment, the author designed novel dithiolate ligands containing very bulky hydrophobic moieties. In this thesis, the author describes the stepwise modeling of the hydrophobic microenvironment at the active site of molybdoenzymes.

In Chapter II, the synthesis and properties of toluene-soluble anionic molybdenum(IV, VI) complexes containing bulky hydrophobic groups are described (Figure 4). The tungsten analogues are known to be isostructural with the corresponding molybdenum complex and relatively stable in the higher oxidation state; thus, tungsten(IV, VI) complexes were also synthesized to investigate the structure in the M(VI) state. The bulky groups can encapsulate the counterions, and the model complexes and toluene as media successfully constructed the hydrophobic environment around the active center. The polar Me_3NO accessed efficiently in the hydrophobic media.

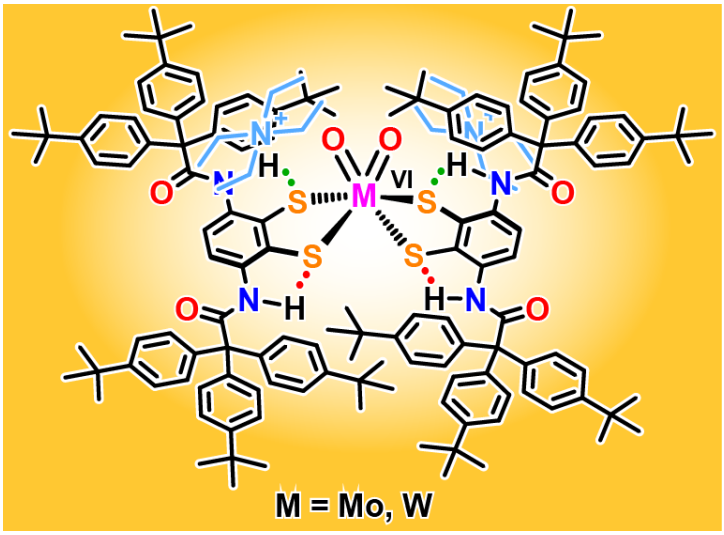

Figure 4. Schematic drawing of the structure of the molybdenum and tungsten complexes containing bulky hydrophobic moieties and NH···S hydrogen bonds.

In Chapter III, a desoxomolybdenum(IV) complex and the related compounds are described as the reaction model of DMSO reductase (Figure 5). The approach of Me_3NO was more efficient in nonpolar solvent as described in Chapter II, whereas the reduction rate of DMSO in toluene was found comparable with that in a polar solvent. These results indicate the construction of the hydrophobic microenvironment at the active center which can uptake DMSO effectively.

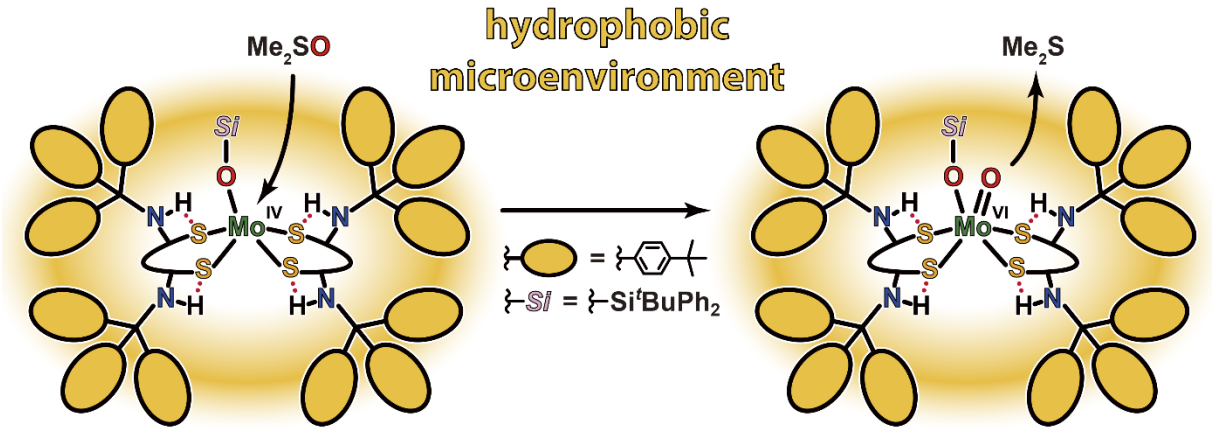

Figure 5. Efficient uptake and reduction of DMSO by the desoxomolybdenum(IV) complex having bulky hydrophobic dithiolate ligands.

In Chapter IV, the catalysis of an enzyme model complex is described. The catalytic reduction of amine *N*-oxide (DDAO) by an NADH analog (BNAH) proceeds both in water-containing toluene and an aqueous micellar solution using Triton X-100 (Scheme 2, Figure 6). The protonation of Mo^{IV}=O was revealed to be involved in the rate-determining-step by kinetic isotope effect. The synthetic approach toward a unimer-micellar type model complex using amphiphilic dithiolate ligands is also described.

Scheme 2. Catalytic Cycle of the OAT Reaction between DDAO and BNAH

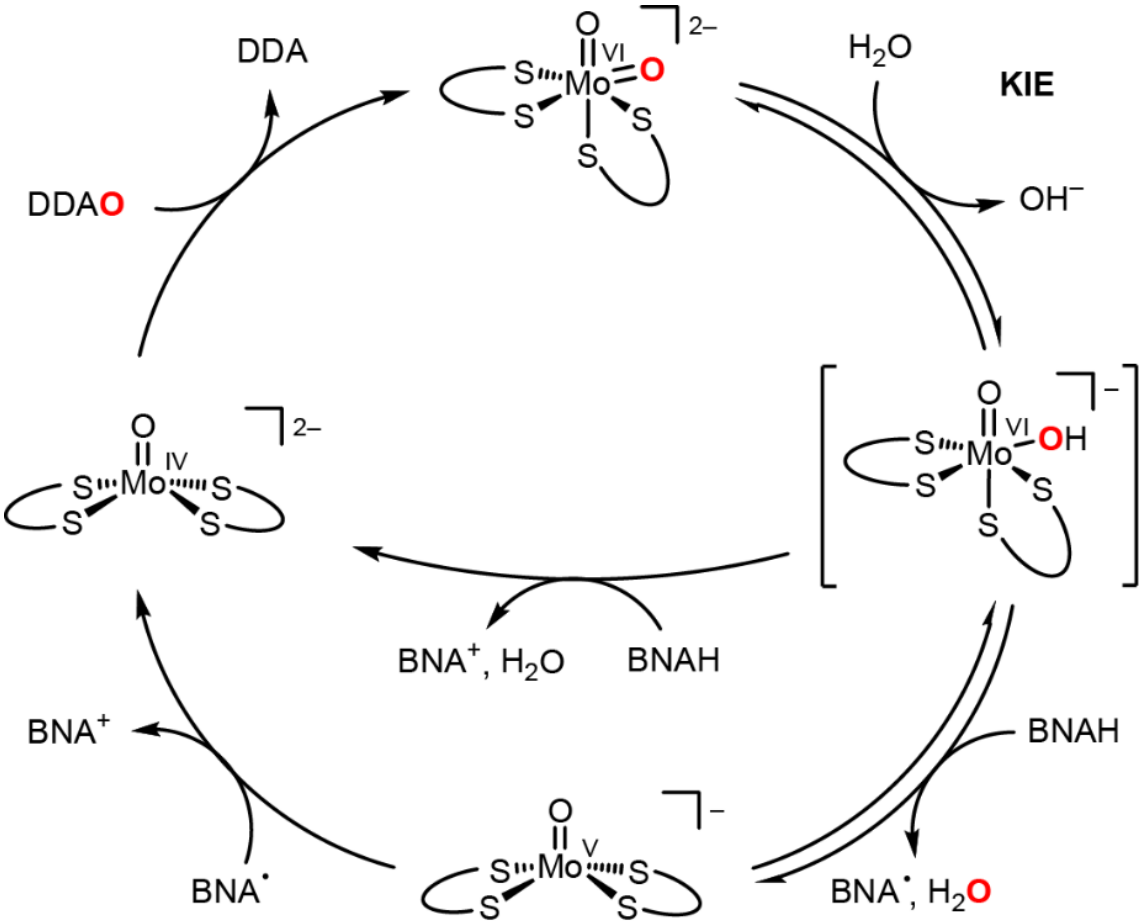

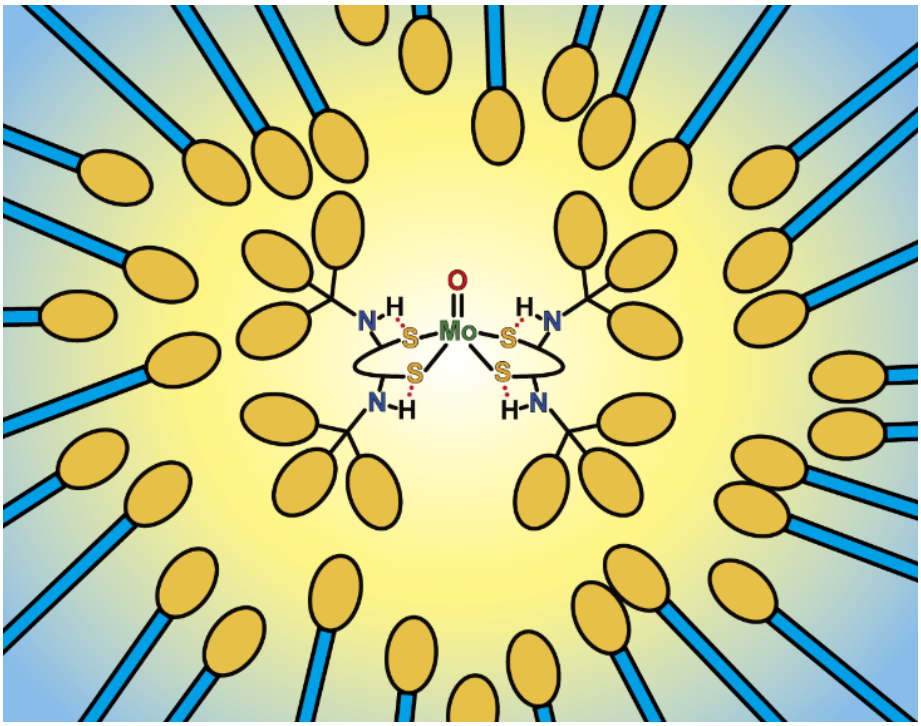

Figure 6. Aqueous micellar solution of molybdenum complex containing bulky hydrophobic dithiolate ligands using Triton X-100 (represented by blue sticks and orange ovals).

The bottom-up modeling of the active site of molybdoenzymes described above is achieved by the precise investigation of the fundamental complexes. The solubility and reactivity of the complexes can be easily modified maintaining the coordination structures and hydrophobic pocket. Thus, the hydrophobic microenvironment at the active site of molybdoenzymes seems to regulate the enzyme activity.

References

(1) Alberts, B.; Bray, D.; Hopkin, K.; Johnson, A.; Lewis, J. *Essential Cell Biology*; Garland Science, 2013.

(2) Warshel, A. *Biochemistry* **1981**, *20*, 3167-3177.

(3) Hille, R. *Trends Biochem. Sci* **2002**, *27*, 360-367.

(4) Hille, R.; Hall, J.; Basu, P. *Chem. Rev.* **2014**, *114*, 3963-4038.

(5) Hille, R. *Chem. Rev.* **1996**, *96*, 2757-2816.

(6) Hille, R.; Nishino, T.; Bittner, F. *Coord. Chem. Rev.* **2011**, *255*, 1179-1205.

(7) Pushie, M. J.; George, G. N. *Coord. Chem. Rev.* **2011**, *255*, 1055-1084.

(8) Magalon, A.; Fedor, J. G.; Walburger, A.; Weiner, J. H. *Coord. Chem. Rev.* **2011**, *255*, 1159-1178.

(9) Dobbek, H. *Coord. Chem. Rev.* **2011**, *255*, 1104-1116.

(10) Grimaldi, S.; Schoepp-Cothenet, B.; Ceccaldi, P.; Guigliarelli, B.; Magalon, A. *Biochim. Biophys. Acta* **2013**, *1827*, 1048-1085.

(11) Schindelin, H.; Kisker, C.; Hilton, J.; Rajagopalan, K. V.; Rees, D. C. *Science* **1996**, *272*, 1615-1621.

(12) McAlpine, A. S.; McEwan, A. G.; Bailey, S. *J. Mol. Biol.* **1998**, *275*, 613-623.

(13) Mondal, S.; Basu, P. *Inorg. Chem.* **2001**, *40*, 192-193.

(14) Johnson, K. E.; Rajagopalan, K. V. *J. Biol. Chem.* **2001**, *276*, 13178-13185.

(15) João Romão, M.; Moura, J. J. G. Aldehyde Oxidoreductase (MOP). In *Encyclopedia of Inorganic and Bioinorganic Chemistry*; John Wiley & Sons, Ltd: 2011.

(16) Knack, D.; Hagel, C.; Szaleniec, M.; Dudzik, A.; Salwinski, A.; Heider, J. *Appl. Environ. Microbiol.* **2012**, *78*, 6475-6482.

(17) Dobbek, H.; Gremer, L.; Meyer, O.; Huber, R. CO Dehydrogenase. In *Encyclopedia of Inorganic and Bioinorganic Chemistry*; John Wiley & Sons, Ltd: 2011.

(18) Cao, H.; Pauff, J. M.; Hille, R. *J. Biol. Chem.* **2010**, *285*, 28044-28053.

(19) Nelson, K. J.; Rajagopalan, K. V. *Biochemistry* **2004**, *43*, 11226-11237.

(20) Kappler, U. *Biochim. Biophys. Acta* **2011**, *1807*, 1-10.

(21) Sun, P. D.; Boyington, J. C.; Stadtman, T. C. Formate Dehydrogenase H. In *Encyclopedia of Inorganic and Bioinorganic Chemistry*; John Wiley & Sons, Ltd: 2011.

(22) Holm, R. H.; Solomon, E. I.; Majumdar, A.; Tenderholt, A. *Coord. Chem. Rev.* **2011**, *255*, 993-1015.

(23) Hine, F. J.; Taylor, A. J.; Garner, C. D. *Coord. Chem. Rev.* **2010**, *254*, 1570-1579.

(24) Ng, V. W. L.; Taylor, M. K.; Young, C. G. *Inorg. Chem.* **2012**, *51*, 3202-3211.

(25) Basu, P.; Burgmayer, S. J. N. *Coord. Chem. Rev.* **2011**, *255*, 1016-1038.

(26) Sugimoto, H.; Tatemoto, S.; Suyama, K.; Miyake, H.; Mtei, R. P.; Itoh, S.; Kirk, M. L. *Inorg. Chem.* **2010**, *49*, 5368-5370.

(27) Majumdar, A.; Sarkar, S. *Coord. Chem. Rev.* **2011**, *255*, 1039-1054.

(28) Lim, B. S.; Donahue, J. P.; Holm, R. H. *Inorg. Chem.* **2000**, *39*, 263-273.

(29) Lim, B. S.; Holm, R. H. *J. Am. Chem. Soc.* **2001**, *123*, 1920-1930.

(30) Basu, P.; Nemykin, V. N.; Sengar, R. S. *Inorg. Chem.* **2003**, *42*, 7489-7501.

(31) Yoshinaga, N.; Ueyama, N.; Okamura, T.; Nakamura, A. *Chem. Lett.* **1990**, *19*, 1655-1656.

(32) Ueyama, N.; Oku, H.; Kondo, M.; Okamura, T.; Yoshinaga, N.; Nakamura, A. *Inorg. Chem.* **1996**, *35*, 643-650.

(33) Baba, K.; Okamura, T.; Suzuki, C.; Yamamoto, H.; Yamamoto, T.; Ohama, M.; Ueyama, N. *Inorg. Chem.* **2006**, *45*, 894-901.

(34) Okamura, T.; Tatsumi, M.; Omi, Y.; Yamamoto, H.; Onitsuka, K. *Inorg. Chem.* **2012**, *51*, 11688-11697.

(35) Okamura, T.; Ushijima, Y.; Omi, Y.; Onitsuka, K. *Inorg. Chem.* **2013**, *52*, 381-394.

(36) Okamura, T.; Kunisue, K.; Omi, Y.; Onitsuka, K. *Dalton Trans.* **2013**, *42*, 7569-7578.

(37) Baba, K.; Okamura, T.; Yamamoto, H.; Yamamoto, T.; Ohama, M.; Ueyama, N. *Chem. Lett.* **2005**, *34*, 44-45.

Chapter II

Behavior of Anionic Molybdenum(IV, VI) and Tungsten(IV, VI) Complexes Containing Bulky Hydrophobic Dithiolate Ligands and Intramolecular NH···S Hydrogen Bonds in Nonpolar Solvents

Introduction

Molybdo- and tungstoenzymes with unique dithiolene ligands called the molybdopterin cofactor (MGD, Chart 1a) catalyze oxygen-atom-transfer (OAT) reactions via M^{IV} and M^{VI} oxidation states (M = Mo, W).[1-8] In the case of dimethyl sulfoxide reductase (DMSOR), a molybdoenzyme with two dithiolene ligands, the molybdenum(IV) center reductively eliminates an oxygen atom from sulfoxides and amine *N*-oxides to form a Mo^{VI}=O bond.[9] The active site is located at the bottom of a large depression and is buried within the protein matrix, and the coordinating ligands are not exposed to the surface. The hydrophobic pocket formed by aromatic residues at the base of the substrate access funnel is conserved in both DMSOR and trimethylamine *N*-oxide reductase, which suggests the importance of hydrophobicity in the enzyme activity.[1]

Chart 1. Structures of (a) the Molybdopterin Cofactor (MGD) and (b) Model Ligand with Intramolecular NH···S Hydrogen Bonds

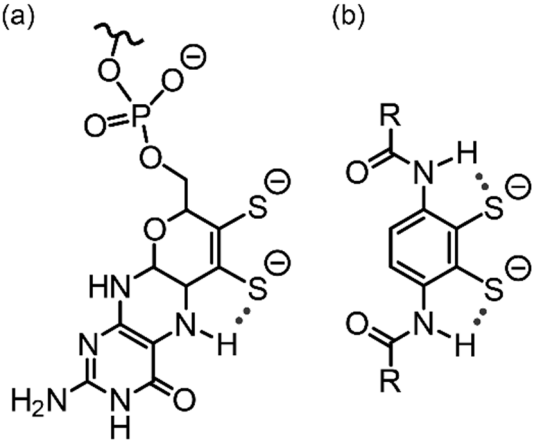

A hydrophobic environment at the active site should support the binding of substrates by weak interactions such as hydrogen bonds, and is probably important for controlling the

electrochemical properties. From this point of view, encapsulation using very bulky dendritic molecules has been reported as models of iron–sulfur proteins, heme proteins, and molybdoenzymes.[10-15]

As one of the weak interactions, hydrogen bonds are known to be supported in nonpolar solvents, and the contribution of the NH···S hydrogen bond to the redox potential has been clearly shown, in iron–sulfur peptide model complexes, to be dependent on the polarity of solvents.[16] Systematic studies using simple model complexes including iron–sulfur proteins,[16-19] cytochrome P450s,[20,21] copper proteins,[22] and molybdo- and tungstoenzymes[23-27] have revealed the positive shift of redox potential by NH···S hydrogen bonds.

A number of complexes have been synthesized to model molybdo- and tungstoenzymes.[28-33] As functional models, monooxomolybdenum(IV) benzene-1,2-dithiolate complexes can eliminate the oxygen atom of trimethylamine *N*-oxide to afford a Mo^{VI}=O bond of dioxomolybdenum(VI) complexes[34,35] although DMSOR uses desoxomolybdenum(IV) and monooxomolybdenum(VI) species. In the research on the NH···S hydrogen bonds of molybdenum benzene-1,2-dithiolate derivatives, it was found that the hydrogen bonds accelerate the OAT reaction between Mo^{IV} complexes and Me_3NO and stabilize the resulting Mo^{VI}=O bonds through a *trans* influence.[23,25-27] These suggestive results inspired the author to propose the presence of an intra-ligand NH···S hydrogen bond in MGD although the NH proton of DMSOR was not observed in crystal structures (Chart 1). As described in detail in previous papers,[23,26] introduction of four bulky triphenylacetylamino groups into the model complex, i.e. $(Et_4N)_2[Mo^{IV}O\{1,2\text{-}S_2\text{-}3,6\text{-}(Ph_3CCONH)_2C_6H_2\}_2]$ (**5-Mo**, Chart 2), resulted in a dramatic acceleration of the OAT reaction via the stabilization of a distorted intermediate by the bulky substituents and intramolecular NH···S hydrogen bonds.[23,36] In the proposed mechanism, the substrate approaches the polar molybdenum center from the upper side, i.e. *cis* to the oxo ligand, and spontaneously a Mo=O bond is formed, similarly to the enzyme. If the polar reactive site

is covered with hydrophobic media, the vacant site probably simulates the hydrophobic pocket of the active site in molybdoenzymes; however, the solubility of **5-Mo** in nonpolar solvents is not enough to confirm this hypothesis. Encapsulation of counterions using hydrophobic groups is one solution. In a previous paper, the (4-^{t}BuC$_6$H$_4$)$_3$CCONH group was used, and it was found that the two substituents partially masked the ionic molybdenum center and created a hydrophobic environment in (Et$_4$N)$_2$[Mo^{IV}O{1,2-S$_2$-3-(4-^{t}BuC$_6$H$_4$)$_3$CCONHC$_6$H$_3$}$_2$].[26] However, the complex was insoluble in nonpolar solvents because of insufficient encapsulation. These results and simulations suggested that introduction of four substituent groups must cover up the ionic parts as shown in this chapter. Another approach to understand the effect of a protein matrix at the active site has already been reported by Basu et al. using dendritic molecules.[14,15]

Chart 2. Designation of Molybdenum and Tungsten Complexes (M = Mo, W)

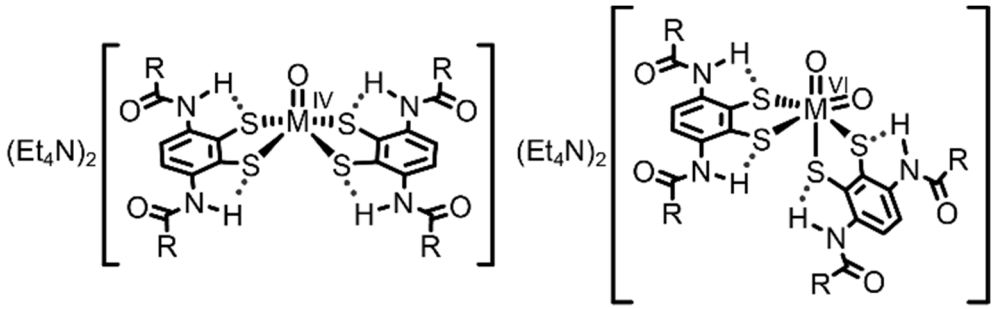

1-M (R = C(C$_6$H$_4$-4-^{t}Bu)$_3$) **2-M**
3-M (R = CH$_3$) **4-M**
5-M (R = CPh$_3$) **6-M**

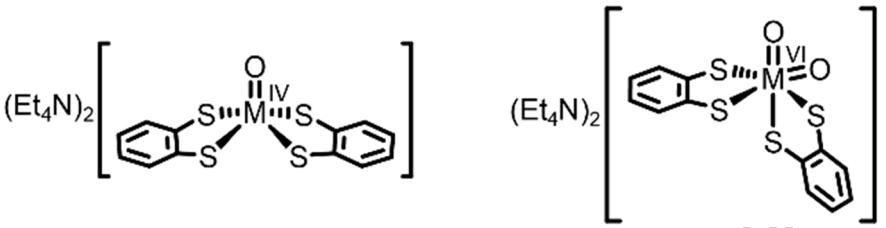

7-M **8-M**

Here, molybdenum(IV, VI) and tungsten(IV, VI) complexes (**1-M**, **2-M**; M = Mo, W; Chart 2) containing bulky hydrophobic dithiolate ligands and intramolecular NH···S hydrogen bonds, which make the complexes soluble in nonpolar solvents like toluene, are reported. The OAT reaction of Me_3NO proceeded faster in nonpolar solvents, which demonstrated that the polar substrate had better access to the active center in hydrophobic surroundings. In addition, the solid and solution state structures of the complexes were spectroscopically investigated in detail.

Results

Synthesis of the ligand. In the process of searching for a precursor of the dithiolate ligand that contained bulky triarylmethyl CAr_3 substituents, a benzotrithiol derivative, 1,2-S_3-3,6-{(4-^{t}BuC_6H_4)$_3$CCONH}$_2C_6H_2$ (**L1**), with a trisulfide bond was found and isolated. To synthesize a diaryl disulfide compound, Bunte salts are generally used as the protecting group for thiophenol derivatives. In a previous paper, a disulfide derivative with bulky CPh_3 substituents {1,2-S_2-3,6-($Ph_3CCONH)_2C_6H_2$}$_2$ was synthesized by deprotecting the corresponding Bunte salt using alkanethiolate in methanol and air oxidation.[23] At first, deprotection of the Bunte salt with bulky hydrophobic substituents, (^{n}Bu$_4$N)$_2$[3,6-{(4-^{t}BuC_6H_4)$_3$CCONH}$_2C_6H_2$-1,2-(SSO_3)$_2$], was attempted using EtSNa by a previously reported procedure. However, the reaction hardly proceeded because of the steric hindrance and the lack of reactant solubility in methanol, and only a small amount of an asymmetric disulfide, 3,6-{(4-^{t}BuC_6H_4)$_3$CCONH}$_2C_6H_2$-1,2-(SSEt)$_2$, was obtained. Another method for deprotecting Bunte salts using thiourea[40] gave a benzotrithiol derivative, **L1**, as yellow blocks which were isolated in a 56% yield (Scheme 1). **L1** was characterized by X-ray structural analysis (Figure 1), ^{1}H NMR, IR, and elemental analysis. Its unexpected structure can be explained by the steric hindrance on the sulfur atoms of a thiourea-bound intermediate, which prefers an intramolecular cyclization reaction to the intermolecular

formation of two disulfide bonds (Scheme 2). The author used **L1** as a precursor for the desired ligand because **L1** is chemically and thermodynamically stable and reducible by borohydride to afford the desired dithiolate ligand.

Scheme 1. Synthetic Route of the Molybdenum and Tungsten Complexes

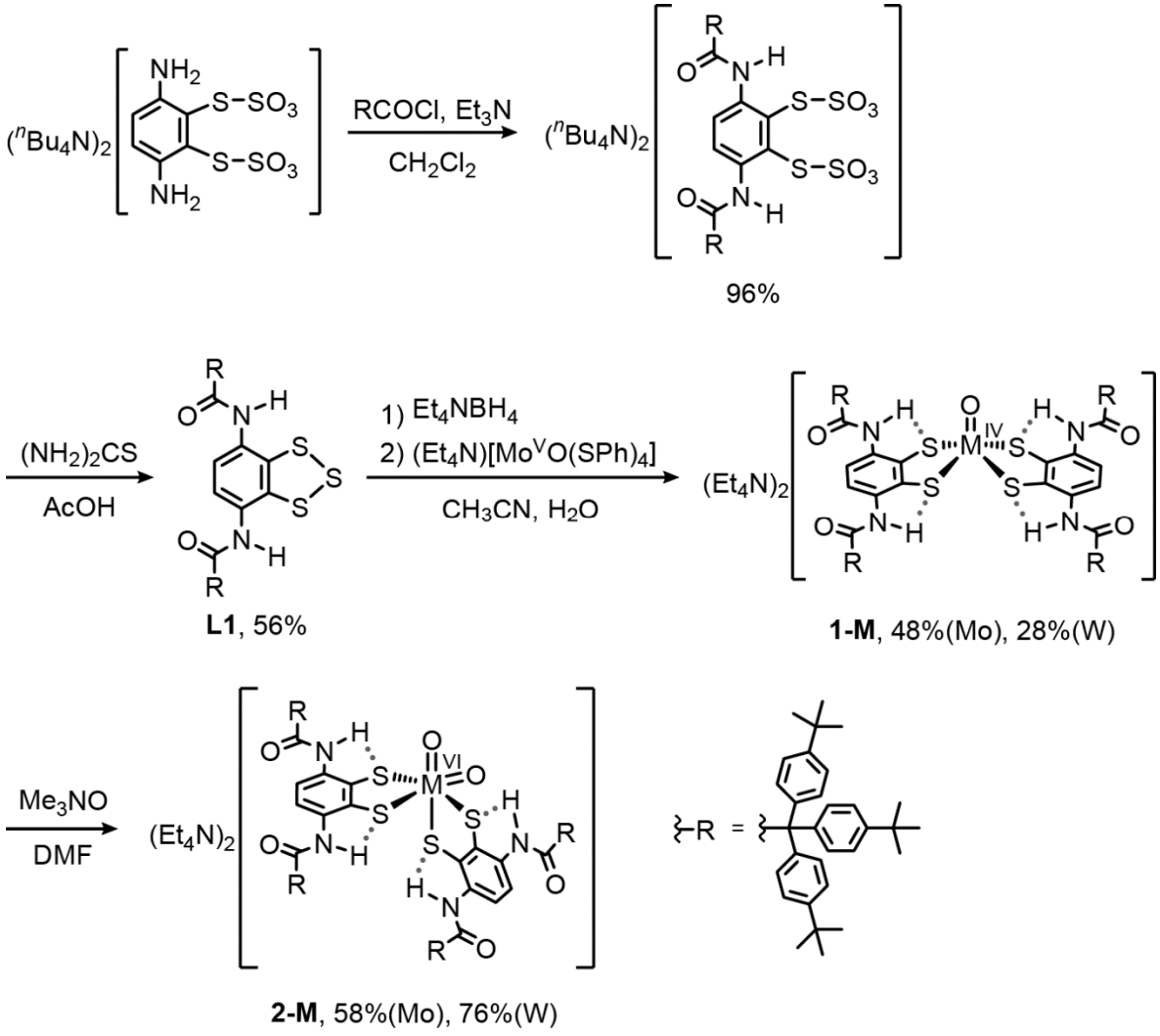

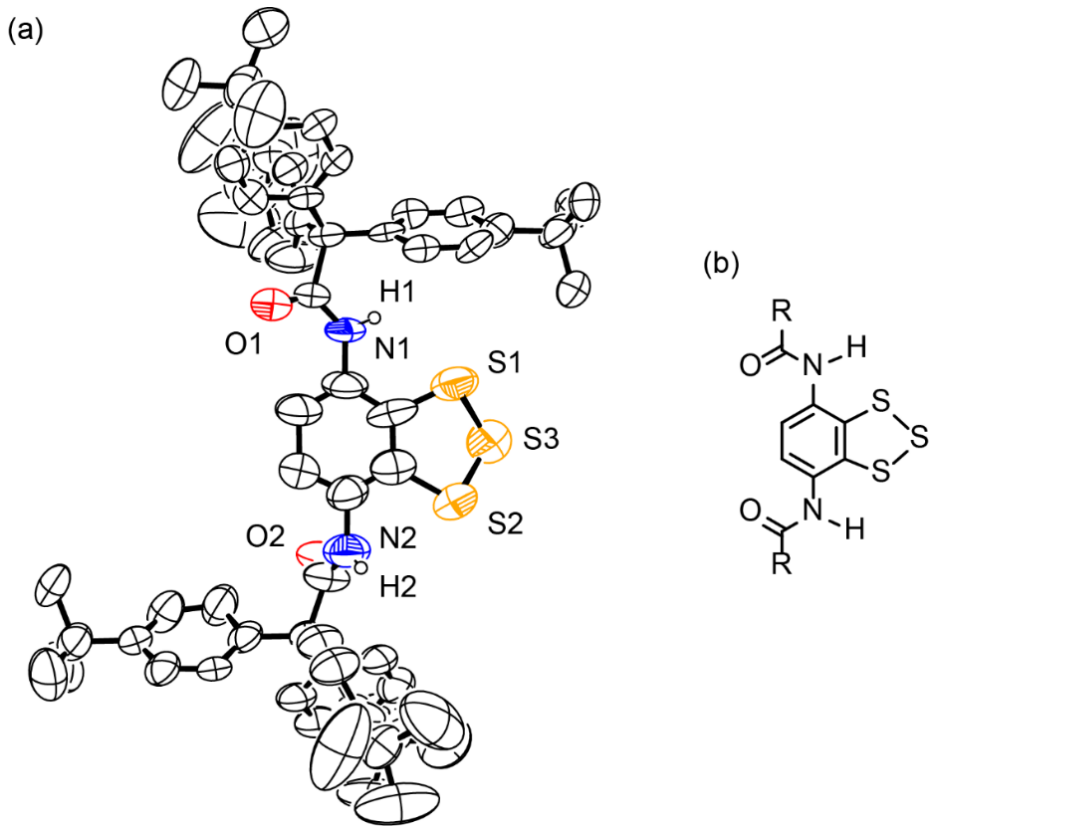

Figure 1. (a) ORTEP drawing at 50% probability (protons are omitted for clarity except amide groups) and (b) simplified structure of **L1**·3.1CH_3OH·H_2O.

Scheme 2. Proposed Mechanism Producing **L1**

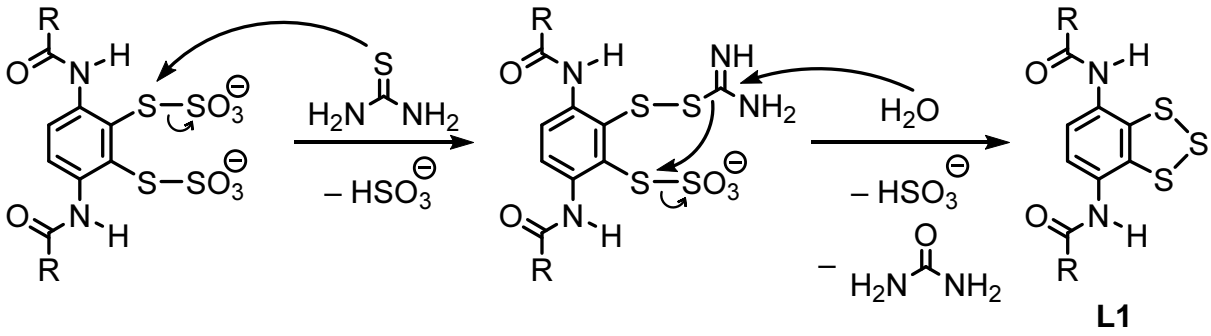

Synthesis of the complexes. Monooxo-molybdenum(IV) and tungsten(IV) complexes, $(Et_4N)_2[M^{IV}O(1,2\text{-}S_2\text{-}3,6\text{-}\{(4\text{-}^tBuC_6H_4)_3CCONH\}_2C_6H_2)_2]$ (**1-M**, M = Mo, W), were obtained using the reactions shown in Scheme 1. These complexes were synthesized by a method similar to that previously reported.[23,24,26] A ligand-exchange reaction in acetonitrile was carried out

between the dithiolate ligand, prepared by reduction of **L1** with excess Et_4NBH_4, and a M^V starting complex, $(Et_4N)[M^VO(SPh)_4]$ (M = Mo, W). The subsequent reduction of the M^V species by residual borohydride anions gave **1-M** as a yellowish-white precipitate. Since the **1-M** complexes have negligible solubility in acetonitrile, the precipitate was thoroughly washed with acetonitrile and selectively extracted with toluene. The pure molybdenum(IV) complex, **1-Mo**, was isolated as yellow blocks via recrystallization from toluene in a 48% yield, and the recrystallization of the tungsten(IV) complex, **1-W**, from a mixture of toluene and acetonitrile resulted in orange blocks in a 28% yield.

Dioxo-molybdenum(VI) and tungsten(VI) complexes, $(Et_4N)_2[M^{VI}O_2(1,2\text{-}S_2\text{-}3,6\text{-}\{(4\text{-}{}^t\text{Bu}C_6H_4)_3CCONH\}_2C_6H_2)_2]$ (**2-M**, M = Mo, W), were obtained by the oxygen-atom-transfer (OAT) reaction between the corresponding complexes, **1-M** and Me_3NO (Scheme 1). The reaction proceeded immediately in DMF at room temperature. The pure molybdenum(VI) complex, **2-Mo**, was isolated as dark brown blocks by recrystallization from acetonitrile in a 58% yield, and the tungsten derivative, **2-W**, was isolated as reddish-orange blocks from acetonitrile in a 76% yield. The dioxomolybdenum(VI) complex **2-Mo** is quite stable in both the solid and solution states compared to other dioxomolybdenum(VI) complexes containing 3,6-bis(acylamino)benzene-1,2-dithiolate ligands, which are too unstable to be isolated.[23,24,26] The complex is considered to be thermodynamically stabilized by its bulky substituents and NH···π hydrogen bonds between amide NH and the adjacent CAr_3 group, which weaken the NH···S hydrogen bond as described in the following section.

Molecular structures in the crystals. The molecular structures of **1-M** and **2-M** (M = Mo, W) were determined by X-ray analysis. These complexes were apparently recrystallized easily but the crystallinity was very low like gel because of the highly-disordered structures inside the organic frameworks or capsules. Although careful recrystallization and selection of crystals were repeated, the quality of the data was quite poor, resulting in large *R* factors. Unfortunately,

the structural details cannot be described; however, the backbone structures and the packing must be correct. Here, the author mainly discusses the relative location of counter cations and conformation of substituents. The preliminary structure of **2-Mo** was only used to confirm that **2-Mo** was isomorphous and isostructural to **2-W**.

Two molecular structures of **1-Mo** were obtained and varied depending on the crystallization solvents. The molecular structures of **1-Mo**·8(toluene) and **1-Mo**·toluene·5CH_3CN, obtained by crystallization from toluene and toluene/acetonitrile, respectively, are shown in Figure 2. The CAr_3 moieties are bulky enough to interlock with each other in the crystal, so the possible symmetries of the four CAr_3 moieties are C_2 and C_i. As shown in Figure 2c,d, the anion part of **1-Mo**·8(toluene) has a pseudo-C_i symmetry (the molecular structure showed a pseudo-center of symmetry), and the anion part of **1-Mo**·toluene·5CH_3CN has a C_2 symmetry. The crystal of **1-W**·4(toluene)·3CH_3CN·H_2O is essentially isomorphous to that of **1-Mo**·toluene·5CH_3CN with similar cell parameters (Table 1). The anion part is also C_2 symmetry. In this chapter, the author discusses the molecular structure of **1-Mo**·8(toluene) because it is the highest quality crystal.

The Mo center of **1-Mo**·8(toluene) shows a square pyramidal geometry similar to $(Et_4N)_2[Mo^{IV}O\{1,2\text{-}S_2\text{-}3,6\text{-}(CH_3CONH)_2C_6H_2\}_2]$ (**3-Mo**, Chart 2). All of the amide NH moieties were directed toward the sulfur atoms of the dithiolate ligand, which indicated the presence of NH···S hydrogen bonds. The aromatic ring of the substituent is close to the NH group suggesting the formation of an NH···π hydrogen bond.[44] Bifurcated (NH···S and NH···π) hydrogen bonds are known[45] and can perturb the strength of the N–H bond. The change was not detected by structural analysis but was found in the IR spectra described later. One of the two Et_4N^+ counterions was found close to the terminal oxo ligand suggesting the formation of a CH···O=Mo interaction (Figure 2e). Similar interactions between an oxo ligand and counter cations have been reported.[46-49] In the space-filling model of **1-Mo**·8(toluene) (Figure 2f), the

polar MoO moiety and Et_4N^+ counterions (blue) are covered by the walls formed by the bulky hydrophobic ligands. These ligand walls can prevent intermolecular ionic interactions, and this makes the complex soluble in nonpolar solvents like toluene.

Table 1. Crystallographic Data for **1-M** and **2-M** (M = Mo, W)

	1-Mo·8(toluene)	**1-Mo**·toluene·5CH_3CN	**1-W**·4(toluene)·3CH_3CN·H_2O	**2-Mo**·5CH_3CN	**2-W**·5CH_3CN
empirical formula	$C_{212}H_{268}MoN_6O_5S_4$	$C_{173}H_{227}MoN_{11}O_5S_4$	$C_{190}H_{247}N_9O_6S_4W$	$C_{166}H_{219}MoN_{11}O_6S_4$	$C_{166}H_{219}N_{11}O_6S_4W$
formula weight	3204.49	2764.82	3065.19	2688.81	2776.72
color	yellow	green	orange	reddish-brown	reddish-orange
crystal system	triclinic	monoclinic	monoclinic	orthorhombic	orthorhombic
a, Å	16.140(4)	39.1189(16)	39.235(5)	14.4864(14)	14.503(2)
b, Å	18.083(4)	23.7467(11)	23.938(3)	25.173(3)	25.170(5)
c, Å	18.963(4)	20.0641(14)	20.131(3)	21.753(2)	21.806(4)
α, deg	116.758(6)				
β, deg	91.907(8)	107.993(8)	108.061(5)		
γ, deg	99.703(8)				
V, Å^3	4833.6(18)	17726.9(18)	17976(4)	7932.6(14)	7960(3)
space group	*P*1	*C*2/*c*	*C*2/*c*	*Pnn*2	*Pnn*2
Z	1	4	4	2	2
D_{calc}, g/cm^3	1.101	1.036	1.133	1.126	1.158
F (000)	1728	5952	6544	2892	2956
μ(MoKα), mm^{-1}	0.166	0.172	0.744	0.191	0.834
scan type	ω	ω	ω	ω	ω
$2\theta_{max}$, deg	50	50	50	50	50
No. of reflections unique	28442	15566	15799	13942	13726
No. variables	2017	1037	929	767	804
residuals; $R1^a$ (I > 2σ(I)), w$R2^b$ (all data)	0.0931, 0.2819	0.1148, 0.3668	0.1265, 0.3323	0.2043, 0.5205	0.1164, 0.3496
GOF	1.032	1.274	1.109	1.463	1.035

$^aR1 = \Sigma||F_o| - |F_c|| / \Sigma|F_o|$. ^{b}w$R2 = \{\Sigma[w(F_o^2 - F_c^2)^2] / \Sigma[w(F_o^2)^2]\}^{1/2}$

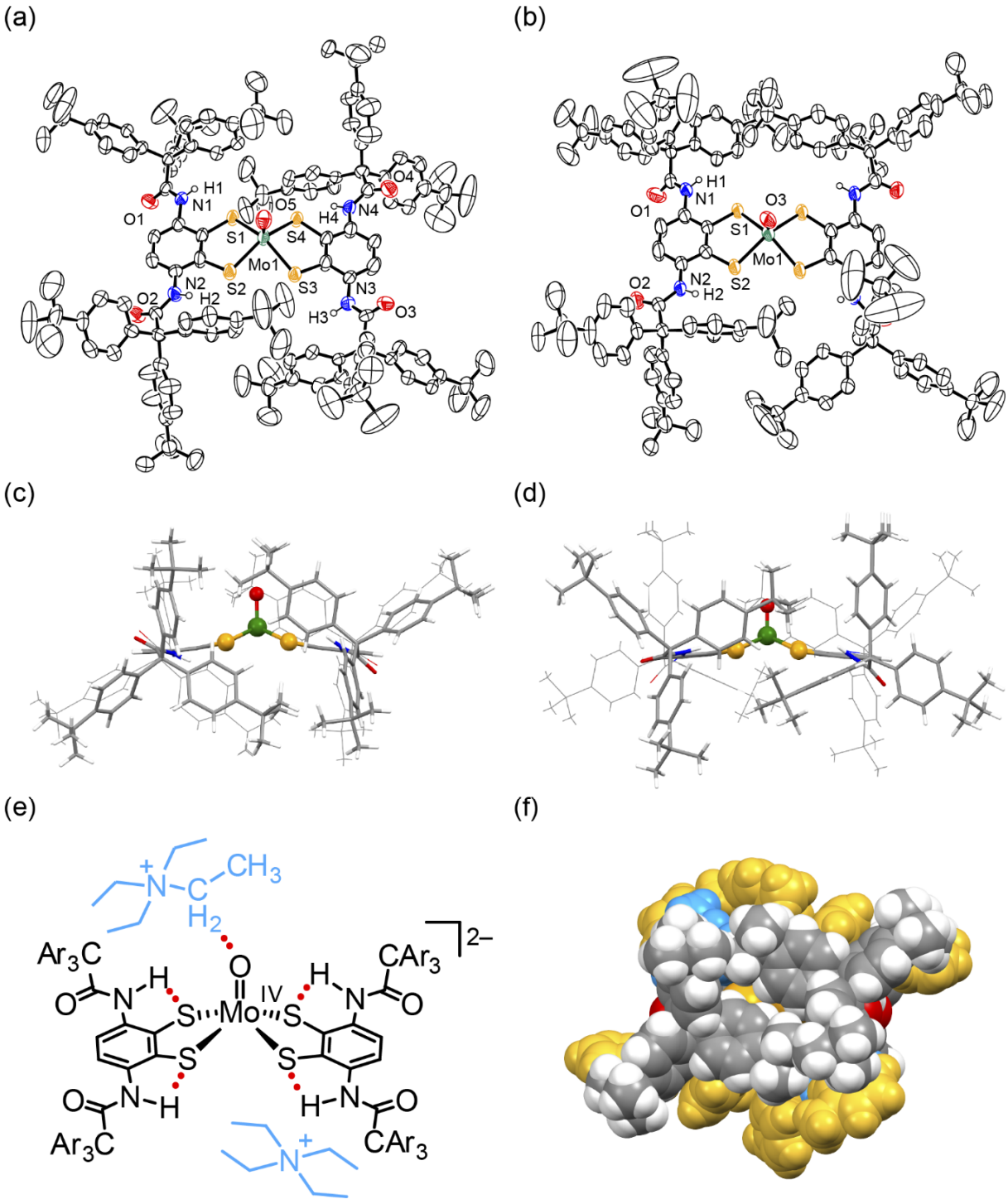

Figure 2. (a, b) ORTEP drawings at 50% probability (protons are omitted for clarity except amide groups) and (c, d) side-view structures of the anion part of (a, c) **1-Mo**·8(toluene) and (b, d) **1-Mo**·toluene·5CH_3CN. (e) Schematic drawing of the interionic CH···O=Mo interaction in the crystal. (f) Space-filling model of **1-Mo**·8(toluene) with Et_4N^+ (blue) and toluene (yellow).

The W center of **2-W**·5CH_3CN shows a slightly distorted octahedral geometry similar to $(Et_4N)_2[W^{VI}O_2\{1,2\text{-}S_2\text{-}3,6\text{-}(CH_3CONH)_2C_6H_2\}_2]$ (**4-W**). The molecular structure of **2-W**·5CH_3CN is shown in Figure 3. The crystals of **2-Mo**·5CH_3CN and **2-W**·5CH_3CN are isomorphous (Table 1). The two dithiolate ligands are crystallographically equivalent owing to the C_2 axial symmetry across the bisector of the O–W–O angle. Two Et_4N^+ counterions were found close to the terminal oxo ligands with CH···O=W interactions (Figure 3c).

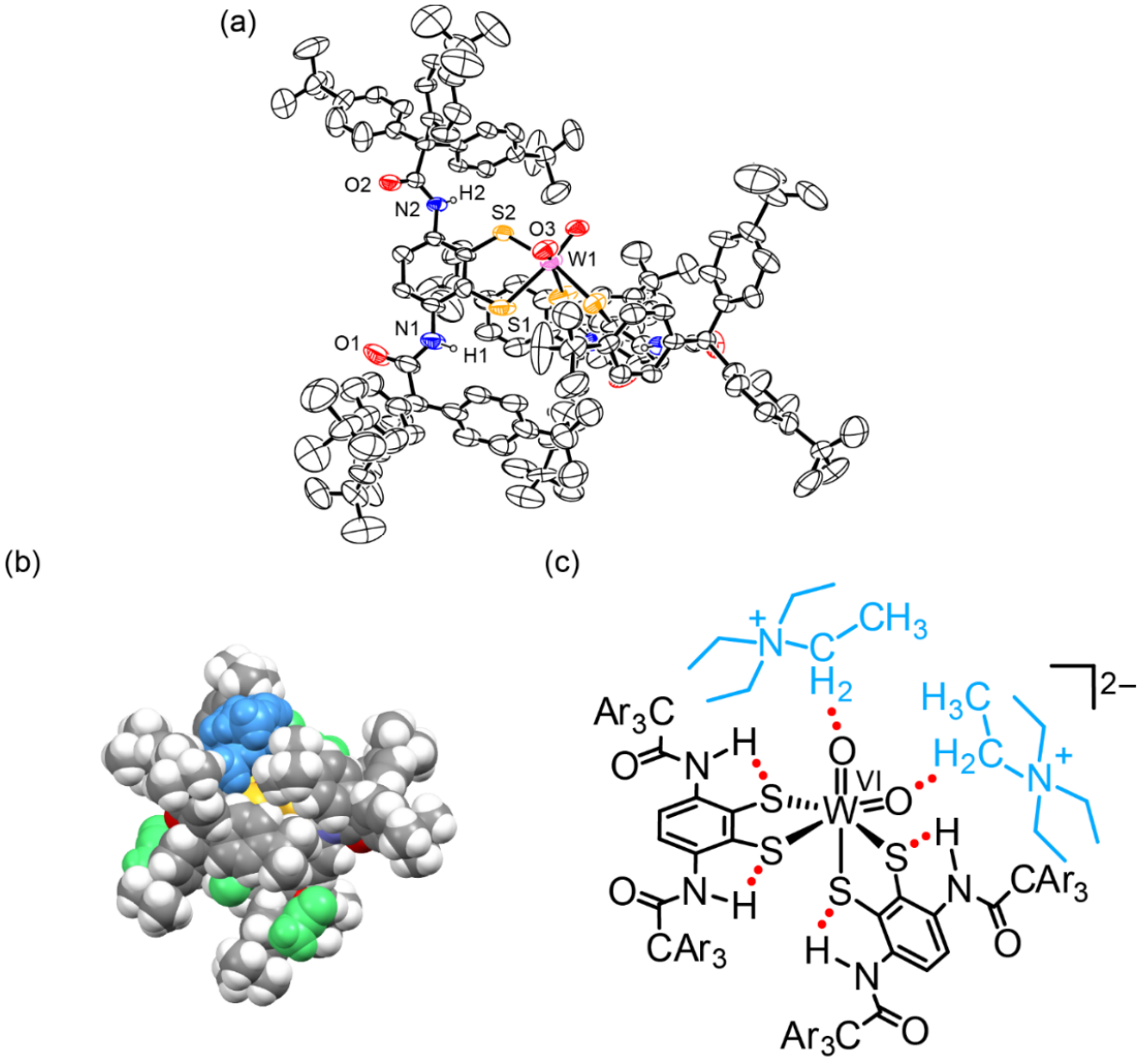

Figure 3. (a) ORTEP drawing at 50% probability (anion part, protons are omitted for clarity except amide groups) and (b) space-filling model of **1-Mo**·toluene·5CH_3CN with Et_4N^+ (blue), toluene (yellow), and acetonitrile (light green). (c) Schematic drawing of interionic CH···O=Mo hydrogen bond in the crystal.

As shown in Figure 4 and Table 2, the geometrical parameters of **2-W** were similar to the reported values of **4-W**, showing the longer W–S at the position *trans* to W=O owing to a strong *trans* influence of the oxo ligand and the unsymmetrical structure with the stronger (red) and the weaker (green) NH···S hydrogen bonds. The amide NH at the position *cis* to the oxo ligand is directed towards the benzene ring of the CAr_3 moiety rather than the sulfur atom suggesting the presence of an NH···π hydrogen bond. The NH···π hydrogen bond decreases the contribution of NH···S, resulting in an increase in donation from S to W. The W–S bond at the position *cis* to the oxo ligand is thought to be stabilized by the intermolecular NH···π hydrogen bond between the amide NH and benzene ring of the neighboring dithiolate ligand. On the other hand, an NH···π hydrogen bond is only seen in an intermolecular fashion in the crystal of **4-W**.

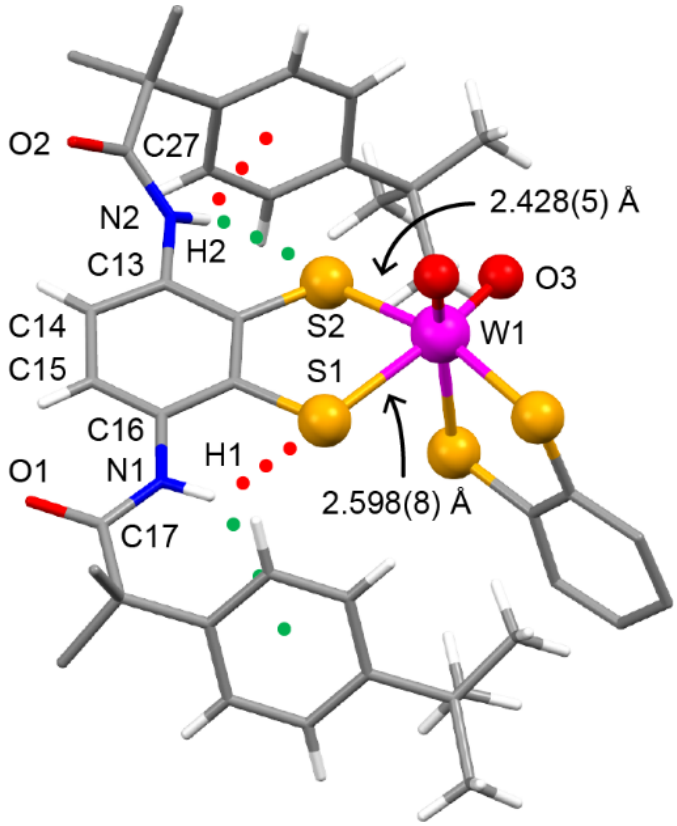

Figure 4. A simplified molecular structure of the anion part of **2-W**·5CH_3CN. Four 4-^{t}BuC_6H_4 moieties and two of acylamino groups were omitted for clarity.

Table 2. Comparison of Selected Bonds and Angles (Å, deg) for the Dioxotungsten(VI) Complexes **2-W** and **4-W**

	2-W	**4-W**
W=O	1.76(2)	1.735(4)
W–S (*trans*)	2.598(8)	2.607(3)
W–S (*cis*)	2.428(5)	2.426(4)
W–S (mean)	2.51	2.52
Δ(W–S)	0.17	0.18
NH···S[a] (*trans*)	2.45	2.47
NH···S (*cis*)	2.65	2.74
NH···π[a] (*trans*)	3.10	—[b]
NH···π (*cis*)	2.78	2.74[c]
dihedral angle[d] (*trans*)	8(5)	7.9(9)
dihedral angle (*cis*)	44(3)	49.7(8)

[a]Hydrogen atoms are located at the calculated positions. Distance between the amide proton and the centroid of the closest benzene ring. [b]No NH···π interaction. [c]Intermolecular NH···π interaction. [d]Dihedral angle between benzene ring and amide CONH plane (C17-N1-C16-C15 for **2-W**).

IR and Raman spectra. The presence of NH···S hydrogen bonds was confirmed by IR spectroscopy. IR data for **1-M** and **2-M** in the solid state are listed in Table 3 along with the values of the related complexes, $(Et_4N)_2[M^{IV}O\{1,2\text{-}S_2\text{-}3,6\text{-}(CH_3CONH)_2C_6H_2\}_2]$ (**3-M**) and $(Et_4N)_2[W^{VI}O_2\{1,2\text{-}S_2\text{-}3,6\text{-}(CH_3CONH)_2C_6H_2\}_2]$ (**4-W**). As described in a previous paper,[26] the strength of the hydrogen bond is evaluated using the negative shift of *ν*(NH) compared to the corresponding compound without a hydrogen bond. RCONHPh is used as a reference in this chapter. The Δ*ν*(NH) values of **1-Mo** and **1-W** (−97 and −99 cm^{-1}, respectively) are more negative than those of **3-Mo** and **3-W** (−85 and −85 cm^{-1}, respectively), which by conventional estimation indicates stronger hydrogen bonds in the complexes with bulky substituents. However, **1-M** forms bifurcated (NH···S and NH···π) hydrogen bonds and not the simple NH···S hydrogen bonds seen in **3-M**. In this case, it is necessary to take into account the contribution of the NH···S hydrogen bond. The NH···π hydrogen bond is favorably formed with a fixed orientation of the aromatic ring to the NH group seen in **1-M** and lowers *ν*(NH)

significantly. The NH···π hydrogen bond is not as strongly formed in the reference compound, RCONHPh, compared to **1-M**. The conventional evaluation based on the obtained Δν(NH) for **1-M** must overestimate the strength of the NH···S hydrogen bond. Therefore, the net strength should be weaker. Moreover, the perturbation of the NH···π hydrogen bond likely weakens the competing NH···S hydrogen bond.

In IR spectra of **2-W**, a single but relatively broad band was observed even though the presence of two distinct hydrogen bonds was suggested in the crystal (Figure 5). On the other hand, **4-W**, with CH_3 substituents, exhibited two distinct ν(NH) bands (3370 and 3316 cm^{-1}) in the solid state. The ν(NH) at the position *cis* to the oxo ligand was observed at a wavenumber 54 cm^{-1} higher. The ν(NH) band at 3316 cm^{-1} of **2-W** can be fitted by a single Gaussian curve (Figure 5b, curve 1) with a full width at half maximum (FWHM) of 66 cm^{-1}. The curve is reasonably separated into two equivalent Gaussian curves at 3326 and 3306 cm^{-1} (curve 2). The difference of the two peaks is only 20 cm^{-1} smaller than the FWHM; therefore the stretching vibrations could not be detected as two bands. The results indicate that the relatively stronger NH bond at the *cis* position was significantly weakened by the formation of the NH···π hydrogen bond in **2-W** (see Figure 4).

Table 3. IR Bands of ν(NH) (cm^{-1}) in the Molybdenum and Tungsten Complexes in the Solid State

	ν(NH)[a]	Δν(NH)[b]
1-Mo	3306	–97
1-W	3304	–99
2-Mo	3307	–96
2-W	3316	–87
3-Mo[c]	3346	–85
3-W[d]	3346	–85
4-W[d]	3370, 3316	–61, –115

[a]Nujol. [b]Differences from the value (3403 cm^{-1} for **1-M** and **2-M**, 3431 cm^{-1} for **3-M** and **4-M**) of the corresponding compound, RCONHPh in solution (10 mM in CH_2Cl_2). [c]Ref. 23. [d]Ref. 24.

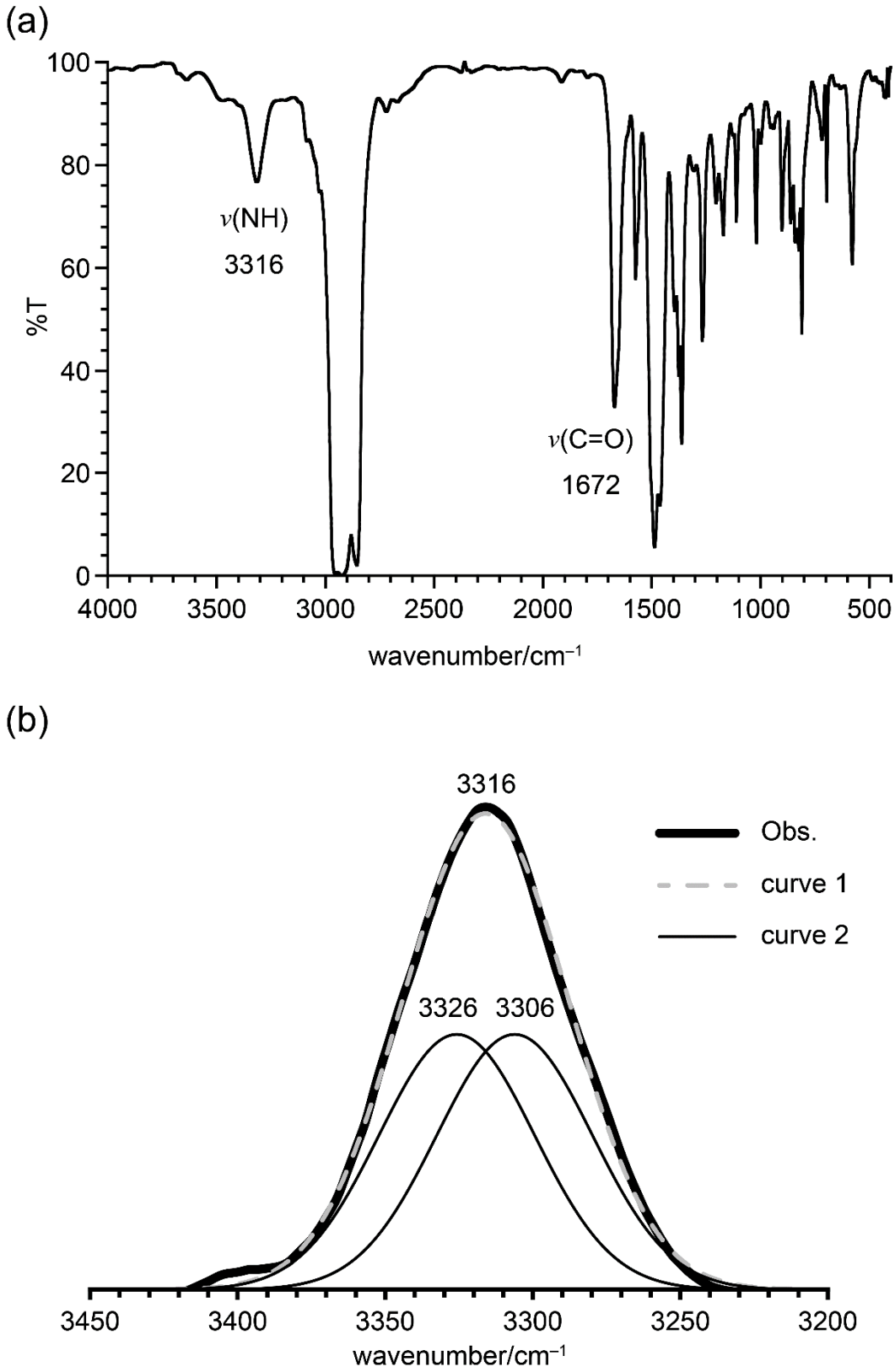

Figure 5. (a) IR spectrum of the dioxotungsten complex **2-W** in the solid state (Nujol method) and (b) Curve-fitting data at the region around *v*(NH) bands by Gaussian distribution using a open sourse software fityk 0.9.8.[50] Curve 1 (gray, dashed) represents the single Gaussian curve fitting, and curve 2 (black, thin solid) represents two Gaussian curves.

IR ν(MO) bands of **1-M** are listed in Table 4 along with those of the related complexes, **3-M** and $(Et_4N)_2[M^{IV}O(1,2\text{-}S_2C_6H_4)_2]$ (**7-M**) without the hydrogen bond.[51-53] The stabilization of the M^{IV}=O bonds of monooxo-molybdenum(IV) and tungsten(IV) complexes by NH···S hydrogen bonds was observed for **1-M**, as well as **3-M**. The results are consistent with the tendency of the NH···S hydrogen-bonded complexes described in previous papers.[23,26]

Table 4. IR Bands of ν(MO) (cm^{-1}) in the Monooxo-Molybdenum(IV) and Tungsten(IV) Complexes in the Solid State

	ν(MO)	$\Delta\nu$(MO)[a]
1-Mo	921	+16
1-W	920	+14
3-Mo[b]	922	+17
3-W[c]	912	+6
7-Mo[d]	905	
7-W[e]	906	

[a]Differences from the value of $(Et_4N)_2[M^{IV}O(1,2\text{-}S_2C_6H_4)_2]$ (**7-M**). [b]Ref. 23. [c]Ref. 24. [d]Ref. 51. [e]Ref. 53.

The symmetric and asymmetric MO_2 stretching bands of **2-Mo** and **2-W**, ascribed to the *cis*-dioxo configuration, were clearly observed by resonance Raman spectroscopy excited at 514.5 nm in the LMCT band (Figure 6). These values are listed in Table 5 together with the related compounds and the differences from $(Et_4N)_2[M^{VI}O_2(1,2\text{-}S_2C_6H_4)_2]$ (**8-M**) are shown in parentheses. Because a dioxomolybdenum(VI) complex with CH_3 substituents (**4-Mo**) was not isolated by thermodynamic instability,[23] only the values for **4-W** are shown.[24] The wavenumber shifts of **2-M** (23 and 21 cm^{-1}) were larger than those of **4-W** (14 cm^{-1}).

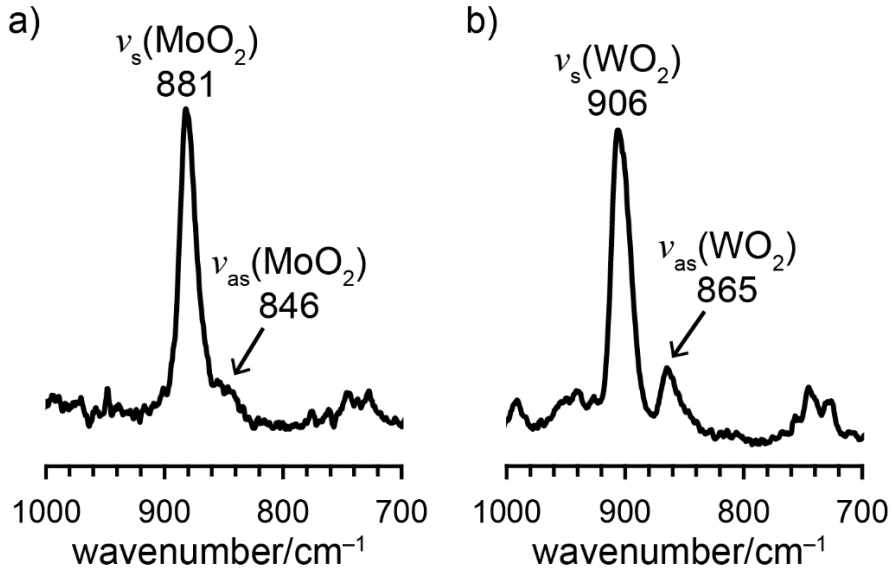

Figure 6. Resonance Raman spectra of (a) **2-Mo** and (b) **2-W** excited at 514.5 nm in the solid state.

Table 5. Resonance Raman Bands of $\nu(WO_2)$ (cm^{-1}) in the Dioxotungsten(VI) Complexes in the Solid State[a]

	Mo		W	
	$\nu_s(MoO_2)$	$\nu_{as}(MoO_2)$	$\nu_s(WO_2)$	$\nu_{as}(WO_2)$
2-M	881 (+23)	846 (+17)	906 (+21)	865 (+22)
4-M[b]			899 (+14)	854 (+9)
8-M[c]	858	829	885	843

[a]Differences from the value of $(Et_4N)_2[M^{VI}O_2(1,2\text{-}S_2C_6H_4)_2]$ (**8-M**) are shown in the parentheses. [b]Refs. 23,24. [c]Refs. 34,53.

^{1}H NMR studies. ^{1}H NMR spectra of the monooxo-molybdenum(IV) and tungsten(IV) complexes (**1-M**) are shown in Figure 7. Because the **1-M** complexes are only slightly soluble in acetonitrile, the ^{1}H NMR measurements were carried out in DMF-d_7 (Figure 7a and c) and toluene-d_8 (Figure 7b and d). **1-M** exhibited well defined signals in DMF-d_7 as did the related molybdenum(IV) complexes in CD_3CN,[25-27] but some crystal solvent signals (labeled by asterisks) were observed. On the other hand, the broadened and upfield-shifted signals of the Et_4N^+ counterions, **e** and **g**, were observed in toluene-d_8. These results probably arose from shielding by the benzene rings of the ligand. In the crystal of **1-M**, the Et_4N^+ counterions are

located at a position shielded by the benzene rings of the dithiolate ligand and CAr_3 groups. Though the shielding effect depends on the spatial position and direction, only a single set of signals was observed, because the molecular motion was faster than the NMR timescale. Upon cooling to –45 °C, the signals of Et_4N^+ broadened and the signal g split into two distinct signals (Figure 8). The result can be explained by a decrease in the molecular motion, resulting in the construction of two distinct environments by shielding of the MoO moiety, which has a triple bond character (formally expressed as $Mo{\equiv}O^+$)[54] and whose effect was the stronger the closer the Et_4N^+ counterion is to the oxo ligand (upper side of Figure 2e).

The ^1H NMR spectrum of **2-W** showed a single set of broad signals in a polar solvent, CD_3CN, although the green and red protons of one ligand are essentially nonequivalent in the *cis*-dioxo octahedral configuration but two ligands are equivalent in C_2-symmetric molecular structures (Figure 9). The observation is caused by fast conformational changes, which are relatively slow in the nonpolar solvent, toluene-d_8 (Figure 9b). Upon cooling to –45 °C in toluene-d_8, the signals sharpened and a pair of signals separated into two sets of signals (Figure 9c). Because the NH proton forming the stronger NH···S hydrogen bond is observed at the lower field[26] and the NH···S at the position *trans* to the oxo ligand is stronger than *cis*,[24] the lowest signal is reasonably assigned to the NH proton at the position *trans* to the oxo ligand. Therefore the other signals were assigned to each side of the ligand at the positions *trans* (red) and *cis* (green) to the oxo ligand using TOCSY and ROESY spectra (Figure 10). The rotating frame Overhauser effects (ROE) between red **f** and green **a**, **b** were observed indicating the fixed conformation, but were absent between green **f** and red **a** in ROESY spectra, which are in accord with the molecular structure in the crystal. These observations prove the validity of the assignments. In addition, the interionic ROE was observed between signals **b** and **g**, which is consistent with the relative location of Et_4N^+ in the crystal.

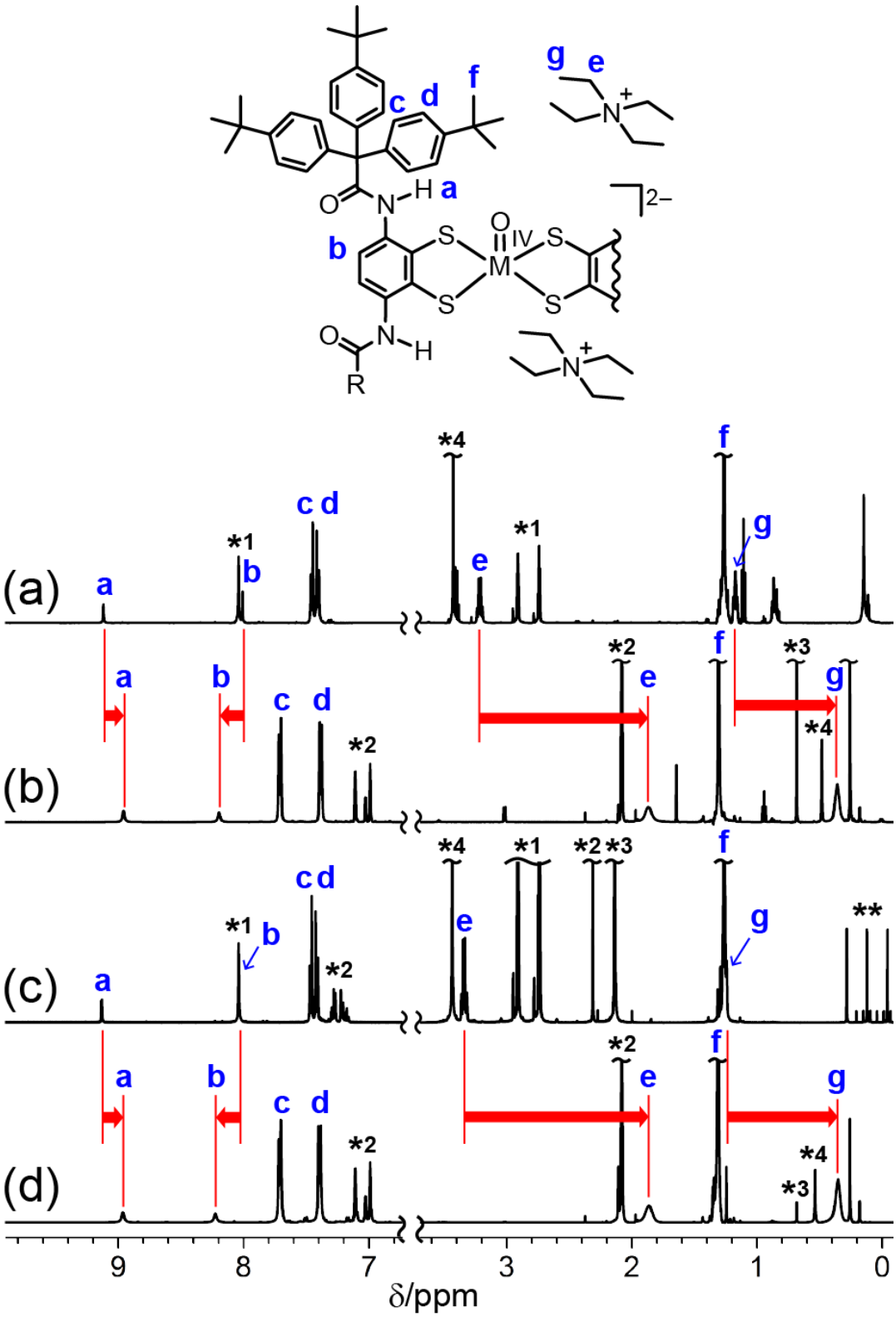

Figure 7. ^{1}H NMR spectra of (a) **1-Mo** in DMF-d_7, (b) **1-Mo** in toluene-d_8, (c) **1-W** in DMF-d_7, and (d) **1-W** in toluene-d_8 at 30 °C. The asterisks denote solvents as a contaminant (*1: DMF; *2: toluene; *3: acetonitrile; *4: water). The double asterisk (**) denotes BH_4^- used for clear spectrum by reducing a trace amount of $W^{V}O$ species.

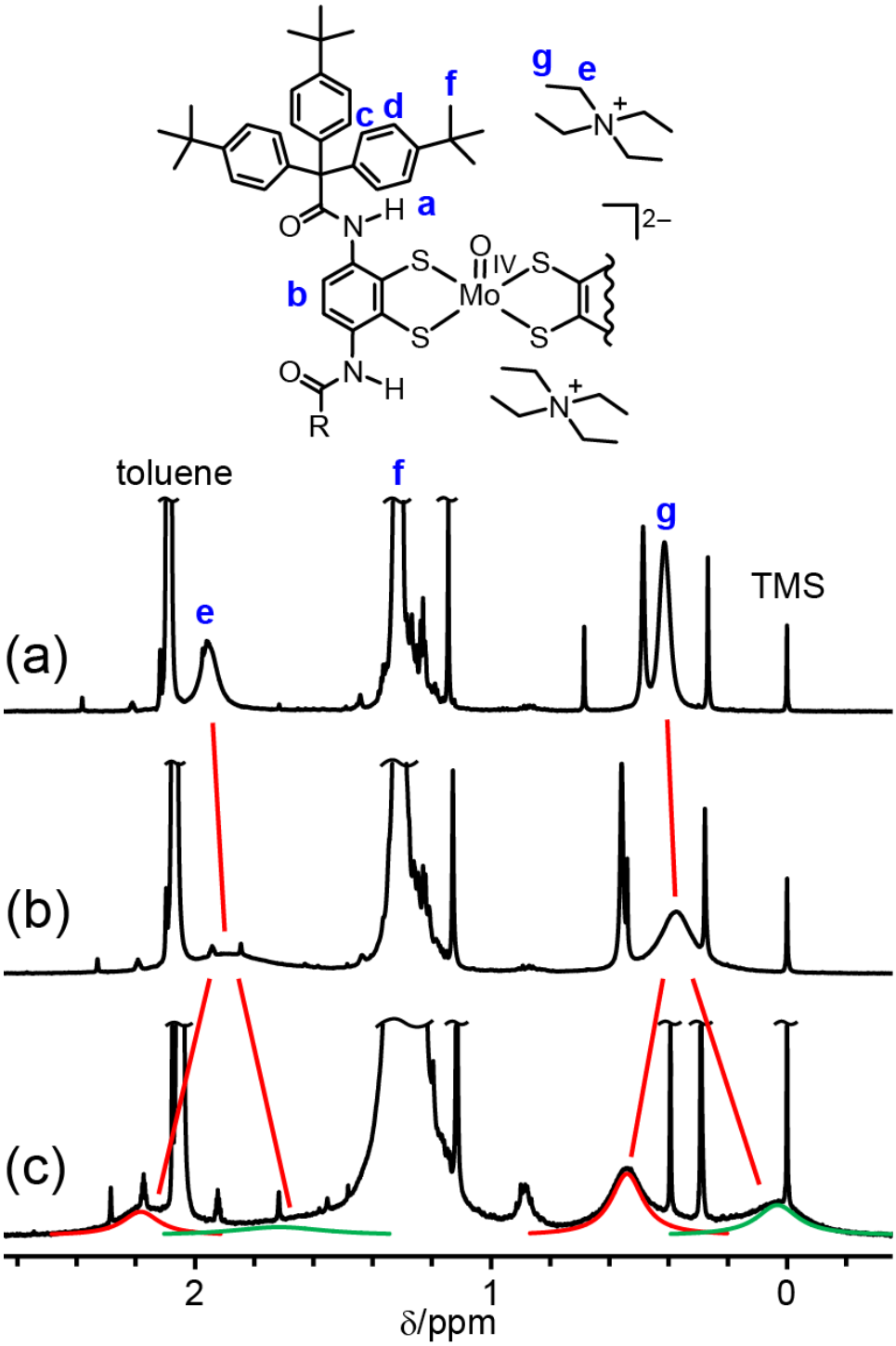

Figure 8. VT NMR spectra and fitted curves using Lorentzian distribution[50] (green and red lines) of the monooxomolybdenum complex **1-Mo** in toluene-d_8 at (a) 30 °C, (b) –10 °C, and (c) –45 °C.

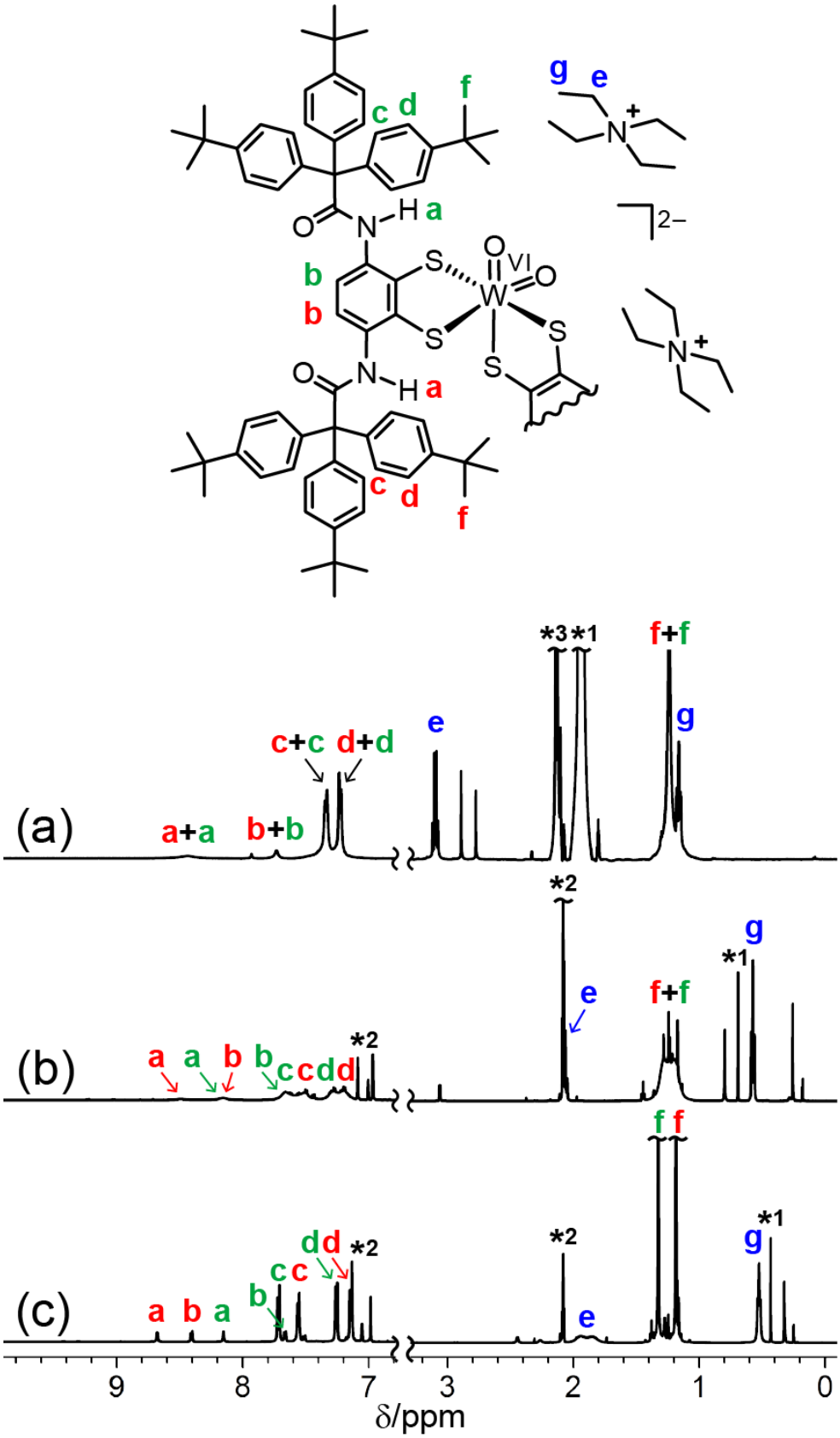

Figure 9. ^{1}H NMR spectra of **2-W** in (a) CD_3CN at 30 °C, (b) toluene-d_8 at 30 °C, and (c) toluene-d_8 at –45 °C. The asterisks denote solvents as a contaminant (*1: acetonitrile; *2: toluene; *3: water).

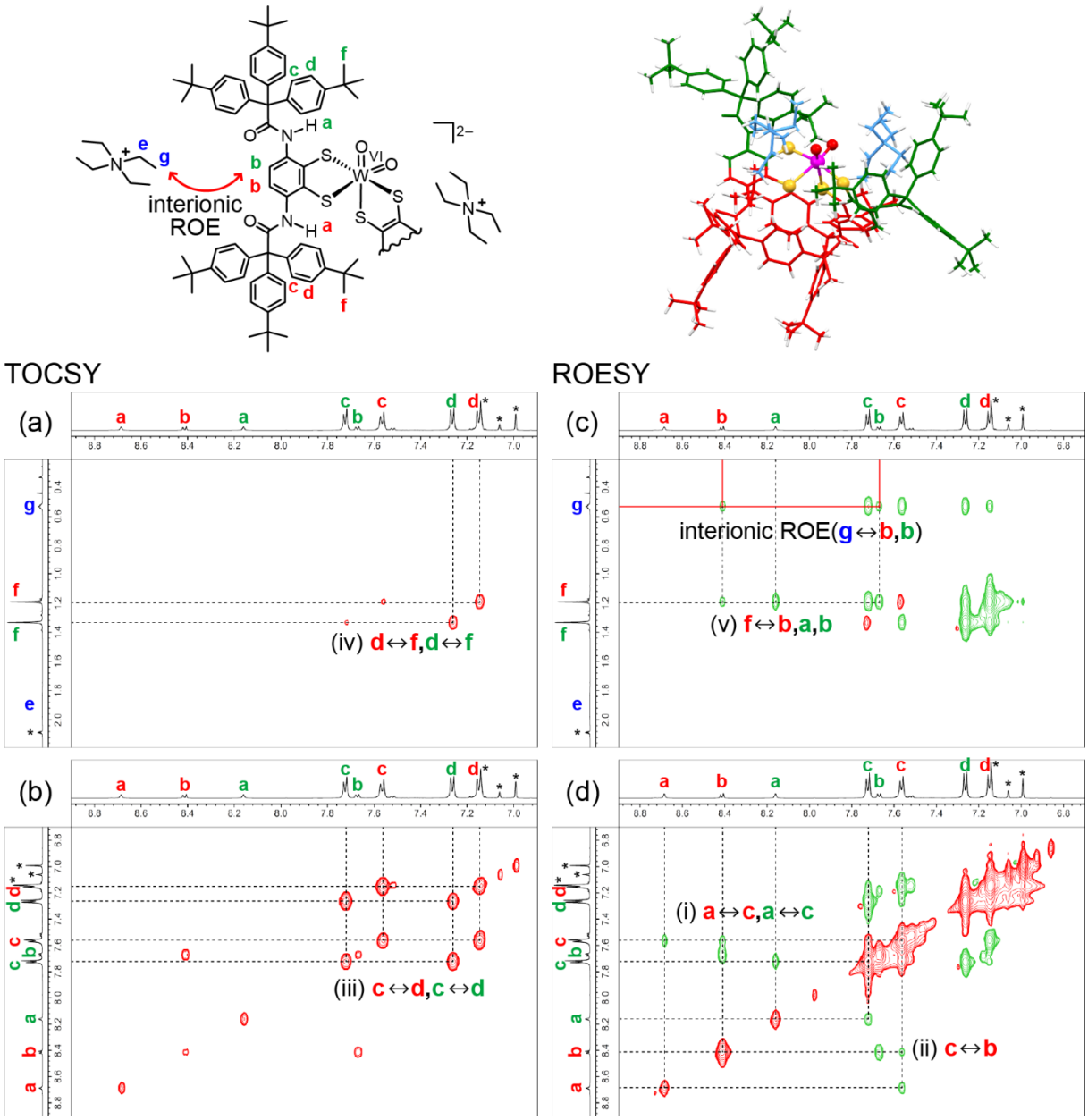

Figure 10. (a,b) TOCSY and (c,d) ROESY spectra of **2-W** in toluene-d_8 at –45 °C. The asterisks denote the residual signals of toluene-d_8. Assignment of red and green protons is represented in (i) to (v).

Variable temperature (VT) NMR analysis of **2-W** confirmed that the signals separated in various solvents at low temperature. Thermodynamic parameters of the chemical exchange estimated from VT NMR spectra using line shape analysis are summarized in Table 6. The Eyring plot in various solvents gave $\Delta H^{\ddagger}$, $\Delta S^{\ddagger}$, and $\Delta G^{\ddagger}$. The activation free energies, $\Delta G^{\ddagger}$, were estimated to be 58.1–64.1 kJ mol^{-1} which are larger than that ($\Delta G^{\ddagger}$ = 43.2 kJ mol^{-1}) of the

related complex without hydrogen bonds, $(Et_4N)_2[W^{VI}O_2(1,2\text{-}S_2\text{-}3,6\text{-}Cl_2C_6H_2)_2]$ in THF-d_8.[55] The activation entropies, $\Delta S^{\ddagger}$, were negative in all cases, which indicates that the conformational change proceeds through a Bailar twist mechanism without dissociation of the ligands as shown in Figure 11, where two enantiomers are identical in NMR spectroscopy.[56-58] The bulky substituents are expected to restrict the possible conformations, which enlarges the negative entropy of activation. In addition, the activation enthalpies, $\Delta H^{\ddagger}$, were relatively large in nonpolar solvents, which allowed observation of the green and red protons in Figure 9 even at room temperature. The small entropy of activation in DMF with a large donor number suggests the presence of a dissociative isomerization mechanism. VT NMR analysis of **2-Mo** in toluene-d_8 gave a relatively small activation free energy ($\Delta G^{\ddagger}$ = 55.1 kJ mol^{-1}) compared to **2-W**. In the case of **2-Mo**, two distinct signals were not observed in toluene-d_8 at room temperature owing to the fast conformational change, which was probably caused by the lability of the Mo–S bonds.

Table 6. Thermodynamic Parameters of **2-W** in Various Solvents

solvent	ε_r[a]	$\Delta H^{\ddagger}$/kJ·mol^{-1}	$\Delta S^{\ddagger}$/J·K^{-1}·mol^{-1}	$\Delta G^{\ddagger}$/kJ·mol^{-1} [b]
CD_3CN	35.9	43.4	–48.7	58.1
DMF-d_7	36.7	59.5	–5.6	61.1
CD_2Cl_2	8.93	53.9	–33.8	64.1
toluene-d_8	2.38	51.9	–39.0	63.7
toluene-d_8[c]	2.38	47.1	–26.6	55.1

[a]Ref. 59. [b]Calculated from the formula $\Delta G^{\ddagger} = \Delta H^{\ddagger} - T\Delta S^{\ddagger}$ at 303 K. [c]**2-Mo**.

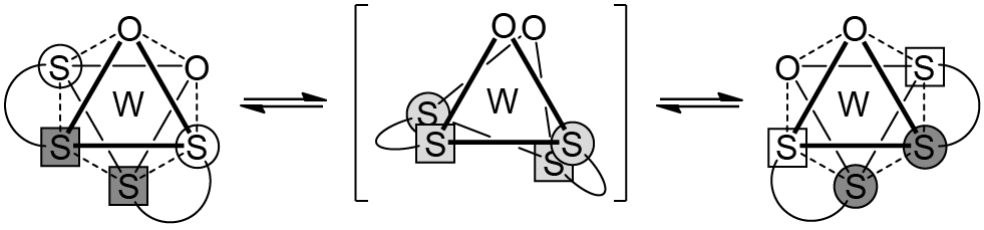

Figure 11. Proposal mechanism of the conformational change of **2-W** in solution. The square and the circle represent two different environments. The color of squares and circles (gray and white) corresponds to the assignment of ^{1}H NMR signals (red and green).

Electrochemical properties. The redox potentials of **1-M** in DMF are listed in Table 7 along with those of **3-M** with CH_3 substituents and **7-M** without hydrogen bonds. The cyclic voltammogram of **1-M** exhibits a reversible Mo(IV)/Mo(V) redox couple at $E_{1/2}$ = –0.20 V vs. SCE and W(IV)/W(V) at −0.40 V, respectively. The redox potentials of **1-M** are 0.15 V and 0.23 V more positive than those of the corresponding **7-M**, which lacks NH···S hydrogen bonds. This is a common tendency for the molybdenum(IV) and tungsten(IV) complexes with NH···S hydrogen bonds. The redox potential of **1-M** is less positive than that of **3-M**, which has methyl groups. As described in the section "IR and Raman spectra", the evaluation of the strength of the NH···S hydrogen bond in **1-M** is difficult because of the significant contribution of the NH···π hydrogen bond. The less positive shift is explained by two reasons. One is that the NH···π hydrogen bond weakened the NH···S hydrogen bond of **1-M**, even though the total contribution of the NH···S and NH···π hydrogen bonds was larger than that of **3-M**. The other is the hydrophobic microenvironment formed by the bulky ligands reported in experimental[60,61] and theoretical[62] examinations on iron–sulfur proteins.

Table 7. Redox Potentials of Monooxo-Molybdenum(IV) and Tungsten(IV) Complexes

	Mo		W	
	$E_{1/2}$	$\Delta E_{1/2}$[a]	$E_{1/2}$	$\Delta E_{1/2}$[a]
1-M	–0.20	+0.15	–0.40	+0.23
3-M[b]	–0.13	+0.22	–0.34	+0.29
7-M[c]	–0.35	—	–0.63	—

[a]Differences from the value of $(Et_4N)_2[M^{IV}O(1,2\text{-}S_2C_6H_4)_2]$ (**7-M**). [b]Refs. 23,24. [c]Refs. 51,53.

Complex **2-W** exhibits a pseudo-reversible W(VI)/W(V) redox couple at $E_{1/2}$ = –0.86 V vs. SCE (Figure 12). As shown in previous reports, the redox couples of the dioxotungsten(VI) complexes with unsubstituted benzene-1,2-dithiolate ligands (**8-W**) and with 3,6-bis(acetylamino)benzene-1,2-dithiolate ligands (**4-W**) were irreversible because of the instability of the one electron reduced $W^{V}O_2$ species.[24,52,53] The electron-rich $W^{V}O_2$ species is thought to degrade via O-atom releasing reactions.[53,55,63] Improved reversibility was observed for $(Et_4N)_2[W^{VI}O_2\{1,2\text{-}S_2\text{-}3,6\text{-}(^t\text{BuCONH})_2C_6H_2\}_2]$, which contains relatively bulky ^{t}Bu

groups. The explanation for this was that the ^{t}Bu groups prevented intermolecular reactions.[24] In the case of **2-W** with bulky hydrophobic CAr_3 groups, the reversibility was improved (i_{pa}/i_{pc} = 0.81) but quantitative evaluation of the reversibility was difficult because of the successive irreversible redox process. The i_{pa}/i_{pc} value is the highest of the *cis*-dioxotetrathiolato-tungsten(VI) complexes ($[W^{VI}O_2(SR)_4]^{2-}$) previously reported.[24,52,53,55,64] The reduction potential (E_p = –0.92 V) of **2-W** is positively shifted compared to −1.26 V of **8-W**, which lacks NH···S hydrogen bonds, and is negatively shifted compared to −0.82 V of **4-W** with CH_3 groups, and this is thought to be the effect of NH···S and NH···π hydrogen bonds and/or the hydrophobic microenvironment described for **1-M**. Unfortunately, **2-Mo** did not give well-defined Mo(VI)/Mo(V) redox couple although **2-Mo** is significantly stable compared to **4-Mo**.

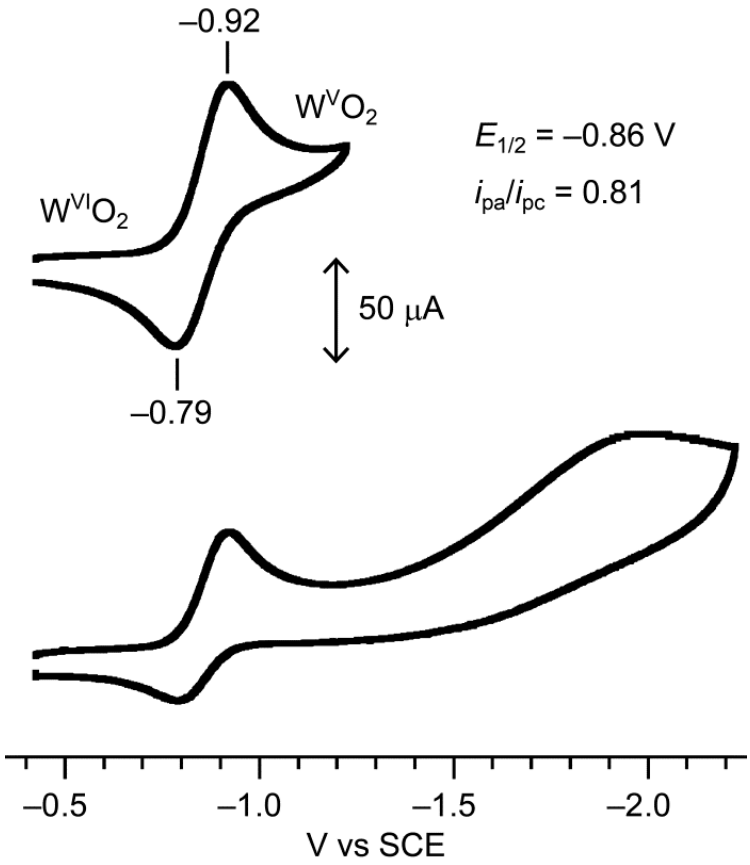

Figure 12. Cyclic voltammogram of **2-W** in DMF scanning from –0.4 to –1.4 V (upper) and from –0.4 to –2.2 V (lower).

Absorption spectra and reactivity. The UV-vis spectra of **1-Mo** and **2-Mo** in DMF are shown in Figure 13. The spectrum of **1-Mo** shows absorption bands at 348, 412, and 452 nm and is similar to **5-Mo** with CPh_3 groups (348, 406, and 457 nm).[23] The spectrum of **2-Mo** shows absorption bands at 364, 398, and 531 nm, and the lowest transition energy assigned to the LMCT band (531 nm) was equal to that of **6-Mo**.[23] Upon addition of 2 eq. of Me_3NO to **1-Mo**, a rapid oxygen-atom-transfer reaction proceeded to afford **2-Mo**. The reaction was monitored by examining the absorption maximum of **2-Mo** at 531 nm in DMF. The second-order rate constant of **1-Mo** in DMF ($k_2 = 27 \pm 12$ M^{-1} s^{-1}) was comparable to the estimated k_2 ($k_{obs}/[\mathbf{5\text{-}Mo}]_0 = 26 \pm 0.1$ M^{-1} s^{-1}) of **5-Mo** from the reported pseudo-first-order rate constant, k_{obs},[23] which indicates that the reaction proceeds via *cis*-attack of Me_3NO, as well as **5-Mo**.[23,26] In the case of **1-W**, the OAT reaction is too fast to evaluate the exact rate constant using the author's instruments, but at least approximately three times faster than **1-Mo**. This result indicates a similar tendency to previous studies.[24]

Surprisingly, in the nonpolar solvent (toluene) the reduction of Me_3NO proceeded about ten times faster than in DMF. In a medium polarity solvent, THF, the complex exhibited moderate reactivity (Figure 14). The calculated k_2 values under these conditions are listed in Table 8 with the dielectric constant of the solvents, ε_r.[59] The results indicate that the substrate can easily approach the active center and efficiently interact with the complex in the hydrophobic environment, which supports attracting interactions between polar molecules.

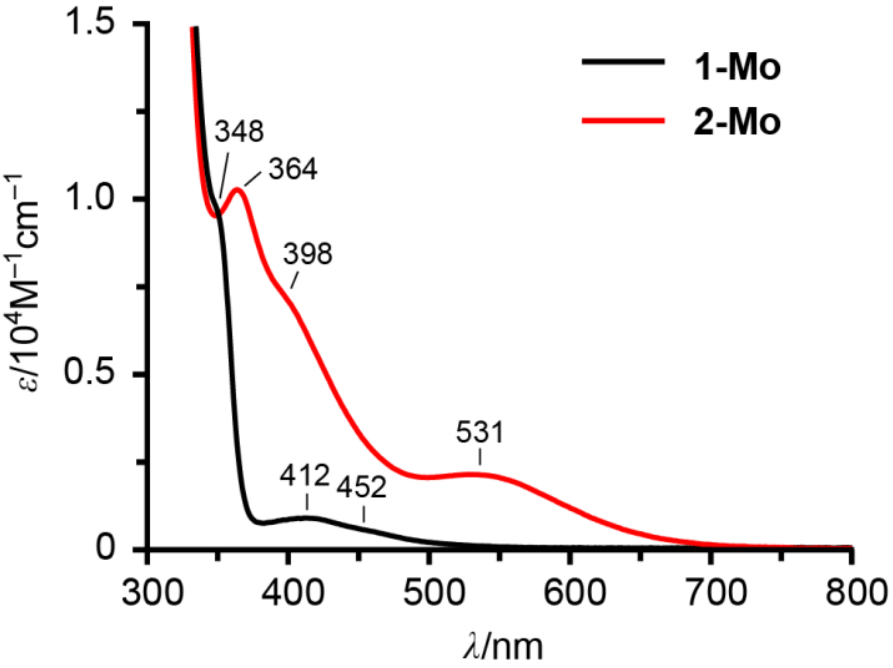

Figure 13. UV-vis spectra of **1-Mo** (black) and **2-Mo** (red) in DMF.

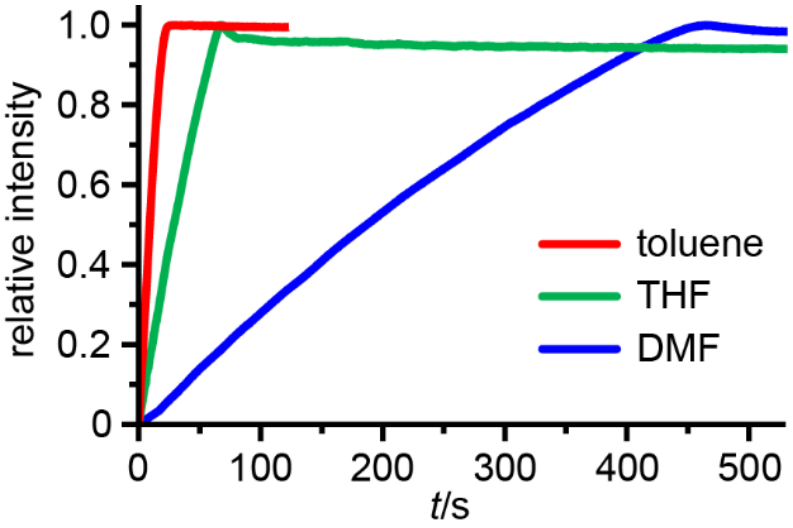

Figure 14. Time course of relative intensity of the absorption maximum of **2-Mo** in toluene (red), THF (green), and DMF (blue).

Table 8. Kinetic Parameters of the Reaction of **1-Mo** with Me_3NO in Various Solvents

solvent	ε_r[a]	$k_2/M^{-1}\cdot s^{-1}$
DMF	36.7	26.6 ± 12.2
THF	7.58	106 ± 10
toluene	2.38	384 ± 51

[a]Ref. 59.

Discussion

The molybdenum(IV, VI) and tungsten(IV, VI) complexes with NH···S hydrogen bonded hydrophobic benzene-1,2-dithiolate ligands are soluble in nonpolar solvents like toluene. The solubility allows a precise discussion about the solution structure and reactivity in various solvents. Here, the author discusses the weak interactions in a hydrophobic environment and the effect of the triarylmethyl groups, in conjunction with their relevance to the nature of the molybdoenzyme.

Weak interactions in a hydrophobic environment. The **1-M** complexes with hydrophobic substituents are soluble in nonpolar solvents like toluene, allowing the observation of weak interionic interactions. Both of the solid state structures of **1-Mo** with different crystal solvents show interionic CH···O=Mo interactions, even though the configuration of four bulky CAr_3 groups is different. Generally such interactions cannot be observed in polar solvents because each ion is completely solvated. However, the ^{1}H NMR spectra in toluene-d_8 clearly showed the nonequivalent Et_4N^+ cations and proximity of the cation to the terminal oxo ligand.

The results correspond with the *cis*-attack of Me_3NO on the $Mo^{IV}O$ moiety in the reported mechanism.[23,36] In the attack of polar Me_3NO, the positively charged Me_3N moiety tended to be drawn by the basic terminal oxo ligand based on theoretical calculations.[26] Such interactions should be stabilized in nonpolar solvents and result in the acceleration of the reduction of Me_3NO, which is consistent with the experimental results for the reactivity of **1-Mo**.

A hydrophobic environment around the active site is a key factor for the activity of the enzymes involving substrate uptake and stabilization of transition states. In the latter case, Warshel proposed that enzymes can be considered as “supersolvents” that stabilize (solvate) ionic transition states by using noncovalent interactions more effectively than do aqueous

solutions.[65] Experimentally, the artificial enzyme with a hydrophobic chain showed much large k_{cat} for catalytic transamination of pyruvic acid.[66]

On the basis of the X-ray structure of DMSOR, the presence of hydrogen bonds from the amino acid residues to the coordinated atoms at the base of the substrate access funnel has been proposed.[6,9,67-69] The mutation study revealed that an OH···O–Mo hydrogen bond between tyrosine 114 and the oxygen atom of the coordinated DMSO increases the affinity of the substrate for the metal center and the rate of the catalytic reaction.[68] Tryptophan 116 is thought to form an NH···O=Mo hydrogen bond between the oxo ligand of the oxidized enzyme, which stabilizes the coordination of the dithiolene ligand and accelerates the reduction process.[70] However, it is very difficult to observe the weak interactions around the active site in solution. The model study with hydrophobic substituents allows observation of noncovalent interactions in solution and investigation of the effect of the hydrophobicity of the surrounding environment by altering the polarity of the solvents.

The effect of the triarylmethyl groups. The CAr_3 groups make the complexes stable and restrict undesirable intermolecular reactions by maintaining interionic and intramolecular weak interactions. With respect to the stability of the complexes, the dioxomolybdenum(VI) complex, **2-Mo**, is much more stable than **4-Mo** with CH_3 groups. The stabilization is attributed to the bulkiness of the ligand and the intra-ligand NH···π hydrogen bond, which stabilizes the Mo–S bond. In cyclic voltammetry of **2-W**, the improved reversibility indicates the stabilization of the one electron reduced $W^{V}O_2$ species. The bulky dithiolate ligand can restrict the intermolecular side reactions.

Concerning weak interactions described in the previous section, the Et_4N^+ counterion was found close to the terminal oxo ligand of **1-M** in both the solid and solution states, and efficient uptake of Me_3NO is observed. There is a confined space around the active center that interacts with counterions or neutral small molecules. In addition, the ^{1}H NMR spectrum of **2-W**

indicates that the unsymmetrical geometry remains in the hydrophobic environment even at room temperature.

In DMSOR, the huge protein is thought to stabilize the coordination of the dithiolene ligand and restrict undesirable intermolecular reactions, while the large depression enables efficient transport of the substrate to the active site. In order to understand the weak interactions and realize the catalytic activity in model systems, the inclusive design of an enzyme model is required. When the outer hydrophilic sphere of the enzyme is removed, the simplest model should contain limited space for electrostatic interactions surrounded by the hydrophobic sphere with a narrow gateway for substrate uptake. The present complexes satisfy these requirements and allow investigation of weak interactions in the hydrophobic environment.

Conclusions

Monooxomolybdenum(IV), monooxotungsten(IV), dioxomolybdenum(VI), and dioxotungsten(VI) complexes (**1-M**, **2-M**; M = Mo, W) with bulky hydrophobic dithiolate ligands and NH···S hydrogen bonds are soluble in nonpolar solvents like toluene. The thermodynamic stability of **2-M** with a *cis*-dioxo octahedral geometry is effectively enhanced by the bulkiness of the dithiolate ligands, intra-ligand bifurcated NH···S and NH···π hydrogen bonds, and the hydrophobicity of the media. The polar Me_3NO can effectively approach the active center in hydrophobic surroundings, resulting in faster oxygen-atom-transfer reaction. These results indicate that a steady structure in hydrophobic media allows observation of the unsymmetrical coordination structure and noncovalent interactions in solution. This concept of reconstructing the active site with the hydrophobic surroundings will provide new insights for enzyme modeling.

Experimental

All procedures were performed under an argon atmosphere by the Schlenk technique. All solvents were dried and distilled under argon before use. Reagents were obtained commercially and used without further purification. (4-^{t}BuC$_6$H$_4$)$_3$CCOOH,[26] 3,6-(NH$_2$)$_2$C$_6$H$_2$-1,2-(SSO$_3$K)$_2$,[37] (Et$_4$N)[Mo^{V}O(SPh)$_4$],[38] and (Et$_4$N)[W^{V}O(SPh)$_4$][39] were prepared by reported methods.

(4-^{t}BuC$_6$H$_4$)$_3$CCOCl. A suspension of (4-^{t}BuC$_6$H$_4$)$_3$CCOOH (8.88 g, 19.5 mmol) in SOCl$_2$ (60 mL, 0.84 mol) was refluxed for 1.5 h to afford a yellow solution. After removal of volatile materials, the white residue was suspended in CH$_2$Cl$_2$ and concentrated to dryness under reduced pressure. This procedure was repeated for several times to remove completely the residual SOCl$_2$. The resulting white powder was recrystallized from CH$_2$Cl$_2$/*n*-hexane to afford colorless blocks. Yield: 9.29 g, quant. Mp: 235 °C. Anal. Calcd for C$_{32}$H$_{39}$ClO: C, 80.90; H, 8.27; Cl, 7.46. Found: C, 80.69; H, 8.23; Cl, 7.58.‡ ^{1}H NMR (CDCl$_3$): δ 7.32 (d, J = 8.9 Hz, 6H, Ar), 7.25 (d, J = 8.9 Hz, 6H, Ar), 1.31 (s, 27H, ^{t}Bu). IR (KBr): 1795, 1768 ($\nu_{C=O}$) cm^{-1}.

‡The chlorine (Cl) content in (4-^{t}BuC$_6$H$_4$)$_3$CCOCl was analyzed by the silver absorption method with an elemental analyzer (Yanaco New Science Inc.).

(4-^{t}BuC$_6$H$_4$)$_3$CCONHPh. A solution of (4-^{t}BuC$_6$H$_4$)$_3$CCOCl (136 mg, 285 μmol) in CH$_2$Cl$_2$ (4 mL) was added to a mixture of aniline (27.7 mg, 297 μmol) and Et$_3$N (29.8 mg, 294 mmol) in CH$_2$Cl$_2$ (3 mL) at 0 °C, and the reaction mixture was stirred at 0 °C for 17 h to afford a colorless solution. After removal of volatile materials, the resulting white residue was extracted with AcOEt and washed successively with water, sat. NaCl aq., 2% HCl aq., sat. NaCl aq., 4% NaHCO$_3$ aq., and sat. NaCl aq. The organic layer was dried over Na$_2$SO$_4$, filtered, and concentrated to dryness to afford colorless solid. Recrystallization from AcOEt/*n*-hexane gave colorless needles. Yield: 285 mg, quant. Mp: 241 °C (dec.). Anal. Calcd for C$_{38}$H$_{45}$NO: C,

85.83; H, 8.53; N, 2.63. Found: C, 85.72; H, 8.54; N, 2.62. ^{1}H NMR ($CDCl_3$): δ 7.49 (s, 1H, NH), 7.42 (d, *J* = 7.9 Hz, 2H, Ph), 7.32 (d, *J* = 8.7 Hz, 6H, Ar), 7.28 (t, *J* = 7.9 Hz, 2H, Ph), 7.22 (d, *J* = 8.7 Hz, 6H, Ar), 7.08 (t, *J* = 7.9 Hz, 1H, Ph), 1.31 (s, 27H, ^{t}Bu). IR (10 mM in CH_2Cl_2): 3403 (ν_{NH}), 1683 ($\nu_{C=O}$) cm^{-1}.

(^{n}Bu$_4$N)$_2$[3,6-(NH$_2$)$_2$C$_6$H$_2$-1,2-(SSO$_3$)$_2$]. To a mixture of 3,6-$(NH_2)_2C_6H_2$-1,2-$(SSO_3K)_2$ (6.04 g, 14.8 mmol) and ^{n}Bu$_4$NCl (8.24 g, 29.7 mmol) were added water (~30 mL) and CH_2Cl_2 (~20 mL). The organic layer was separated, and then the remnant product was extracted from aqueous layer with CH_2Cl_2 (50 mL and 2 × 10 mL). The combined organic layer was washed with water (3 × 5 mL), dried over Na_2SO_4, and concentrated to dryness under reduced pressure. The green residue was recrystallized from acetone/THF to afford greenish yellow blocks. Yield: 9.19 g, 76%. Mp: 148 °C (dec.). Anal. Calcd for $C_{38}H_{78}N_4O_6S_4 \cdot H_2O$: C, 54.77; H, 9.68; N, 6.72. Found: C, 54.98; H, 9.46; N, 6.77. ^{1}H NMR ($CDCl_3$): δ 6.58 (s, 2H, 4,5-H), 4.50 (br, 4H, NH_2), 3.13 (m, 16H, ^{n}Bu$_4$N$^+$), 1.59 (m, 16H, ^{n}Bu$_4$N$^+$), 1.43 (m, 16H, ^{n}Bu$_4$N$^+$), 0.98 (t, *J* = 7.3 Hz, 24 H, ^{n}Bu$_4$N$^+$). IR (KBr): 3436, 3338 (ν_{NH}), 1017 (ν_{SO}) cm^{-1}.

(^{n}Bu$_4$N)$_2$[3,6-{(4-^{t}BuC$_6$H$_4$)$_3$CCONH}$_2$C$_6$H$_2$-1,2-(SSO$_3$)$_2$]. A solution of (4-^{t}BuC$_6$H$_4$)$_3$CCOCl (4.95 g, 10.4 mmol) in CH_2Cl_2 (37 mL) was added to a mixture of (^{n}Bu$_4$N)$_2$[3,6-$(NH_2)_2C_6H_2$-1,2-$(SSO_3)_2$] (4.08 g, 5.01 mmol) and Et_3N (2.8 mL, 20 mmol) in CH_2Cl_2 (10 mL) at 0 °C, and the reaction mixture was stirred at 0 °C for 15 h to afford a yellow solution. After removal of volatile materials, the yellow residue was washed with water and AcOEt, and then dried under reduced pressure to afford white powder. Recrystallization from hot AcOEt gave colorless blocks. Yield: 8.15 g, 96%. Mp: 251 °C (dec.). Anal. Calcd for $C_{102}H_{154}N_4O_8S_4 \cdot H_2O$: C, 71.62; H, 9.19; N, 3.28. Found: C, 71.52; H, 9.14; N, 3.32. ^{1}H NMR ($CDCl_3$): δ 9.71 (s, 2H, NH), 8.18 (s, 2H, 4,5-H), 7.28 (d, *J* = 9.0 Hz, 12H, Ar), 7.25 (d, *J* = 9.0 Hz, 12H, Ar), 3.04 (m, 16H, ^{n}Bu$_4$N$^+$), 1.51 (m, 16H, ^{n}Bu$_4$N$^+$), 1.30 (m, 16H, ^{n}Bu$_4$N$^+$), 1.30 (s,

54H, ^{t}Bu), 0.87 (t, J = 7.3 Hz, 24H, ^{n}Bu$_4$N$^+$). IR (KBr): 3298 (ν_{NH}), 1669 ($\nu_{C=O}$), 1018 (ν_{SO}) cm^{-1}.

1,2-S$_3$-3,6-{(4-^{t}BuC$_6$H$_4$)$_3$CCONH}$_2$C$_6$H$_2$ (L1). This compound was synthesized by a modified method reported in the literature.[40] A suspension of (^{n}Bu$_4$N)$_2$[3,6-{(4-^{t}BuC$_6$H$_4$)$_3$CCONH}$_2$C$_6$H$_2$-1,2-(SSO$_3$)$_2$] (1.51 g, 889 μmol) and (NH$_2$)$_2$CS (129 mg, 1.69 mmol) in AcOH (15 mL) was heated at 100 °C to afford a light yellow solution, and the reaction mixture was stirred for 5 h. The resulting light yellow powder was filtered off, washed with MeOH, and recrystallized from CH$_2$Cl$_2$/MeOH to afford yellow blocks. Yield: 539 mg, 56%. Mp: >300 °C. Anal. Calcd for C$_{70}$H$_{82}$N$_2$O$_2$S$_3$: C, 77.88; H, 7.66; N, 2.59. Found: C, 77.68; H, 7.65; N, 2.87. ^{1}H NMR (CDCl$_3$): δ 7.62 (s, 2H, NH), 7.42 (s, 2H, 4,5-H), 7.32 (d, J = 8.6 Hz, 12H, Ar), 7.20 (d, J = 8.6 Hz, 12H, Ar), 1.30 (s, 54H, ^{t}Bu). IR (KBr): 3358 (ν_{NH}), 1696 ($\nu_{C=O}$) cm^{-1}.

(Et$_4$N)$_2$[Mo^{IV}O(1,2-S$_2$-3,6-{(4-^{t}BuC$_6$H$_4$)$_3$CCONH}$_2$C$_6$H$_2$)$_2$] (1-Mo). A suspension of **L1** (237 mg, 219 μmol) and Et$_4$NBH$_4$ (85 mg, 586 μmol) in a mixture of acetonitrile (5 mL) and water (0.5 mL) was heated at 70 °C for 0.5 h to afford a greenish-yellow solution and a colorless precipitate. After adding acetonitrile (19 mL) to dissolve the precipitate, a solution of (Et$_4$N)[Mo^{V}O(SPh)$_4$] (38.0 mg, 56.0 μmol) in acetonitrile (3 mL) was added dropwise to afford an orange suspension. The reaction mixture was stirred for 72 h at 30 °C to afford a yellow solution and a yellowish-white precipitate. The supernatant was removed, and the precipitate was washed several times with acetonitrile by centrifugation. The product was extracted with toluene and recrystallized from toluene/acetonitrile to afford yellow blocks. Yield: 66.0 mg, 48%. ^{1}H NMR (toluene-d_8): δ 8.95 (s, 4H, NH), 8.18 (s, 4H, 4,5-H), 7.70 (d, J = 8.4 Hz, 24H, Ar), 7.37 (d, J = 8.4 Hz, 24H, Ar), 1.88 (br, 16H, Et$_4$N$^+$), 1.31 (s, 108H, ^{t}Bu), 0.37 (br, 24H, Et$_4$N$^+$). ^{1}H NMR (DMF-d_7): δ 9.10 (s, 4H, NH), 8.02 (s, 4H, 4,5-H), 7.43 (d, J = 8.7 Hz, 24H, Ar), 7.38 (d, J = 8.7 Hz, 24H, Ar), 3.21 (q, J = 7.3 Hz, 16H, Et$_4$N$^+$), 1.26 (s, 108H, ^{t}Bu), 1.17

(tt, $J_{H–H}$ = 7.3 Hz, $J_{H–N}$ = 1.6 Hz, 24H, Et_4N^+). ESI-MS (CH_3CN) calcd for $[Mo^{IV}O(1,2\text{-}S_2\text{-}3,6\text{-}\{(4\text{-}^t BuC_6H_4)_3CCONH\}_2C_6H_2)_2]^{2-}$: m/z 1103.8. Found: 1103.5. Absorption spectrum (DMF): λ_{max} (ε, M^{-1} cm^{-1}) 348 (sh) (10000), 412 (920), 452 (sh) (590) nm. Absorption spectrum (toluene): λ_{max} (ε, M^{-1} cm^{-1}) 337 (sh) (11000), 395 (1000), 455 (sh) (550) nm. Anal. Calcd for $C_{156}H_{204}N_6O_5S_4Mo$: C, 75.93; H, 8.33; N, 3.41. Found: C, 74.91; H, 8.35; N, 3.43.

The disagreement with elemental analysis results for molybdenum and tungsten complexes is probably caused by their nanoporous structure in the solid state. After removal of the solvent molecules from the crystals, the resulting voids might be able to trap gaseous water molecules. Formal addition of water to the chemical formula improved the results. The calculated values for $C_{156}H_{204}N_6O_5S_4Mo\cdot(H_2O)_{1.8}$: C, 74.95; H, 8.37; N, 3.36, which agree with the found ones. The water molecules were also detected in ^{1}H NMR spectra, but the amount of water depended on the reaction conditions. Similar results were also found for **1-W**, **2-Mo**, and **2-W**.

$(Et_4N)_2[W^{IV}O(1,2\text{-}S_2\text{-}3,6\text{-}\{(4\text{-}^t BuC_6H_4)_3CCONH\}_2C_6H_2)_2]$ (1-W). A suspension of **L1** (1.01 g, 0.936 mmol) and Et_4NBH_4 (1.42 g, 9.81 mmol) in a mixture of acetonitrile (53 mL) and water (2 mL) was refluxed at 70 °C for 3 h to afford a greenish-yellow solution and a colorless precipitate. The supernatant was separated, and a solution of $(Et_4N)[W^VO(SPh)_4]$ (288 mg, 0.375 mmol) in acetonitrile (25 mL) was added dropwise to the solution to afford a yellowish-white precipitate. The reaction mixture was stirred for 15 h at room temperature to afford a yellow suspension. The supernatant was removed, and the precipitate was washed several times with acetonitrile using centrifugation. The product was extracted with toluene and concentrated to dryness to afford a yellow powder. The crude product was recrystallized from toluene/acetonitrile to afford yellowish-orange blocks. Yield: 252 mg, 28%. ^{1}H NMR (toluene-d_8): δ 8.94 (s, 4H, NH), 8.20 (s, 4H, 4,5-H), 7.69 (d, J = 8.5 Hz, 24H, Ar), 7.37 (d, J = 8.5 Hz, 24H, Ar), 1.86 (br, 16H, Et_4N^+), 1.31 (s, 108H, ^{t}Bu), 0.35 (br, 24H, Et_4N^+). ^{1}H NMR (DMF-d_7): δ 9.11 (s, 4H, NH), 8.01 (s, 4H, 4,5-H), 7.44 (d, J = 8.7 Hz, 24H, Ar), 7.39 (d, J = 8.7 Hz,

24H, Ar), 3.34 (q, J = 7.3 Hz, 16H, Et_4N^+), 1.26 (s, 108H, ^{t}Bu), 1.26 (tt, $J_{H–H}$ = 7.3 Hz, $J_{H–N}$ = 1.8 Hz, 24H, Et_4N^+). Absorption spectrum (toluene): λ_{max} (ε, M^{-1} cm^{-1}) 342 (sh) (9100), 425 (sh) (1300) nm. Anal. Calcd for $C_{156}H_{204}N_6O_5S_4W \cdot CH_3CN \cdot (H_2O)_{1.6}$: C, 72.28; H, 8.07; N, 3.73. Found: C, 72.27; H, 7.95; N, 3.93.

$(Et_4N)_2[Mo^{VI}O_2(1,2\text{-}S_2\text{-}3,6\text{-}\{(4\text{-}^tBuC_6H_4)_3CCONH\}_2C_6H_2)_2]$ (2-Mo). A solution of Me_3NO (0.42 mg, 5.6 μmol) in DMF (0.2 mL) was added to a solution of **1-Mo** (6.8 mg, 2.8 μmol) in DMF (1.2 mL). The solution immediately turned reddish-purple. After removal of the solvent under reduced pressure, the reddish-purple residue was extracted with toluene. The solution was concentrated to dryness under reduced pressure, and the resulting reddish-purple solid was recrystallized from acetonitrile to afford dark brown blocks. Yield: 4.0 mg, 58%. ^{1}H NMR (CD_3CN): δ 8.49 (s, 4H, NH), 7.73 (s, 4H, 4,5-H), 7.33 (d, J = 8.7 Hz, 24H, Ar), 7.23 (d, J = 8.7 Hz, 24H, Ar), 3.04 (q, J = 7.3 Hz, 16H, Et_4N^+), 1.24 (s, 108H, ^{t}Bu), 1.12 (tt, $J_{H–H}$ = 7.3 Hz, $J_{H–N}$ = 1.9 Hz, 24H, Et_4N^+). ESI-MS (CH_3CN, $M^{2–}$ = $[Mo^{VI}O_2(1,2\text{-}S_2\text{-}3,6\text{-}\{(4\text{-}^tBuC_6H_4)_3CCONH\}_2C_6H_2)_2]^{2–}$) calcd for $M^{2–}$: m/z 1111.2. Found: 1111.5. Absorption spectrum (DMF): λ_{max} (ε, M^{-1} cm^{-1}) 364 (10000), 398 (sh) (7500), 531 (2100) nm. Absorption spectrum (toluene): λ_{max} (ε, M^{-1} cm^{-1}) 357 (12000), 392 (sh) (7800), 548 (2300) nm. Anal. Calcd for $C_{156}H_{204}N_6O_6S_4Mo \cdot (H_2O)_3$: C, 73.84; H, 8.34; N, 3.31. Found: C, 73.82; H, 8.15; N, 3.32.

$(Et_4N)_2[W^{VI}O_2(1,2\text{-}S_2\text{-}3,6\text{-}\{(4\text{-}^tBuC_6H_4)_3CCONH\}_2C_6H_2)_2]$ (2-W). To a mixture of **1-W** (131.7 mg, 51.5 μmol) and Me_3NO (8.74 mg, 116 μmol) was added DMF (5 mL), and the mixture was stirred for 2 h to afford a reddish-orange solution. After removal of the solvent under reduced pressure, the reddish-orange residue was extracted with toluene. The solution was concentrated to dryness under reduced pressure, and the resulting reddish-orange solid was recrystallized from acetonitrile to afford reddish-orange blocks. Yield: 100.7 mg, 76%. ^{1}H NMR (CD_3CN): δ 8.44 (br, 4H, NH), 7.73 (s, 4H, 4,5-H), 7.34 (d, J = 8.2 Hz, 24H, Ar), 7.23 (d, J = 8.2 Hz, 24H, Ar), 3.10 (q, J = 7.2 Hz, 16H, Et_4N^+), 1.24 (br, 108H, ^{t}Bu), 1.16 (tt, $J_{H–H}$ = 7.2 Hz,

J_{H-N} = 1.9 Hz, 24H, Et_4N^+). ESI-MS (CH_3CN, M^{2-} = $[W^{VI}O_2(1,2\text{-}S_2\text{-}3,6\text{-}\{(4\text{-}{}^tBuC_6H_4)_3CCONH\}_2C_6H_2)_2]^{2-}$) calcd for M^{2-}: m/z 1155.1. Found: 1155.7. IR (Nujol): 3316 (ν_{NH}), 1671 ($\nu_{C=O}$) cm^{-1}. Absorption spectrum (toluene): λ_{max} (ε, M^{-1} cm^{-1}) 360 (sh) (9200), 436 (2100), 495 (840) nm. Anal. Calcd for $C_{156}H_{204}N_6O_6S_4W\cdot H_2O$: C, 72.36; H, 8.02; N, 3.25. Found: C, 72.34; H, 7.93; N, 3.36.

Physical measurements. The elemental analyses were performed on a Yanaco CHN CORDER MT-5. ^1H NMR spectra were obtained with JEOL ECA-500, GSX-400, and ECS-400 spectrometers in chloroform-*d*, dichloromethane-d_2, acetonitrile-d_3, *N*,*N*-dimethylformamide-d_7, or toluene-d_8 at 30 °C. Totally correlated spectroscopy (TOCSY) and rotating frame Overhauser enhancement (ROE) and exchange spectroscopy (ROESY) spectra were recorded on a VARIAN VNS-600 spectrometer in toluene-d_8 at –45 °C with a mixing time of 500 ms. Electrospray ionization mass spectroscopy (ESI-MS) measurements were performed on a Finnigan MAT LCQ ion trap mass spectrometer using an acetonitrile solution. UV-visible absorption spectra were recorded using a SHIMADZU UV-3100PC spectrometer. Infrared (IR) spectroscopic measurements were done on a Jasco FT/IR-4000 spectrometer. Raman spectra were measured on a Jasco NR-1800 spectrophotometer with a liq. N_2 cooled CCD detector. Exciting radiation was provided by an Ar^+ ion laser (514.5 nm). The measurements of cyclic voltammograms (CVs) in a DMF solution were carried out on a BAS 100B/W instrument with a three-electrode system: a glassy carbon working electrode, a Pt-wire auxiliary electrode, and a saturated calomel electrode (SCE). The scan rate was 100 mV s^{-1}. The concentration of the sample was 2.5 mM, containing 0.1 M of ${}^nBu_4NClO_4$ as a supporting electrolyte. The result was cross-referenced using the ferrocene/ferrocenium couple as a calibrant. The redox potential of ferrocene/ferrocenium was observed at +0.48 V vs. SCE under the same conditions.

Structural determination. Each single crystal of **L1**·3.1$CH_3OH\cdot H_2O$, **1-Mo**·8(toluene), **1-Mo**·toluene·5CH_3CN, **1-W**·4(toluene)·3$CH_3CN\cdot H_2O$, **2-Mo**·5CH_3CN and **2-W**·5CH_3CN

was selected carefully and mounted on MicroMount™ 200 μm with Nujol, which was frozen immediately in a stream of cold nitrogen at 200 K. Data collection was made on a Rigaku RAPID II Imaging Plate area detector with Mo-Kα radiation (0.71075 Å) using MicroMax-007HF microfocus rotating anode X-ray generator and VariMax-Mo optics. The structures were solved by direct methods (SIR2008[41] for **L1**·3.1CH_3OH·H_2O, SHELX-97[42] for **1-Mo**·8(toluene), **2-Mo**·5CH_3CN and **2-W**·5CH_3CN, and SIR97[43] for **1-Mo**·toluene·5CH_3CN, **1-W**·4(toluene)·3CH_3CN·H_2O) and expanded Fourier techniques using SHELXL-2014/6.[42]

Kinetic measurements. A reaction system containing **1-Mo** and Me_3NO was monitored spectrophotometrically in the range 280–800 nm. The measurements were carried out in a 1 cm UV cell containing a solution of **1-Mo** (0.1 mM, 3.0 mL) at 27 °C (solvents: DMF, THF, toluene). After thermal equilibrium, a Me_3NO solution (60 mM, 10 μL) in DMF was injected through a silicone rubber cap, and the cell contents were quickly mixed by shaking. The time course of the reaction was monitored using the absorption maximum of **2-Mo**. All calculations for the data analysis were performed at 531, 537, and 548 nm in DMF, THF, and toluene, respectively.

References

(1) Hille, R.; Hall, J.; Basu, P. *Chem. Rev.* **2014**, *114*, 3963-4038.

(2) Hille, R. *Chem. Rev.* **1996**, *96*, 2757-2816.

(3) Hille, R.; Nishino, T.; Bittner, F. *Coord. Chem. Rev.* **2011**, *255*, 1179-1205.

(4) Pushie, M. J.; George, G. N. *Coord. Chem. Rev.* **2011**, *255*, 1055-1084.

(5) Magalon, A.; Fedor, J. G.; Walburger, A.; Weiner, J. H. *Coord. Chem. Rev.* **2011**, *255*, 1159-1178.

(6) Dobbek, H. *Coord. Chem. Rev.* **2011**, *255*, 1104-1116.

(7) Johnson, M. K.; Rees, D. C.; Adams, M. W. W. *Chem. Rev.* **1996**, *96*, 2817-2840.

(8) Grimaldi, S.; Schoepp-Cothenet, B.; Ceccaldi, P.; Guigliarelli, B.; Magalon, A. *Biochim. Biophys. Acta* **2013**, *1827*, 1048-1085.

(9) Schindelin, H.; Kisker, C.; Hilton, J.; Rajagopalan, K. V.; Rees, D. C. *Science* **1996**, *272*, 1615-1621.

(10) Smith, D. K.; Diederich, F. *Chem. Eur. J.* **1998**, *4*, 1353-1361.

(11) Gorman, C. B.; Smith, J. C. *Acc. Chem. Res.* **2001**, *34*, 60-71.

(12) Vögtle, F.; Gestermann, S.; Hesse, R.; Schwierz, H.; Windisch, B. *Prog. Polym. Sci.* **2000**, *25*, 987-1041.

(13) Cardona, C. M.; Mendoza, S.; Kaifer, A. E. *Chem. Soc. Rev.* **2000**, *29*, 37-42.

(14) Basu, P.; Nemykin, V. N.; Sengar, R. S. *Inorg. Chem.* **2003**, *42*, 7489-7501.

(15) McNaughton, R. L.; Mondal, S.; Nemykin, V. N.; Basu, P.; Kirk, M. L. *Inorg. Chem.* **2005**, *44*, 8216-8222.

(16) Ueyama, N.; Terakawa, T.; Nakata, M.; Nakamura, A. *J. Am. Chem. Soc.* **1983**, *105*, 7098-7102.

(17) Okamura, T.; Takamizawa, S.; Ueyama, N.; Nakamura, A. *Inorg. Chem.* **1998**, *37*, 18-28.

(18) Ueyama, N.; Okamura, T.; Nakamura, A. *J. Chem. Soc., Chem. Commun.* **1992**, 1019-1020.

(19) Ueyama, N.; Yamada, Y.; Okamura, T.; Kimura, S.; Nakamura, A. *Inorg. Chem.* **1996**, *35*, 6473-6484.

(20) Ueyama, N.; Nishikawa, N.; Yamada, Y.; Okamura, T.; Nakamura, A. *J. Am. Chem. Soc.* **1996**, *118*, 12826-12827.

(21) Ueyama, N.; Nishikawa, N.; Yamada, Y.; Okamura, T.; Oka, S.; Sakurai, H.; Nakamura, A. *Inorg. Chem.* **1998**, *37*, 2415-2421.

(22) Okamura, T.; Ueyama, N.; Nakamura, A.; Ainscough, E. W.; Brodie, A. M.; Waters, J. M. *J. Chem. Soc., Chem. Commun.* **1993**, 1658-1660.

(23) Baba, K.; Okamura, T.; Suzuki, C.; Yamamoto, H.; Yamamoto, T.; Ohama, M.; Ueyama, N. *Inorg. Chem.* **2006**, *45*, 894-901.

(24) Baba, K.; Okamura, T.; Yamamoto, H.; Yamamoto, T.; Ohama, M.; Ueyama, N. *Inorg. Chem.* **2006**, *45*, 8365-8371.

(25) Okamura, T.; Tatsumi, M.; Omi, Y.; Yamamoto, H.; Onitsuka, K. *Inorg. Chem.* **2012**, *51*, 11688-11697.

(26) Okamura, T.; Ushijima, Y.; Omi, Y.; Onitsuka, K. *Inorg. Chem.* **2013**, *52*, 381-394.

(27) Okamura, T.; Kunisue, K.; Omi, Y.; Onitsuka, K. *Dalton Trans.* **2013**, *42*, 7569-7578.

(28) Holm, R. H.; Solomon, E. I.; Majumdar, A.; Tenderholt, A. *Coord. Chem. Rev.* **2011**, *255*, 993-1015.

(29) Hine, F. J.; Taylor, A. J.; Garner, C. D. *Coord. Chem. Rev.* **2010**, *254*, 1570-1579.

(30) Ng, V. W. L.; Taylor, M. K.; Young, C. G. *Inorg. Chem.* **2012**, *51*, 3202-3211.

(31) Basu, P.; Burgmayer, S. J. N. *Coord. Chem. Rev.* **2011**, *255*, 1016-1038.

(32) Sugimoto, H.; Tatemoto, S.; Suyama, K.; Miyake, H.; Mtei, R. P.; Itoh, S.; Kirk, M. L. *Inorg. Chem.* **2010**, *49*, 5368-5370.

(33) Majumdar, A.; Sarkar, S. *Coord. Chem. Rev.* **2011**, *255*, 1039-1054.

(34) Yoshinaga, N.; Ueyama, N.; Okamura, T.; Nakamura, A. *Chem. Lett.* **1990**, *19*, 1655-1656.

(35) Ueyama, N.; Oku, H.; Kondo, M.; Okamura, T.; Yoshinaga, N.; Nakamura, A. *Inorg. Chem.* **1996**, *35*, 643-650.

(36) Baba, K.; Okamura, T.; Yamamoto, H.; Yamamoto, T.; Ohama, M.; Ueyama, N. *Chem. Lett.* **2005**, *34*, 44-45.

(37) Green, A. G.; Perkin, A. G. *J. Chem. Soc., Trans.* **1903**, *83*, 1201-1212.

(38) Boyd, I. W.; Dance, I. G.; Murray, K. S.; Wedd, A. G. *Aust. J. Chem.* **1978**, *31*, 279-284.

(39) Hanson, G. R.; Brunette, A. A.; McDonell, A. C.; Murray, K. S.; Wedd, A. G. *J. Am. Chem. Soc.* **1981**, *103*, 1953-1959.

(40) Milligan, B.; Swan, J. M. *J. Chem. Soc.* **1962**, 2172-2177.

(41) Burla, M. C.; Caliandro, R.; Camalli, M.; Carrozzini, B.; Cascarano, G. L.; Caro, L. D.; Giacovazzo, C.; Polidori, G.; Siliqi, D.; Spagna, R. **2007**.

(42) Sheldrick, G. M. *Acta Crystallogr.* **2008**, *A64*, 112-122.

(43) Altomare, A.; Burla, M. C.; Camalli, M.; Cascarano, G. L.; Giacovazzo, C.; Guagliardi, A.; Moliterni, A. G. G.; Polidori, G.; Spagna, R. *J. Appl. Cryst.* **1999**, *32*, 115-119.

(44) Allen, F. H.; Hoy, V. J.; Howard, J. A. K.; Thalladi, V. R.; Desiraju, G. R.; Wilson, C. C.; McIntyre, G. J. *J. Am. Chem. Soc.* **1997**, *119*, 3477-3480.

(45) Aakeroy, C. B.; Seddon, K. R. *Chem. Soc. Rev.* **1993**, *22*, 397-407.

(46) Cooney, J. J. A.; Carducci, M. D.; McElhaney, A. E.; Selby, H. D.; Enemark, J. H. *Inorg. Chem.* **2002**, *41*, 7086-7093.

(47) Sugimoto, H.; Tarumizu, M.; Tanaka, K.; Miyake, H.; Tsukube, H. *Dalton Trans.* **2005**, 3558-3565.

(48) Maiti, R.; Nagarajan, K.; Sarkar, S. *J. Mol. Struct.* **2003**, *656*, 169-176.

(49) Okamura, T.; Taniuchi, K.; Lee, K.; Yamamoto, H.; Ueyama, N.; Nakamura, A. *Inorg. Chem.* **2006**, *45*, 9374-9380.

(50) Wojdyr, M. *J. Appl. Crystallogr.* **2010**, *43*, 1126-1128.

(51) Boyde, S.; Ellis, S. R.; Garner, C. D.; Clegg, W. *J. Chem. Soc., Chem. Commun.* **1986**, 1541-1543.

(52) Ueyama, N.; Oku, H.; Nakamura, A. *J. Am. Chem. Soc.* **1992**, *114*, 7310-7311.

(53) Oku, H.; Ueyama, N.; Nakamura, A. *Bull. Chem. Soc. Jpn.* **1996**, *69*, 3139-3150.

(54) Ueyama, N.; Okamura, T.; Nakamura, A. *J. Am. Chem. Soc.* **1992**, *114*, 8129-8137.

(55) Sugimoto, H.; Tarumizu, M.; Miyake, H.; Tsukube, H. *Eur. J. Inorg. Chem.* **2007**, *29*, 4663-4668.

(56) Rodger, A.; Johnson, B. F. G. *Inorg. Chem.* **1988**, *27*, 3061-3062.

(57) Tenderholt, A. L.; Szilagyi, R. K.; Holm, R. H.; Hodgson, K. O.; Hedman, B.; Solomon, E. I. *Inorg. Chem.* **2008**, *47*, 6382-6392.

(58) Yan, Y.; Chandrasekaran, P.; Mague, J. T.; DeBeer, S.; Sproules, S.; Donahue, J. P. *Inorg. Chem.* **2012**, *51*, 346-361.

(59) Riddick, J. A.; Bunger, W. B.; Sakano, T. K. *Organic Solvents: Physical Properties and Methods of Purification*; 4th ed.; Wiley: New York, 1986.

(60) Hill, C. L.; Renaud, J.; Holm, R. H.; Mortenson, L. E. *Inorg. Chem.* **1977**, *99*, 2549-2557.

(61) Sun, W.-Y.; Ueyama, N.; Nakamura, A. *Tetrahedron* **1992**, *48*, 1557-1566.

(62) Kassner, R. J.; Yang, W. *J. Am. Chem. Soc.* **1977**, *99*, 4351-4355.

(63) De Hayes, L. J.; Faulkner, H. C.; Doub, W. H.; Sawyer, D. T. *Inorg. Chem.* **1975**, *14*, 2110-2116.

(64) Das, S. K.; Biswas, D.; Maiti, R.; Sarkar, S. *J. Am. Chem. Soc.* **1996**, *118*, 1387-1397.

(65) Warshel, A. *Biochemistry* **1981**, *20*, 3167-3177.

(66) Breslow, R. *J. Phys. Org. Chem.* **2006**, *19*, 813-822.

(67) Ridge, J. P.; Aguey-Zinsou, K.-F.; Bernhardt, P. V.; Brereton, I. M.; Hanson, G. R.; McEwan, A. G. *Biochemistry* **2002**, *41*, 15762-15769.

(68) Ridge, J. P.; Aguey-Zinsou, K.-F.; Bernhardt, P. V.; Hanson, G. R.; McEwan, A. G. *FEBS Lett.* **2004**, *563*, 197-202.

(69) McAlpine, A. S.; McEwan, A. G.; Bailey, S. *J. Mol. Biol.* **1998**, *275*, 613-623.

(70) Cobb, N.; Hemann, C.; Polsinelli, G. A.; Ridge, J. P.; McEwan, A. G.; Hille, R. *J. Biol. Chem.* **2007**, *282*, 35519-35529.

Chapter III

Efficient Uptake of Dimethyl Sulfoxide by Desoxomolybdenum(IV) Dithiolate Complex Containing Bulky Hydrophobic Groups

Introduction

Dimethyl sulfoxide reductase (DMSOR), one of the molybdoenzymes with two unique dithiolene ligands and an alkoxo ligand, catalyzes an oxygen-atom-transfer (OAT) reaction of DMSO via Mo(IV) and Mo(VI) oxidation states. A molybdenum(IV) center reductively eliminates an oxygen atom from the substrates such as sulfoxides and amine *N*-oxides, resulting in the formation of a Mo^{VI}=O bond (Chart 1).[1,2]

Chart 1. The Structure of the Active Site and Catalytic Cycle of Dimethyl Sulfoxide Reductase

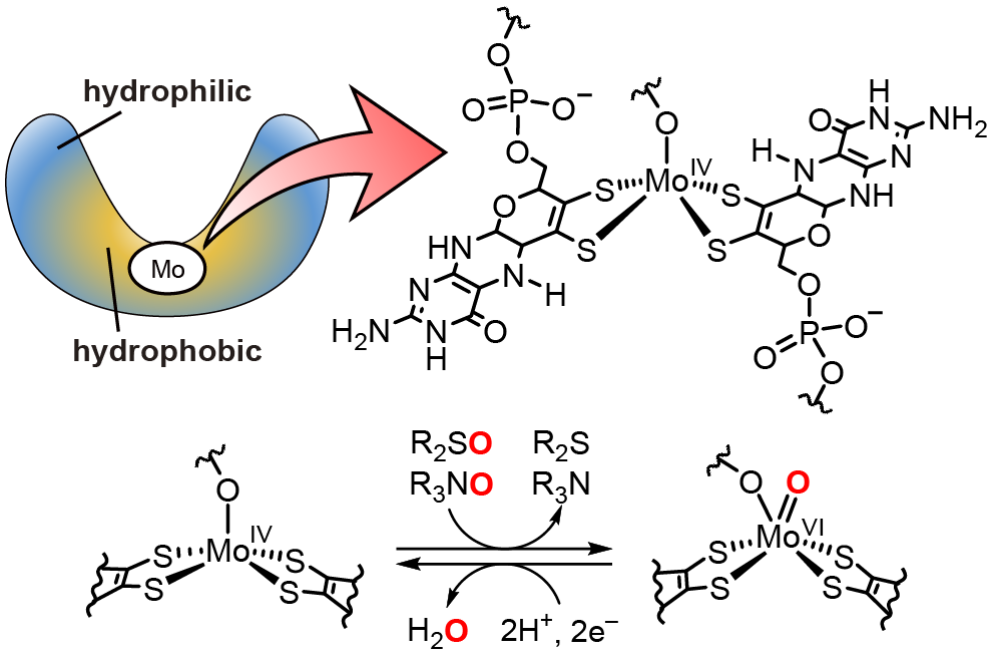

DMSOR is involved in anaerobic respiration using dilute DMSO as an energy source in aqueous media.[3] The enzyme has high affinity for DMSO with K_m values in the micromolar range.[4] Its molecular crystal structure shows that the molybdenum site is located at the base of a large funnel-shaped depression,[2,5] and the ligands are not exposed to the surface (Chart 1).[6] The aromatic residues at the base of the depression provide a hydrophobic pocket to capture the methyl groups of substrate.[1] The above results suggest the importance of the hydrophobic microenvironment for an efficient uptake of the substrates.

Chart 2. Designation of Molybdenum and Tungsten Complexes (**L1** = 1,2-S_2-3,6-{(4-^{t}BuC_6H_4)$_3$CCONH}$_2C_6H_2$)

$(Et_4N)[Mo^{IV}(OSi^tBuPh_2)(\mathbf{L1})_2]$	**1**
$(Et_4N)[Mo^{VI}O(OSi^tBuPh_2)(\mathbf{L1})_2]$	**2**
$(Et_4N)[W^{VI}O(OSi^tBuPh_2)(\mathbf{L1})_2]$	**3**
$(Et_4N)_2[Mo^{IV}O(\mathbf{L1})_2]$	**4**
$(Et_4N)_2[Mo^{VI}O_2(\mathbf{L1})_2]$	**5**
$(Et_4N)_2[W^{VI}O_2(\mathbf{L1})_2]$	**6**
$(Et_4N)[Mo^{IV}(OSi^tBuPh_2)(bdt)_2]$	**7**
$(Et_4N)[Mo^{IV}(OPh)\{S_2C_2(CH_3)_2\}_2]$	**8**

Siloxomolybdenum(IV) complex with benzene-1,2-dithiolate (bdt) ligands (**7**, Chart 2) has been reported as a structural model for the "desoxo"-molybdenum center of DMSOR, synthesized by a simple modification of the corresponding monooxomolybdenum(IV) complex.[7] Moreover, a structural analogue, alkoxomolybdenum(IV) dithiolate complex (**8**, Chart 2), has been reported to promote the OAT reaction of DMSO, a biological substrate; however, because the complex has low reactivity, excess DMSO was used.[8,9]

The DFT calculations of the models indicated that the transient distortion of the square-pyramidal geometry that affords a vacant site *cis* to the apical ligand is important for the binding of the substrate.[10] If the active center is covered with adequately bulky hydrophobic groups, and as a result, distorted by the bulkiness, then both the efficient uptake of the substrate and the enhancement of the reactivity to DMSO are expected to be achieved.

In the earlier studies, it has been demonstrated that the introduction of four bulky CPh_3CONH substituents into the monooxomolybdenum(IV) bdt complex resulted in a dramatic

acceleration of the OAT reaction of Me_3NO via the "*cis*-attack" mechanism. This is due to the stabilization of the distorted intermediate.[11-13]

Furthermore, the author has recently reported that the monooxomolybdenum(IV) complex containing bulky hydrophobic dithiolate ligands, i.e., $(Et_4N)_2[Mo^{IV}O(1,2\text{-}S_2\text{-}3,6\text{-}\{(4\text{-}^tBuC_6H_4)_3CCONH\}_2C_6H_2)_2]$ (**4**, Scheme 1), was soluble in nonpolar solvents such as toluene. The approach of a polar substrate, Me_3NO, to the active center was found to be more efficient in hydrophobic media.[14] The hydrophobic microenvironment formed by bulky hydrophobic moieties was expected to simulate the hydrophobic pocket of DMSOR; however, **4** did not react with DMSO owing to the strong donation of the oxo ligand to the Mo(IV) center.

Here, the synthesis and reactivity of a desoxomolybdenum(IV) complex, $(Et_4N)[Mo^{IV}(OSi^tBuPh_2)(1,2\text{-}S_2\text{-}3,6\text{-}\{(4\text{-}^tBuC_6H_4)_3CCONH\}_2C_6H_2)_2]$ (**1**, Scheme 1), are reported. The author showed that a simple modification of **4** that maintains the solubility and coordination structure results in a dramatic enhancement of the reactivity of the complex to DMSO. Unlike complex **7** with unsubstituted bdt ligands, **1** promotes the OAT reaction of DMSO in both polar and nonpolar solvents, thus demonstrating the efficient uptake of DMSO into the hydrophobic microenvironment. Monooxotungsten(VI) complex **3** was also synthesized and isolated as crystals to investigate its coordination structure in the higher-oxidation state.

Results

Synthesis. Desoxomolybdenum(IV), monooxomolybdenum(VI), and monooxotungsten(VI) complexes, **1-3** (Chart 2), were obtained by the reactions shown in Scheme 1. First, the author monitored the UV-vis spectral change of the silylation of monooxomolybdenum(IV) (**4**) and dioxomolybdenum(VI) (**5**) complexes by using a modified

method reported in the literature (Figure 1).[7,15] Upon adding ^{t}BuPh$_2$SiCl to the complexes in toluene, the absorption spectra changed with sharp isosbestic points. The silylation of complex **4** (k_2 = 0.18 M^{-1} s^{-1}) was slower than that of **5** (k_2 = 0.29 M^{-1} s^{-1}), which is probably ascribed to weak nucleophilicity of the strongly bonded apical oxo ligand.[10,16] On completion of silylation of **4**, the UV-vis spectrum was found to be identical to that of isolated **1**. Therefore, the spectrum of quantitatively silylated complex **5** was regarded as that of **2**. Tungsten analogue **3** was obtained by a similar method. All the complexes were soluble in nonpolar solvents such as toluene, and pure **1** and **3** were isolated as light green and dark purple blocks in a 93% and 74% yields, respectively.

Scheme 1. Synthesis of the Complexes **1-3**

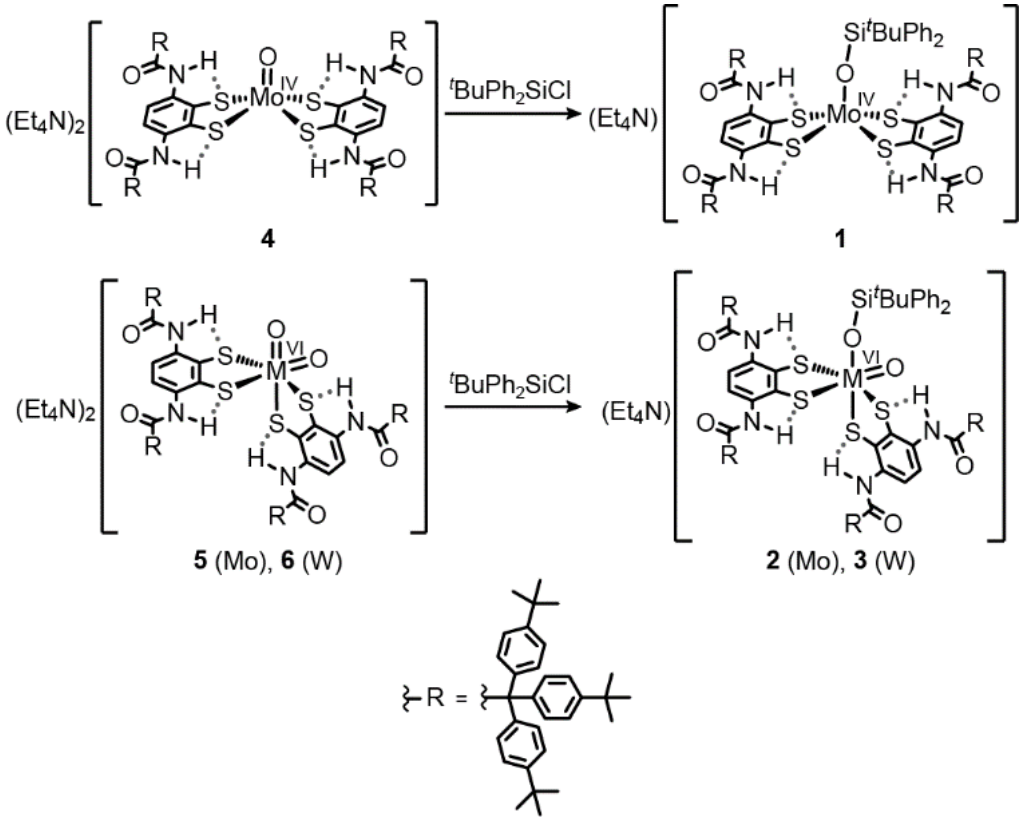

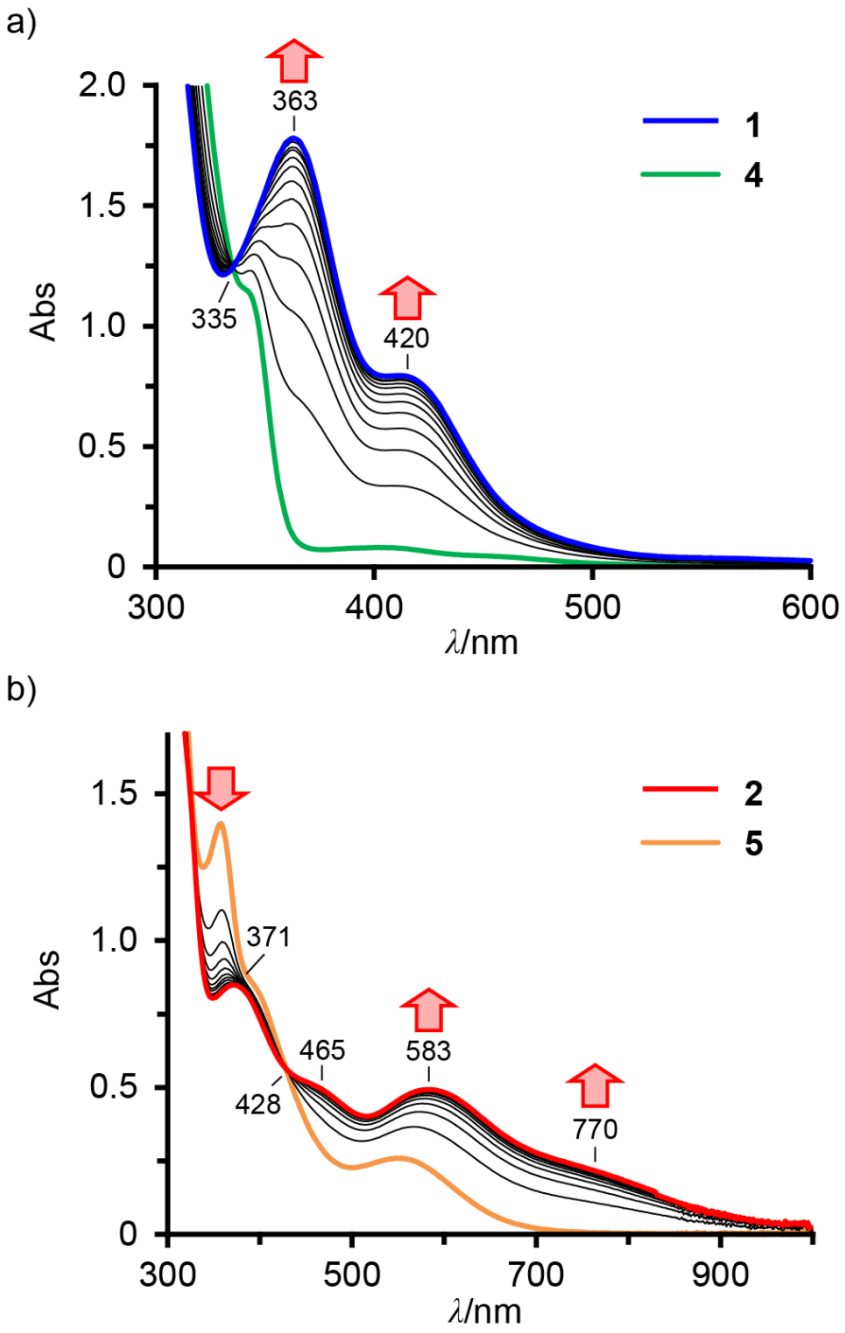

Figure 1. UV-vis spectral change of the reaction of a 1 mM solution of (a) **4** (green) and (b) **5** (orange) with 1.7 eq. of $^{t}BuPh_2SiCl$ in toluene at 27 °C to afford **1** (blue) and **2** (red), respectively.

Molecular structures in the crystals. The molecular structures of **1** and **3** were determined by X-ray analysis. These complexes were apparently recrystallized easily, but their crystallinity was very poor. The result was similar to that observed in case of **4**, **5**, and **6**, as previously described.[14] Here, the author mainly discusses the geometry of the metal center.

The molecular structure of **1**·5CH_3CN·2H_2O is shown in Fig. 1a. The C(C_6H_4-4-^{t}Bu)$_3$ (CAr_3) moieties are bulky enough to interlock with each other in the crystal and to create walls similar to those of as complex **4** that have been previously reported.[14] The resulting hydrophobic microspace was retained both before and after silylation. The square pyramidal geometry and the linearity of Mo–O–Si (164°) were similar to those of the related siloxomolybdenum(IV) complexes (164°–175°).[7,17] All the amide NH moieties were directed toward the sulfur atoms of the dithiolate ligand, indicating the presence of NH···S hydrogen bonds.

The W center of **3**·7/2CH_3CN·5/2H_2O shows a slightly distorted octahedral geometry, which is similar to that of **6** rather than that of a monooxotungsten(VI) complex with bdt ligands (Figure 2b).[14,15] The bulky substituents and hydrogen bonds probably maintain the coordination structure. All the four W–S bonds in **3** were different, and the order of the bond length was W–S1 > W–S3 > W–S4 > W–S2. As described in a previous paper on complex **6**, a strong *trans* influence of the oxo ligand makes W–S1 *trans* to W=O, leading to the most anionic thiolate and the strongest (red) N1H1···S1 hydrogen bond.[14] The moderate (blue) and weak (green) hydrogen bonds were formed at S3 and S2 owing to the medium and weak *trans* influences of the siloxo and thiolate ligands, respectively. The other amide N4H4 is directed toward the benzene ring of the neighboring R4 moiety, probably owing to the packing in the crystal.

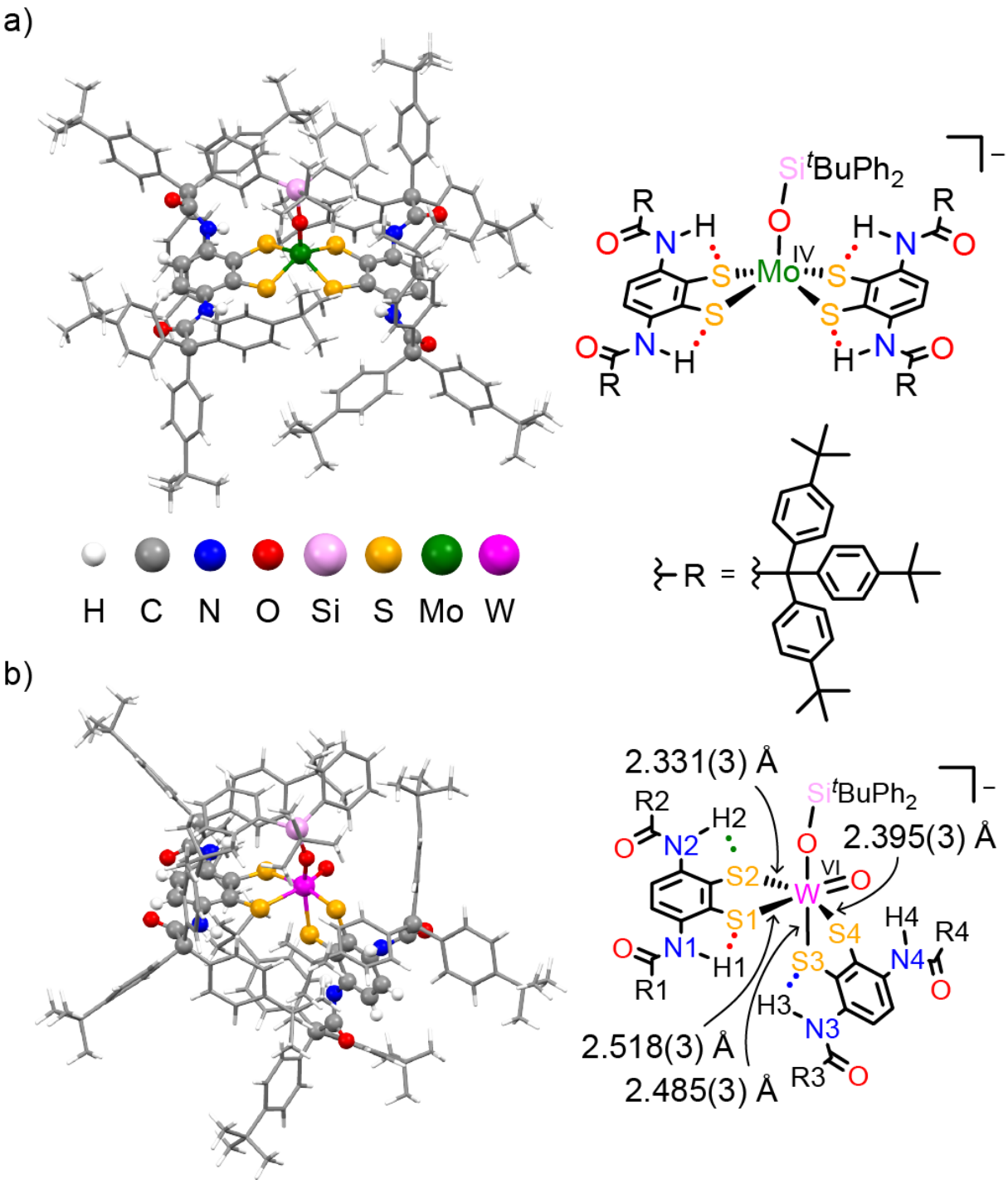

Figure 2. Ball-and-stick models (left) and schematic drawings (right) of the anion part of (a) **1**·5CH_3CN·2H_2O and (b) **3**·7/2CH_3CN·5/2H_2O.

^{1}H NMR studies. Desoxomolybdenum(IV) complex **1** exhibited well-defined ^{1}H NMR signals in toluene-d_8 (Figure 3), which indicated that the four acylamino groups are magnetically equivalent. In the ^{1}H NMR spectrum of monooxotungsten(VI) complex **3**, a single set of broad signals in a polar solvent, CD_3CN, and a couple of broad signals were observed in toluene-d_8 (Figure 3). The separation and broadening of signals are ascribed to the conformational change through the Bailar twist, as described for *cis*-dioxotungsten(VI) complex **5** in a previous paper.[14] As expected, the signals in toluene-d_8 became sharp upon cooling to –45 °C. The partial assignment using ROESY and COSY techniques showed that the four acylamino groups are nonequivalent like in the crystal. The singlet signal at the lowest field (red **a**) was reasonably assigned to the amide NH proton *trans* to the oxo ligand, as observed in **6**.[14] The protons in the other dithiolate ligand (blue and pink) were unassignable because of the relatively weak *trans* influence of the siloxo ligand. The unassignable signals are shown in purple (Figure 4). Interestingly, two distinct **d** protons were observed at 8.2 and 8.5 ppm (Figure 4c), indicating that the two phenyl rings of the ^{t}BuPh$_2$SiO ligand in essentially nonequivalent environments can be distinguished owing to the slowing of the conformational change.

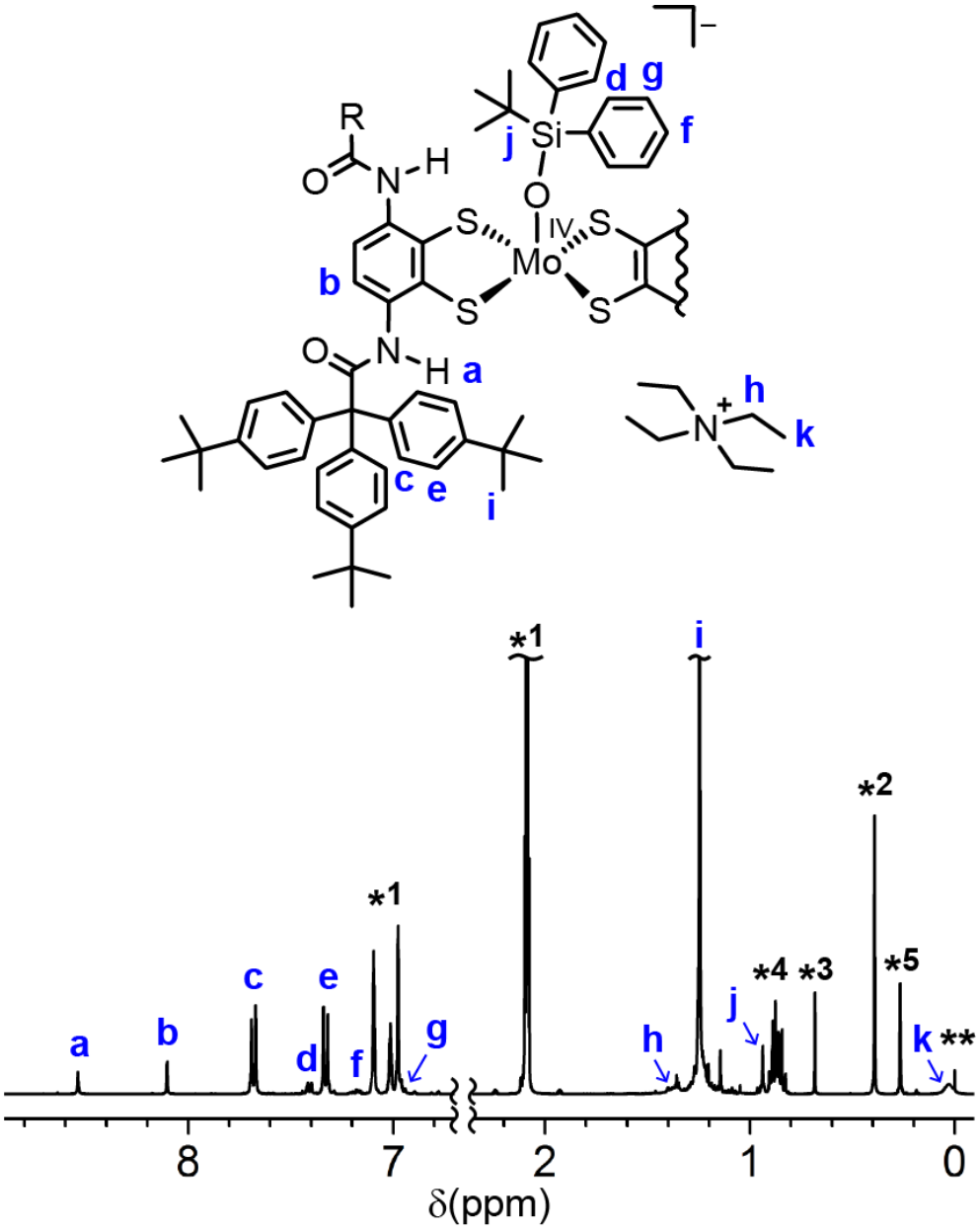

Figure 3. ^{1}H NMR spectrum of **1** in toluene-d_8 at 30 °C. The asterisks denote solvents as a contaminant (*1: toluene; *2: water; *3: acetonitrile; *4: petroleum ether; *5: silicone grease). The double asterisk (**) denotes TMS.

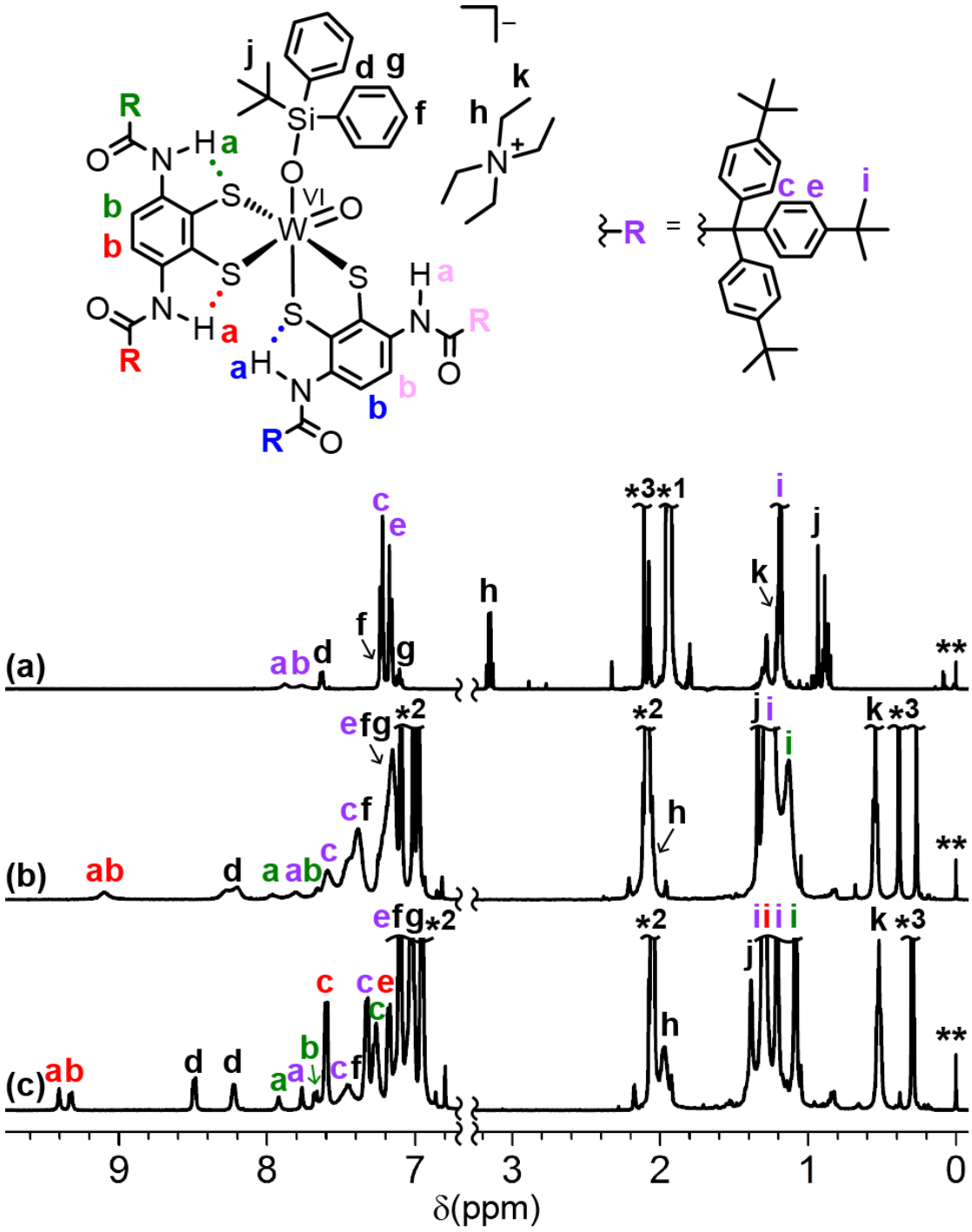

Figure 4. ^{1}H NMR spectra of **3** in (a) CD_3CN at 30 °C, (b) toluene-d_8 at 30 °C, and (c) toluene-d_8 at -45 °C. The two set of assignable siganals and unassignable signals are colored in red, green, and purple, respectively. The asterisks denote solvents as a contaminant (*1: acetonitrile; *2: toluene; *3: water). The double asterisk (**) denotes TMS.

IR and resonance Raman spectra. The presence of NH···S hydrogen bonds was confirmed by IR spectroscopy. Amide NH stretching bands for **1** and **3** in the solid state are listed in Table 1, along with the values of related complexes **4** and **6**.[14] The $\Delta\nu$(NH) values, the lower shifts of ν(NH) than that of the corresponding compound without the NH···S hydrogen bond (RCONHPh), represent the strength of the hydrogen bond, as described in a previous paper.[12,14]

The smaller $\Delta\nu$(NH) values of **1** (–57 cm^{-1}) and **3** (–26, –69 cm^{-1}) than those of **4** and **6** (–97 and –96 cm^{-1}, respectively) indicate the presence of weaker NH···S hydrogen bonds in the complexes with the siloxo ligand, which is consistent with the molecular structures in the crystal.

In monooxotungsten(VI) complex **3**, four ν(NH) values are expected based on the molecular structure, but only two NH stretching bands (3377 and 3334 cm^{-1}) were observed. The NH bands of **3** were considered to be overlapped similar to related complex **6**, which exhibited a single band (3316 cm^{-1}) of two ν(NH) values (3326 and 3306 cm^{-1} by curve-fitting simulation).[14]

Table 1. IR Bands of ν(NH) (cm^{-1}) in the Molybdenum and Tungsten Complexes in the Solid State

	Complexes[a]	Δ(NH)[b]
1	3346	–57
3	3377, 3334	–26, –69
4[c]	3306	–97
6[c]	3316	–87

[a]Nujol. [b]Differences from the value (3403 cm^{-1}) of the corresponding compound, RCONHPh in solution (10 mM in CH_2Cl_2). [c]Ref. 14.

Resonance Raman spectra of desoxomolybdenum(IV) complex **1** excited at 514.5 nm exhibited a single signal at 919 cm^{-1} (Figure 5a). In the IR spectrum of the related complex, $(Et_4N)[Mo^{IV}(OSi^tBuPh_2)(bdt)_2]$ (**7**), the corresponding band at 947 cm^{-1} was assigned to ν(O–Si).[7] In the case of monooxotungsten(VI) complex **3**, strong (924 cm^{-1}) and weak (889 cm^{-1}) signals were observed (Figure 5b), whereas the corresponding signals of $(Et_4N)[W^{IV}O(OSi^tBuPh_2)(bdt)_2]$ at 933 and 888 cm^{-1} were assigned to ν(O–Si) and ν(W=O) by IR, respectively.[15] However, because the sample was excited at the LMCT absorption band, the signal of ν(W=O) should be more intense than that of ν(O–Si) owing to the resonance effect (Figure 6). In order to assign the vibrational mode of these complexes, the frequency was estimated by DFT calculations and compared them with the observed values in the resonance Raman measurements of reported complexes containing bdt ligands (Figure 5c, d).[7,15] As illustrated in Figure 5, the signal of the molybdenum(IV) complex was assigned to a Mo–O stretching combined with O–Si stretching, and the signals of the tungsten(VI) complex were assigned to symmetric and asymmetric WO_2 stretchings combined with O–Si stretching. The bands of **1** and **3** involving the M–O bonds were observed at lower wavenumbers than those of the corresponding bdt complexes; however, it is difficult to evaluate the influence of NH···S hydrogen bonds on the M–O bonds because of the complicated coupling of the stretching bands, as described above.

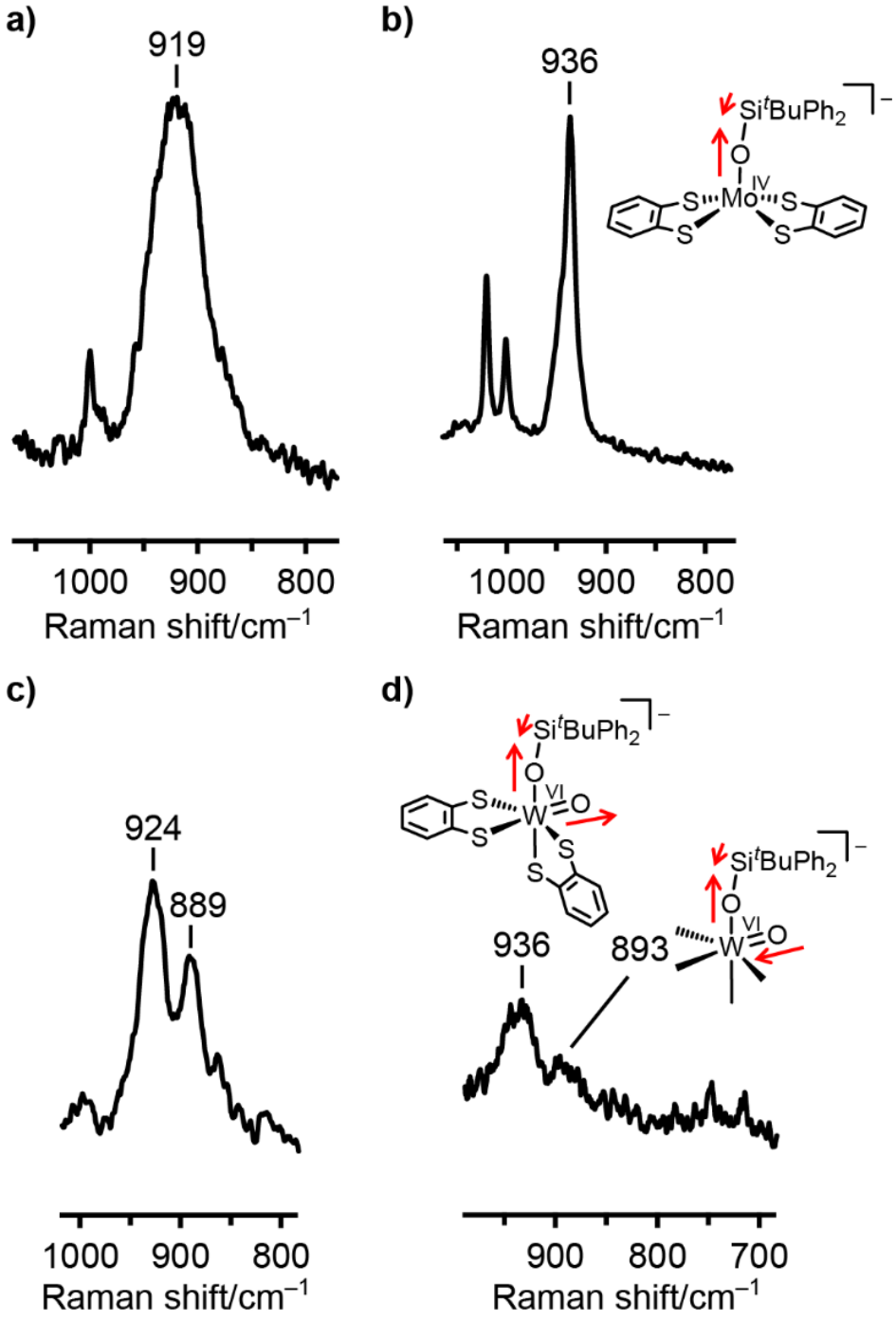

Figure 5. Resonance Raman spectra of (a) **1**, (b) $(Et_4N)[Mo^{IV}(OSi^tBuPh_2)(bdt)_2]$, (c) **3**, (d) $(Et_4N)[W^{VI}O(OSi^tBuPh_2)(bdt)_2]$ excited at 514.5 nm in the solid state. The vibrational mode was assigned using DFT calculation and illustrated in (b) and (d).

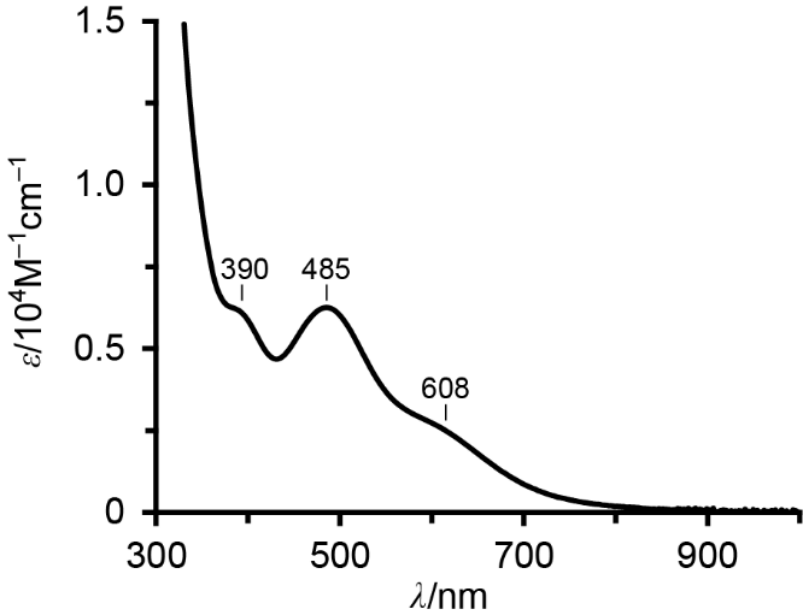

Figure 6. UV-vis spectra of **3** in toluene at 27 °C.

Oxygen-atom-transfer reactions. The OAT reaction between Me_3NO and complex **1** was monitored using UV-vis spectroscopy. Upon adding 2 equiv. of Me_3NO in DMF to **1** in toluene, a fast reaction occurred to afford a dark green solution (Figure 7). The UV-vis spectrum obtained after the OAT reaction (red solid line) was identical with that of **2** (red dotted line), which indicated the clear and quantitative conversion of **1** into **2**. The second-order rate constant, k_2, of the reaction was calculated to be 98 M^{-1} s^{-1}.

In a polar toluene/acetonitrile solution (v/v = 1/1 with a dielectric constant (ε_r) of approximately 25[18]), the reaction rate (k_2 = 8.6 M^{-1} s^{-1}) was about ten times smaller than that in toluene, which was consistent with the results of a previous study, suggesting that the approach of a polar substrate was more efficient in a hydrophobic environment.[14]

Notably, these k_2 values were smaller in both polar and nonpolar solvents than those of the OAT reaction between **4** and Me_3NO (k_2 = 26.6 and 384 M^{-1} s^{-1} in DMF (ε_r = 36.7[19]) and toluene, respectively).[14] This was ascribed to the steric hindrance of bulky CAr_3 moieties and ^{t}BuPh$_2$SiO$^-$ ligand and/or the decrease of ionicity of the active center by the replacement of the dianionic O^{2-} ligand into the monoanionic ^{t}BuPh$_2$SiO$^-$ ligand.

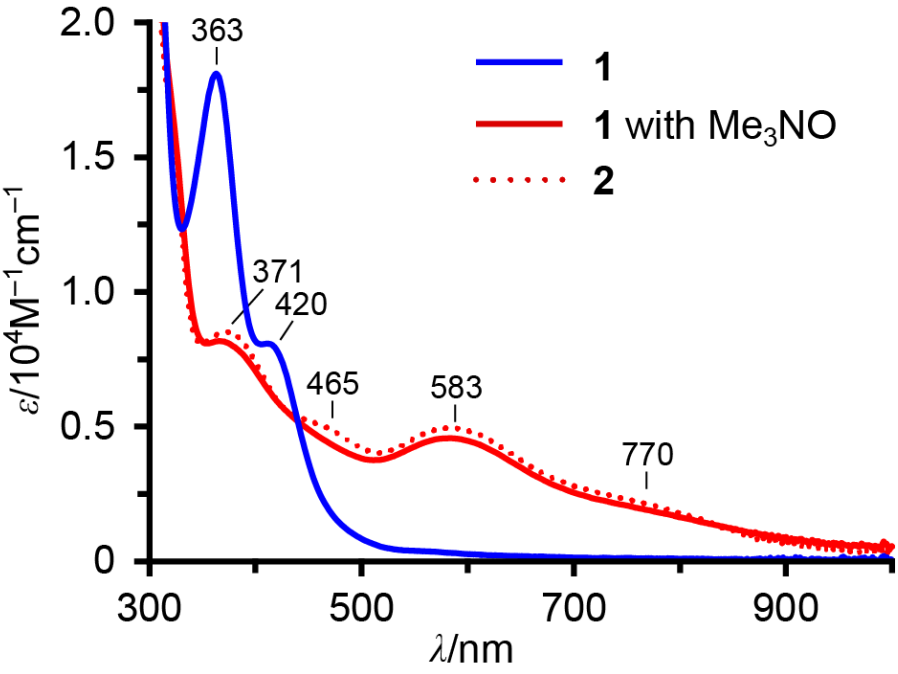

Figure 7. UV-vis spectra of **1** (blue), the reaction mixture of **1** with 2 eq. of Me_3NO (red, solid), and in-situ synthesized **2** by silylation of **5** (red, dotted) in toluene.

Unfortunately, the solubility of complex **1** in acetonitrile was not enough to determine the k_2 of the reaction. In another polar solvent (DMF), **1** was unstable and hence decomposed into **4** by the dissociation of the silyl group, and its reaction with Me_3NO afforded dioxomolybdenum(VI) complex **5**.

On the other hand, complex **1** was stable for several hours in an aqueous micellar solution containing Triton X-100, even in the presence of Me_3NO (Figure 8), indicating the formation of a robust hydrophobic microenvironment that prevents the approach of water molecules and polar substrates.

Addition of a large excess (400 eq.) of DMSO to **1** in toluene at 27 °C resulted in the oxidative dissociation of the dithiolate ligand to afford a disulfide derivative, $L1_2$. These results suggest that a large excess of the coordinating compound with a large donor number (D_N)[19] tends to dissociate the ligands of **1**.

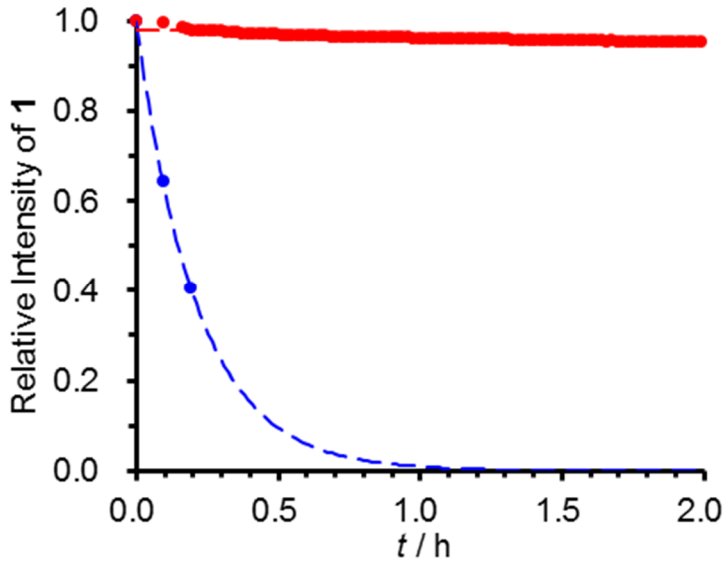

Figure 8. Stability of **1** in an aqueous micellar solution (red) and DMF (blue) monitored by absorption at 418 nm using UV-vis spectroscopy at 27 °C.

Surprisingly, complex **1** could reduce DMSO into Me_2S in toluene-d_8, while no reaction occurred between monooxomolybdenum(IV) complex **4** and DMSO at 80 °C for 20 h. The reaction system containing 1.2 mM of **1** and 4.6 equiv. of DMSO in toluene-d_8 was monitored using ^{1}H NMR spectroscopy. No significant change in the spectrum was observed at r.t. for 24 h; however, heating the mixture at 50 °C resulted in the slow consumption of DMSO and **1**, accompanying the production of Me_2S (Figure 9,10). The reaction accomplished within 600 h, and the second-order kinetic constant estimated from the conversion of **1** was $k_2 = 5.7 \times 10^{-4}$ $M^{-1}s^{-1}$ (Figure 11). Accompanying the decrease in the signals of **1**, neither the signals of amide NH nor the benzenedithiolate protons of the product were observed, whereas a broad signal of ^{t}Bu protons in the CAr_3 moiety was observed. The result suggests the formation of paramagnetic species. After the complete consumption of **1**, the UV-vis spectrum of the reaction mixture showed the absorption band at 756 nm (Figure 12), which is characteristic of five-coordinated monooxomolybdenum(V) complexes. One-electron oxidation of **4** by 1.1 equiv. of $[Fe^{III}Cp_2]BF_4$ proceeded quickly and quantitatively in toluene to afford the

monooxomolybdenum(V) complex, $(Et_4N)[Mo^{V}O(1,2\text{-}S_2\text{-}3,6\text{-}\{(4\text{-}^{t}BuC_6H_4)_3CCONH\}_2\text{-}C_6H_2)_2]$. By comparing the absorbance at 756 nm, the yield of the Mo(V) species was found to be approximately 70%. Moreover, sharp signals of $^{t}BuPh_2SiOH$ were observed. The result is similar to that observed for monooxomolybdenum(VI) complex, **8**, which decomposes by a homolytic cleavage of the Mo^{VI}–OPh bond to afford the corresponding monooxomolybdenum(V) complex and phenol.[9,20] The dissociative mechanism is consistent with the ~60% production of $^{t}BuPh_2SiOH$ (Scheme 2). In addition, 2 equiv. of DMSO was consumed while ~20% of Me_2S based on the initial amount of **1** was detected, probably owing to the decomposition of the product through a radical process.

A similar OAT reaction occurred in a mixture of toluene-d_8 and acetonitrile-d_3 (v/v = 1/1, Figure 13). The similar reaction rate ($k_2 = 6.7 \times 10^{-4}$ $M^{-1}s^{-1}$) to that in toluene-d_8 indicates that the desoxomolybdenum(IV) complex can reduce DMSO without depending on the solvent polarity, unlike the case of Me_3NO. The polar amine *N*-oxide is hardly soluble in nonpolar solvents and considered to be condensed into the ionic active center. Thus, the dramatic acceleration of the OAT reaction was achieved, as described in a previous paper.[14] On the contrary, DMSO can diffuse uniformly even in toluene, and only the hydrophobic microenvironment around the active center affects the uptake of substrate. The similar reactivity in both polar and nonpolar solvents indicates the presence of a hydrophobic microenvironment for an efficient uptake of the substrate.

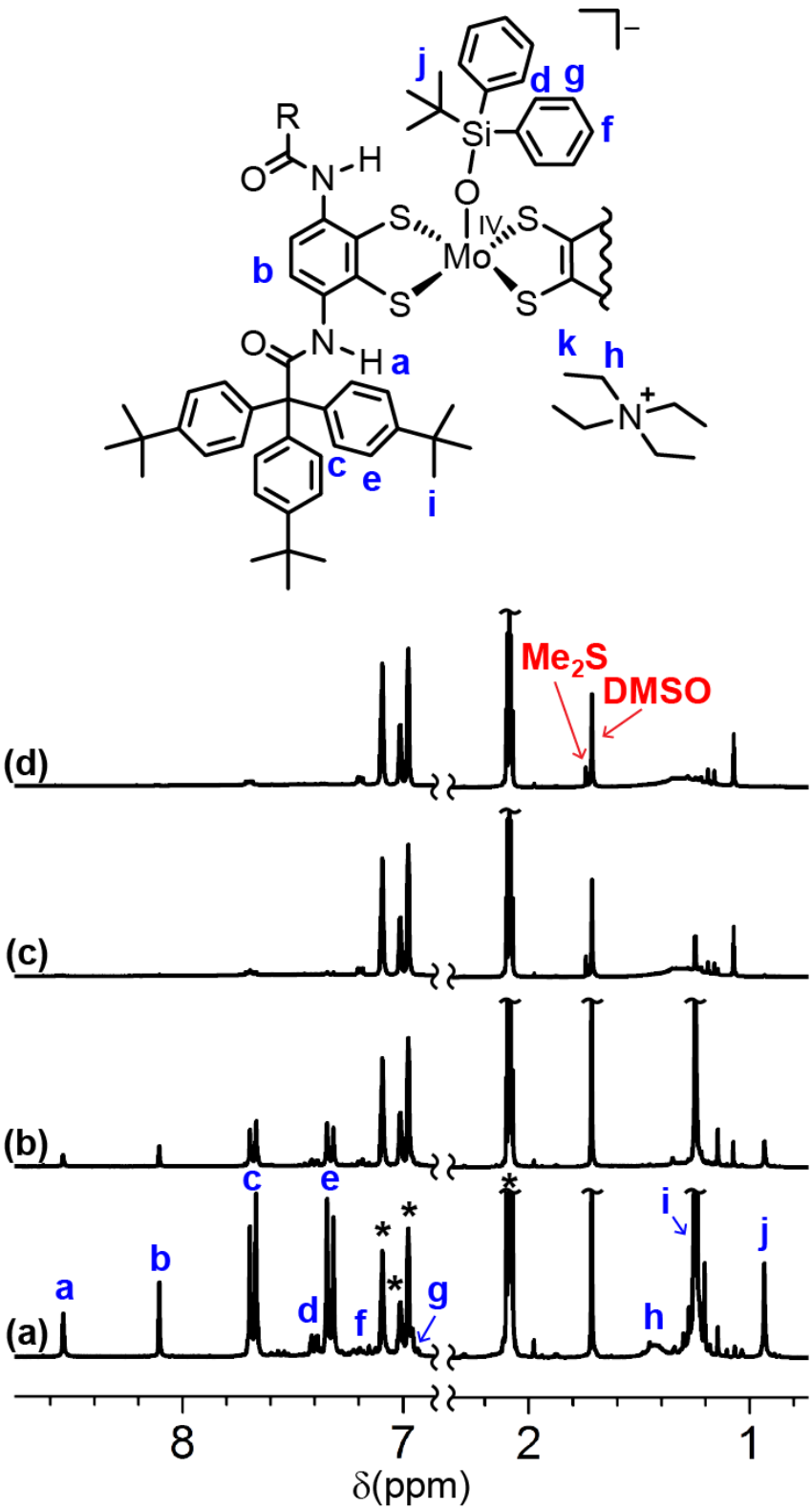

Figure 9. NMR spectral change during the reaction of **1** and 5 eq. of DMSO in toluene-d_8. (a) 0 h, (b) 24 h, (c) 294 h, (d) 576 h. The asterisk (*) denotes toluene.

Scheme 2. The Proposed Mechanism of the OAT Reaction of DMSO

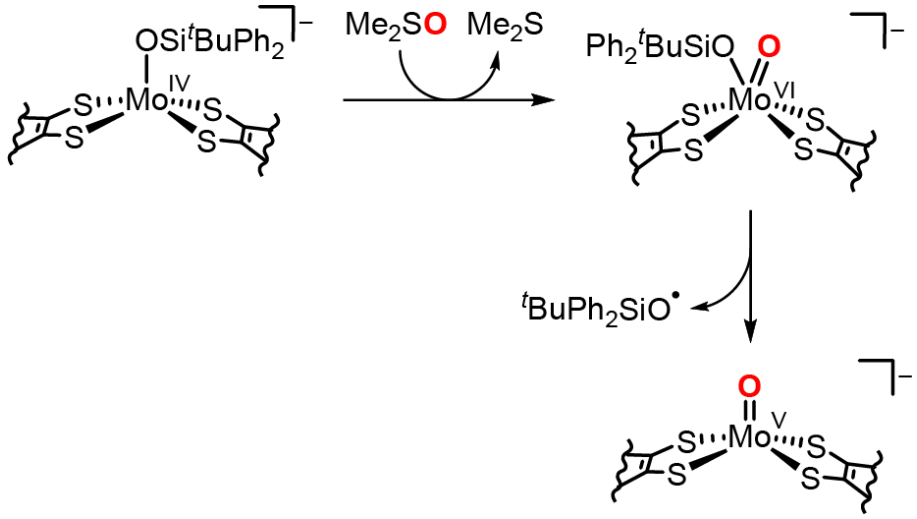

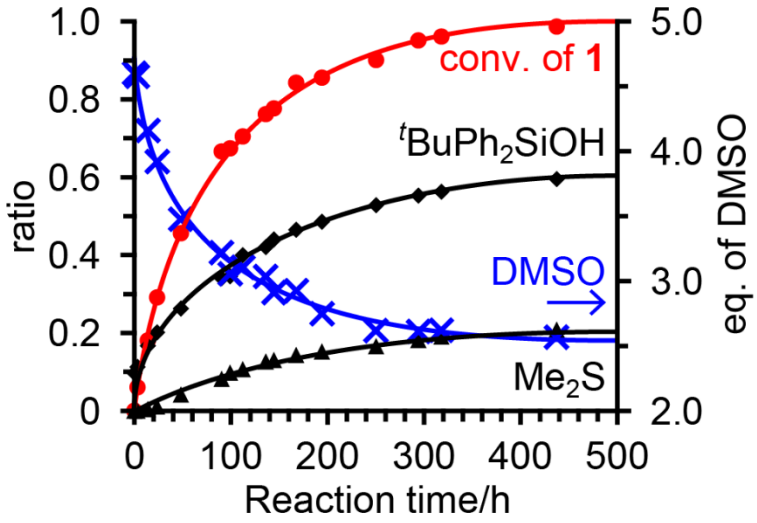

Figure 10. Time course of the conversion of **1** during the reduction of DMSO in toluene-d_8.

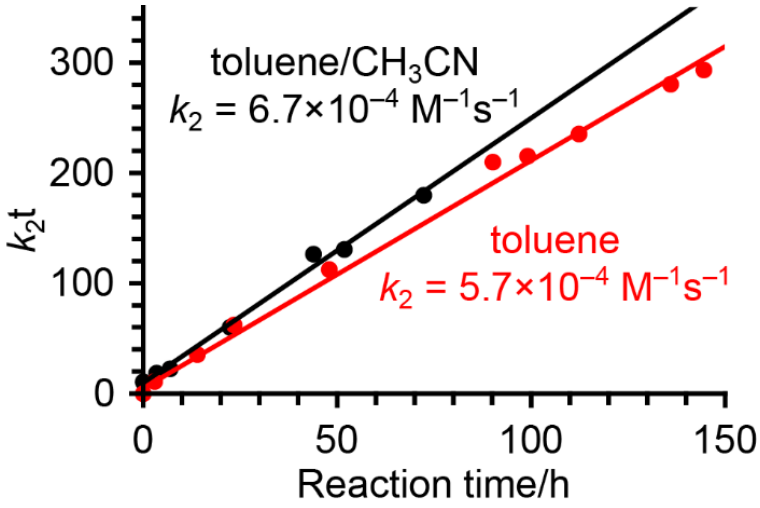

Figure 11. Kinetic plot of the reduction of DMSO.

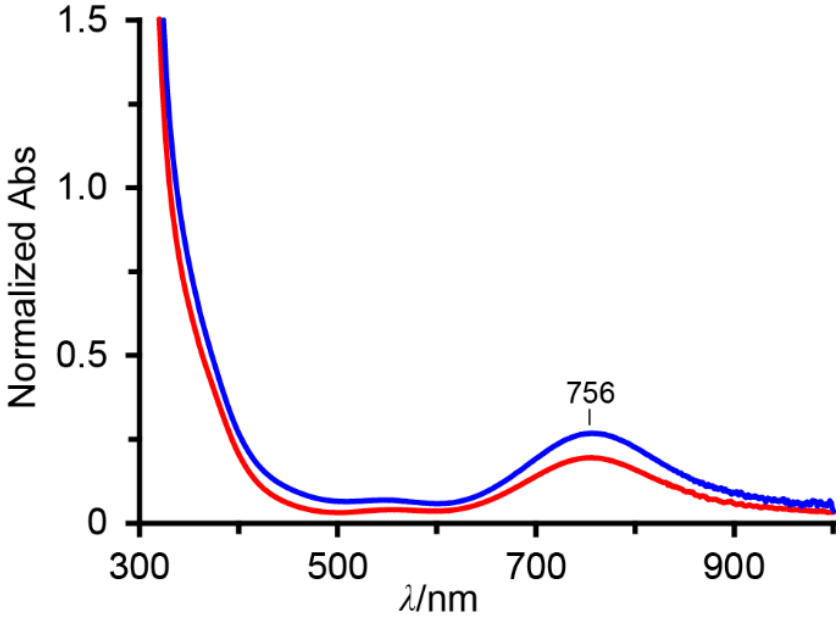

Figure 12. UV-vis spectra of the reaction mixture of **1** and DMSO in toluene (red) and the in-situ generated monooxomolybdenum(V) complex (blue) in toluene at 27 °C.

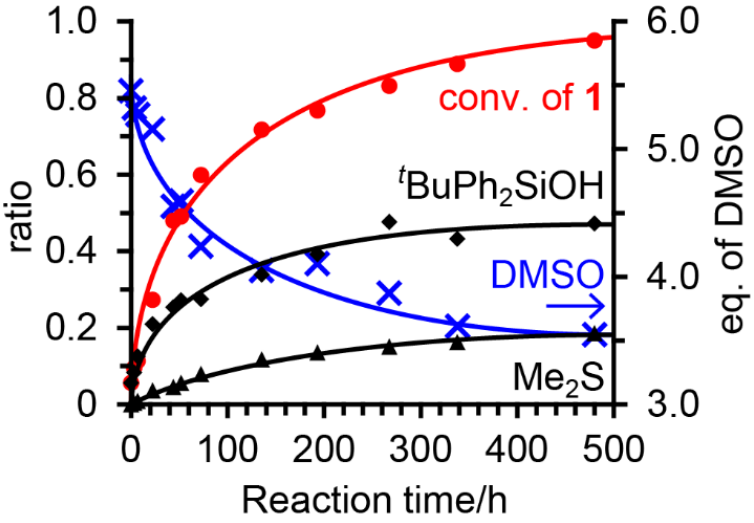

Figure 13. Time course of the conversion of **1** during the reduction of DMSO in a mixed solution of toluene-d_8 and acetonitrile-d_3 (v/v = 1/1).

Discussion

Desoxomolybdenum(IV) complex **1** containing bulky hydrophobic substituents could reduce DMSO in both polar and nonpolar solvents. Although it is difficult to quantitatively discuss the reaction because of the instability of the resulting monooxomolybdenum(VI) complex **2** under the reaction conditions, the production of Me_2S was confirmed by ^1H NMR analysis. Moreover, the clean and quantitative OAT reaction of **1** with Me_3NO was also observed.

In the case of the siloxomolybdenum(IV) complex containing unsubstituted bdt ligands (**7**), no appreciable reaction was observed when large excess of more reactive tetramethylene sulfoxide ($(CH_2)_4SO$) was reacted in CH_3CN on heating at 50 °C, whereas the OAT reaction of Me_3NO occurred, but it was not clean.[7] Phenoxomolybdenum(IV) complex **8** slowly reacted with a large excess of DMSO in CH_3CN on heating, and the kinetic parameters $\Delta H^{\ddagger}$ and $\Delta S^{\ddagger}$ were reported to be 14.8(5) kcal/mol and –36(1) cal/mol, respectively.[9,20] The estimated k_2 at 50 °C from the Eyring plot was 8×10^{-6} $M^{-1}s^{-1}$, which was much smaller than the present system. In another case, a siloxomolybdenum(IV) complex, $(Et_4N)[Mo^{IV}(OSi^tBuPh_2)\{S_2C_2(COOCH_3)_2\}_2]$, was reported to cleanly react with Me_3NO below –15 °C; however, the reaction with DMSO was too slow to be monitored.[17]

The enhanced reactivity of the desoxomolybdenum(IV) complex in the present system is considered to be caused by the stabilization of the DMSO-bound transient structure owing to bulky hydrophobic substituents. The DFT calculations of desoxomolybdenum(IV) complexes indicated that the distortion of the geometry and trigonal-prismatic transition state are important to promote the attack of DMSO *cis* to the alkoxo ligand.[10] In the previous theoretical investigation of monooxomolybdenum(IV) complexes, it has been shown that the four bulky

ligands stabilize the transient distorted structure and promote the very fast OAT reaction of Me_3NO through a direct *cis*-attack mechanism.[12]

Further, the hydrophobic microenvironment around the active center is found to be maintained regardless of the solvent polarity. These results indicate that desoxomolybdenum(IV) complex **1** ensures the substrate-access pocket for DMSO.

Conclusions

Toluene-soluble desoxomolybdenum(IV), monooxomolybdenum(VI), and monooxotungsten(VI) complexes (**1**-**3**, respectively) containing bulky hydrophobic groups were synthesized. The simple modification of an oxo ligand into a siloxo ligand achieved the reduction of not only Me_3NO but also DMSO. Moreover, the reduction of DMSO was accelerated compared to that of the other complexes.

The rate of the OAT reaction of DMSO was independent of the polarity of the reaction media, which suggests the formation of a hydrophobic microenvironment around the active center. The combination of the bulkiness of CAr_3 groups and a hydrophobic microenvironment promoted the OAT reaction of the biological substituent, DMSO, by forming the confined space for substrate binding.

Experimental

All procedures were performed under an argon atmosphere by the Schlenk technique. All solvents were dried and distilled under argon before use. $(Et_4N)_2[Mo^{IV}O(1,2\text{-}S_2\text{-}3,6\text{-}\{(4\text{-}^tBuC_6H_4)_3CCONH\}_2C_6H_2)_2]$ (**4**), $(Et_4N)_2[Mo^{VI}O_2(1,2\text{-}S_2\text{-}3,6\text{-}\{(4\text{-}^tBuC_6H_4)_3CCONH\}_2C_6H_2)_2]$ (**5**), and $(Et_4N)_2[W^{VI}O_2(1,2\text{-}S_2\text{-}3,6\text{-}\{(4\text{-}^tBuC_6H_4)_3CCONH\}_2C_6H_2)_2]$ (**6**) were prepared by the reported method.[14]

$(Et_4N)[Mo^{IV}(OSi^tBuPh_2)(1,2\text{-}S_2\text{-}3,6\text{-}\{(4\text{-}^tBuC_6H_4)_3CCONH\}_2C_6H_2)_2]$ (1). This compound was synthesized by a modified method reported in the literature.[7] To a solution of **4** (17.5 mg, 7.09 μmol) in toluene (0.7 mL) was added ^{t}BuPh$_2$SiCl (3 μL, 12 μmol), and the reaction mixture was stirred for 1 h to afford a brownish-yellow suspension. After removal of colorless precipitates by filtration, the filtrate was evaporated under reduced pressure. The resulting brownish-yellow residue was recrystallized from toluene/acetonitrile to afford light green blocks. Yield: 17.0 mg, 93%. ^{1}H NMR (toluene-d_8): δ 8.54 (s, 4H, NH), 8.10 (s, 4H, 4,5-H), 7.68 (d, J = 8.7 Hz, 24H, Ar), 7.41 (m, 4H, PhSi), 7.33 (d, J = 8.7 Hz, 24H, Ar), 7.18 (m, 2H, PhSi), 6.95 (m, 4H, PhSi), 1.36 (br, 8H, Et_4N^+), 1.25 (s, 108H, ^{t}Bu), 0.94 (s, 9H, ^{t}BuSi), 0.03 (br, 12H, Et_4N^+). Absorption spectrum (toluene): λ_{max} (ε, $M^{-1}cm^{-1}$) 363 (17000), 420 (sh) (7300) nm. Anal. Calcd for $C_{164}H_{203}N_5O_5S_4MoSi$: C, 76.45; H, 7.94; N, 2.72. Found: C, 75.17; H, 7.99; N, 2.66.

As described in a previous paper, the disagreement of elemental analysis for molybdenum complexes is probably caused by their nanoporous structure in the solid state.[14] After removal of the solvent molecules from the crystals, the resulting voids might be able to trap gaseous water molecules. Formal addition of water to the chemical formula improved the results. The calculated values for $C_{164}H_{203}N_5O_5S_4MoSi\cdot(H_2O)_{2.5}$: C, 75.13; H, 8.00 N, 2.67, which agree

with the found ones. The water molecules were also detected in ^{1}H NMR spectra, but the amount of water depended on the conditions.

$(Et_4N)[Mo^{VI}O(OSi^tBuPh_2)(1,2\text{-}S_2\text{-}3,6\text{-}\{(4\text{-}^tBuC_6H_4)_3CCONH\}_2C_6H_2)_2]$ (2). This compound was synthesized in situ to obtain the UV-vis spectrum. To a solution of **5** (1 mM, 0.3 mL) in toluene in a 1-mm UV cell was added a ^{t}BuPh$_2$SiCl solution (128 mM, 4 μL) in toluene, and the cell contents were quickly mixed by shaking and allowed to stand for 8.5 h at 27 °C. The product was used for the spectral measurements without further purification. Absorption spectrum (toluene): λ_{max} (ε, $M^{-1}cm^{-1}$) 371 (8500), 465 (sh) (5000), 583 (4900), 770 (sh) (2100) nm.

$(Et_4N)[W^{VI}O(OSi^tBuPh_2)(1,2\text{-}S_2\text{-}3,6\text{-}\{(4\text{-}^tBuC_6H_4)_3CCONH\}_2C_6H_2)_2]$ (3). This compound was synthesized by a modified method reported in the literature.[15] To a solution of **5** (30.9 mg, 12.0 μmol) in toluene (1 mL) was added ^{t}BuPh$_2$SiCl (5 μL, 19 μmol). The reaction mixture was stirred at r.t. for 10 min. After removal of colorless precipitates by filtration, the filtrate was evaporated. The resulting dark reddish-purple powder was recrystallized from toluene/acetonitrile to afford dark purple plates. Yield: 23.8 mg, 74%. ^{1}H NMR (CD_3CN): δ 7.88 (s, 4H, NH), 7.77 (s, 4H, 4,5-H), 7.63 (d, J = 7.2 Hz, 4H, PhSi), 7.22 (d, J = 8.5 Hz, 24H, Ar), 7.20 (m, 2H, PhSi), 7.16 (d, J = 8.5 Hz, 24H, Ar), 7.11 (dd, J = 7.2, 7.8 Hz, 4H, PhSi), 3.15 (q, J = 7.2 Hz, 8H, Et_4N^+), 1.20 (tt, $J_{H\text{-}H}$ = 7.2 Hz, $J_{H\text{-}N}$ = 1.9 Hz, 12H, Et_4N^+), 1.19 (s, 108H, ^{t}Bu), 0.93 (s, 9H, ^{t}BuSi). Absorption spectrum (toluene): λ_{max} (ε, $M^{-1}cm^{-1}$) 390 (sh) (6100), 485 (6100), 608 (sh) (2600) nm. Anal. Calcd for $C_{164}H_{203}N_5O_6S_4SiW$: C, 73.48; H, 7.63; N, 2.61. Found: C, 73.32; H, 7.51; N, 2.57.

Physical measurements. The elemental analyses were performed on a Yanaco CHN CORDER MT-5. ^{1}H NMR spectra were obtained with JEOL ECA-500 and ECS-400 spectrometers in toluene-d_8 and CD_3CN at 30 °C. UV-visible absorption spectra were recorded using a SHIMADZU UV-3100PC spectrometer. Infrared (IR) spectroscopic measurements

were done on a Jasco FT/IR-6100 spectrometer. Raman spectra were measured on a Jasco NR-1800 laser Raman spectrometer with liq. N_2 cooled or thermoelectrically cooled CCD detector. Exciting radiation was provided by Ar^+ ion laser (514.5 nm).

Structural determination. Each single crystal of **1**·5CH_3CN·2H_2O and **3**·7/2CH_3CN·5/2H_2O was selected carefully and mounted on MicroMount™ 200 μm with Nujol, which was frozen immediately in a stream of cold nitrogen at 200 K. Data collection was made on a Rigaku RAPID II Imaging Plate area detector with Mo-Kα radiation (0.71075 Å) using MicroMax-007HF microfocus rotating anode X-ray generator and VariMax-Mo optics. The structures were solved by direct methods (SIR92[21]) for **1**·5CH_3CN·2H_2O and heavy-atom Patterson methods (PATTY[22]) for **3**·7/2CH_3CN·5/2H_2O and expanded Fourier techniques using SHELXL-97 or SHELXL-2014/7.[23]

Density functional theory (DFT) calculations. Geometry optimization and vibrational calculations were performed using Becke's three-parameter hybrid functionals (B3LYP) in the Gaussian 03 program package.[24] The basis set used for Mo and W was LanL2DZ. For other atoms (H, C, N, O, Si, S), a 6-31G** basis set was employed. The coordinates of the crystal structures, $(Et_4N)[Mo^{IV}(OSi^tBuPh_2)(bdt)_2]$[7] and $(Et_4N)[W^{VI}O(OSi^tBuPh_2)(bdt)_2]$,[15] were used for the initial structures with some modifications.

Kinetic measurements. A reaction system containing **1** and Me_3NO was monitored spectrophotometrically in the region 280–1000 nm. The measurements were carried out in a 1-cm UV cell containing a toluene solution of **1** (0.1 mM, 3.0 mL) at 27 °C. After thermal equilibrium, a Me_3NO solution (60 mM, 10 μL) in DMF was injected through a silicone rubber cap, and the cell contents were quickly mixed by shaking. The time course of the reaction was monitored by using the absorption maximum of **2** at 583 nm. In the case in toluene/acetonitrile solution, a 1 mM solution of **1** in toluene/acetonitrile (v/v = 1/1) was treated with an acetonitrile solution of Me_3NO (60 mM, 10 μL).

The reaction between **1** and DMSO was monitored by ^{1}H NMR spectroscopy. A sealed-NMR tube containing **1** (1.2 mM) and DMSO (5.7 mM) in toluene-d_8 (0.6 mL) was heated at 50 °C. The measurement was carried out at 30 °C. In the case in toluene/acetonitrile solution, a mixed solution of **1** (0.99 mM) and DMSO (5.4 mM) in toluene-d_8/CD_3CN (v/v = 1/1) was used.

References

(1) Hille, R.; Hall, J.; Basu, P. *Chem. Rev.* **2014**, *114*, 3963-4038.

(2) Schindelin, H.; Kisker, C.; Hilton, J.; Rajagopalan, K. V.; Rees, D. C. *Science* **1996**, *272*, 1615-1621.

(3) Cobb, N.; Hemann, C.; Polsinelli, G. A.; Ridge, J. P.; McEwan, A. G.; Hille, R. *J. Biol. Chem.* **2007**, *282*, 35519-35529.

(4) Johnson, K. E.; Rajagopalan, K. V. *J. Biol. Chem.* **2001**, *276*, 13178-13185.

(5) McAlpine, A. S.; McEwan, A. G.; Bailey, S. *J. Mol. Biol.* **1998**, *275*, 613-623.

(6) Mondal, S.; Basu, P. *Inorg. Chem.* **2001**, *40*, 192-193.

(7) Donahue, J. P.; Goldsmith, C. R.; Nadiminti, U.; Holm, R. H. *J. Am. Chem. Soc.* **1998**, *120*, 12869-12881.

(8) Lim, B. S.; Donahue, J. P.; Holm, R. H. *Inorg. Chem.* **2000**, *39*, 263-273.

(9) Lim, B. S.; Holm, R. H. *J. Am. Chem. Soc.* **2001**, *123*, 1920-1930.

(10) Ha, Y.; Tenderholt, A. L.; Holm, R. H.; Hedman, B.; Hodgson, K. O.; Solomon, E. I. *J. Am. Chem. Soc.* **2014**, *136*, 9094-9105.

(11) Baba, K.; Okamura, T.; Suzuki, C.; Yamamoto, H.; Yamamoto, T.; Ohama, M.; Ueyama, N. *Inorg. Chem.* **2006**, *45*, 894-901.

(12) Okamura, T.; Ushijima, Y.; Omi, Y.; Onitsuka, K. *Inorg. Chem.* **2013**, *52*, 381-394.

(13) Baba, K.; Okamura, T.; Yamamoto, H.; Yamamoto, T.; Ohama, M.; Ueyama, N. *Chem. Lett.* **2005**, *34*, 44-45.

(14) Hasenaka, Y.; Okamura, T.; Tatsumi, M.; Inazumi, N.; Onitsuka, K. *Dalton Trans.* **2014**, *43*, 15491-15502.

(15) Lorber, C.; Donahue, J. P.; Goddard, C. A.; Nordlander, E.; Holm, R. H. *J. Am. Chem. Soc.* **1998**, *120*, 8102-8112.

(16) Ueyama, N.; Okamura, T.; Nakamura, A. *J. Am. Chem. Soc.* **1992**, *114*, 8129-8137.

(17) Sugimoto, H.; Tatemoto, S.; Suyama, K.; Miyake, H.; Mtei, R. P.; Itoh, S.; Kirk, M. L. *Inorg. Chem.* **2010**, *49*, 5368-5370.

(18) Ritzoulis, G.; Papadopoulos, N.; Jannakoudakis, D. *Journal of Chemical & Engineering Data* **1986**, *31*, 146-148.

(19) Riddick, J. A.; Bunger, W. B.; Sakano, T. K. *Organic Solvents: Physical Properties and Methods of Purification*; 4th ed.; Wiley: New York, 1986.

(20) Lim, B. S.; Sung, K.-M.; Holm, R. H. *J. Am. Chem. Soc.* **2000**, *122*, 7410-7411.

(21) Altomare, A.; Cascarano, G.; Giacovazzo, C.; Guagliardi, A. *J. Appl. Cryst.* **1994**, *27*, 435-436.

(22) Beurskens, P. T.; Admiraal, G.; Behm, H.; Beurskens, G.; Smits, J. M. M.; Smykalla, C. *Z. f. Kristallogr.* **1991**, *Suppl.4*, 99.

(23) Sheldrick, G. M. *Acta Crystallogr.* **2008**, *A64*, 112-122.

(24) Frisch, M. J.; Trucks, G. W.; Schlegel, H. B.; Scuseria, G. E.; Robb, M. A.; Cheeseman, J. R.; Montgomery, J. A.; Jr, T. V.; Kudin, K. N.; Burant, J. C.; Millam, J. M.; Iyengar, S. S.; Tomasi, J.; Barone, V.; Mennucci, B.; Cossi, M.; Scalmani, G.; Rega, N.; Petersson, G. A.; Nakatsuji, H.; Hada, M.; Ehara, M.; Toyota, K.; Fukuda, R.; Hasegawa, J.; Ishida, M.; Nakajima, T.; Honda, Y.; Kitao, O.; Nakai, H.; Klene, M.; Li, X.; Knox, J. E.; Hratchian, H. P.; Cross, J. B.; Bakken, V.; Adamo, C.; Jaramillo, J.; Gomperts, R.;

Stratmann, R. E.; Yazyev, O.; Austin, A. J.; Cammi, R.; Pomelli, C.; Ochterski, J. W.; Ayala, P. Y.; Morokuma, K.; Voth, G. A.; Salvador, P.; Dannenberg, J. J.; Zakrzewski, V. G.; Dapprich, S.; Daniels, A. D.; Strain, M. C.; Farkas, O.; Malick, D. K.; Rabuck, A. D.; Raghavachari, K.; Foresman, J. B.; Ortiz, J. V.; Cui, Q.; Baboul, A. G.; Clifford, S.; Cioslowski, J.; Stefanov, B. B.; Liu, G.; Liashenko, A.; Piskorz, P.; Komaromi, I.; Martin, R. L.; Fox, D. J.; Keith, T.; Al-Laham, M. A.; Peng, C. Y.; Nanayakkara, A.; Challacombe, M.; Gill, P. M. W.; Johnson, B.; Chen, W.; Wong, M. W.; Gonzalez, C.; Pople, J. A. *Gaussian 03, Revision E.01*; Gaussian, Inc., Wallingford CT, 2004.

Chapter IV

Modeling of Hydrophobic Microenvironment of Water-Soluble Molybdoenzymes in Aqueous Micellar Solution

Introduction

Trimethylamine *N*-oxide reductase (TMAOR), a molybdoenzyme with two dithiolene ligands called pterin cofactor, catalyzes oxygen-atom-transfer (OAT) reactions via Mo(IV) and Mo(VI) oxidation states (Figure 1).[1-4] The molybdenum(IV) center reductively eliminates an oxygen atom from amine *N*-oxides to form a Mo^{VI}=O bond and is regenerated via protonation and reduction accompanied with the production of water. Nicotinamide adenine dinucleotide (phosphate), NAD(P)H, can be used as an electron source in the catalytic cycle.[5] In the case of biotin sulfoxide reductase (BSOR), the direct hydride transfer from NADPH to the active site has been proposed by using kinetic analyses.[6-8] The active site is located at the bottom of a large depression, and the ligands are not exposed to the surface.[1,9] The hydrophobic pocket formed by aromatic residues at the base of the depression is conserved in both TMAOR and BSOR,[1,7] which suggests the importance of the hydrophobicity in the enzyme activity. A hydrophobic environment around the active site should support weak interactions such as binding of substrates and hydrogen bonds, and is probably important for controlling the electrochemical properties. Studies on encapsulated model compounds with dendritic architecture have demonstrated the importance of the hydrophobic pocket.[10-15]

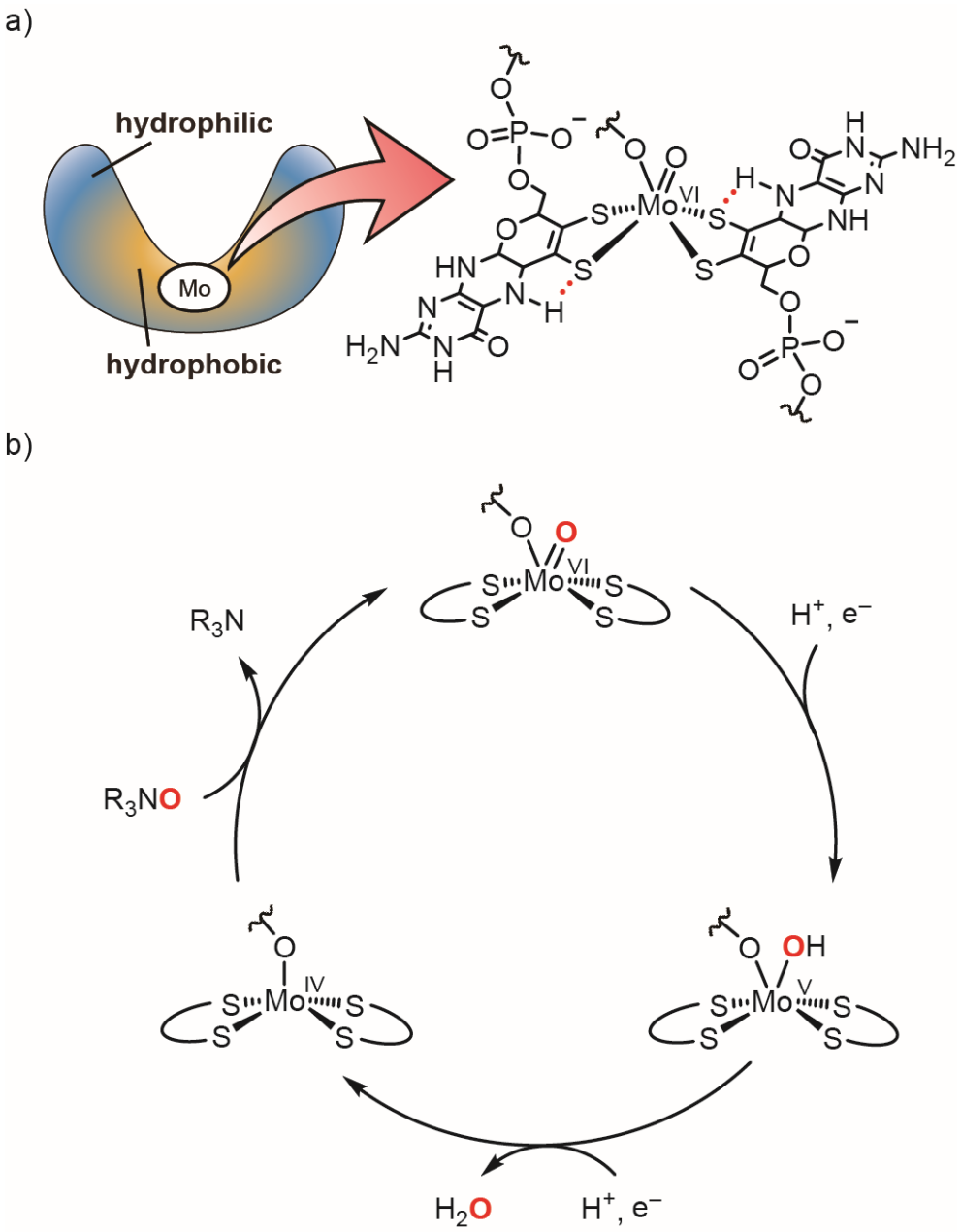

Figure 1. (a) The structure of the active site and (b) catalytic cycle of trimethylamine *N*-oxide reductase.

A number of molybdoenzyme models have been synthesized,[16-21] some of which have simulated the catalytic reduction of amine *N*-oxides by phosphines by double OAT reactions.[22-26] Monooxomolybdenum(IV) complexes with benzene-1,2-dithiolate (bdt) ligands can eliminate the oxygen atom of trimethylamine *N*-oxide to afford a Mo^{VI}=O bond; the

resulting dioxomolybdenum(VI) complexes can be reduced by benzoin to regenerate the original monooxomolybdenum(IV) complexes with the production of water.[27,28]

Introduction of four bulky triphenylacetylamino groups into the model complex, i.e. $(Et_4N)_2[Mo^{IV}O\{1,2\text{-}S_2\text{-}3,6\text{-}(Ph_3CCONH)_2C_6H_2\}_2]$, dramatically accelerated the OAT reaction via the stabilization of a distorted intermediate by the bulky substituents.[29,30] In the proposed mechanism, the substrate approaches the polar molybdenum center from the upper side, i.e. *cis* to the oxo ligand, and spontaneously a Mo=O bond is formed, similar to the enzyme. As described in Chapter II, a toluene-soluble monooxomolybdenum complex, $(Et_4N)_2[Mo^{IV}O\{1,2\text{-}S_2\text{-}3\text{-}(4\text{-}^tBuC_6H_4)_3CCONHC_6H_3\}_2]$ (**1**) has been designed and synthesized. Introduction of *tert*-butyl groups covered the polar molybdenum center completely with a hydrophobic barrier, and amine *N*-oxide was found to approach the active center more efficiently in hydrophobic media.

The author presents here the biomimetic catalytic reduction of amine *N*-oxide by an NADH analog in an aqueous micellar solution. There are a few reports on models promoting the OAT reaction in aqueous media; however, the reports are limited to the use of a mixture of polar solvents and water or wet organic solvents.[31,32]

Results

Catalysis in nonpolar solvent. Since the importance of hydrophobicity around the reactive center has been revealed in Chapters II and III, the author expanded the model system to a catalytic reaction using toluene-soluble dodecyldimethylamine *N*-oxide (DDAO) and the NADH analog, 1-benzyl-1,4-dihydronicotinamide (BNAH). At first, a stoichiometric reaction in toluene/THF was examined using UV-vis spectroscopy (Scheme 1, Figure 2). When 2 eq. of DDAO was added to a toluene solution of complex **1** (0.1 mM), a rapid OAT reaction occurred in a manner similar to the reaction of Me_3NO. Subsequently, 2 eq. of BNAH was added, but no

reaction occurred. The characteristic absorption of BNAH at 355 nm remained unchanged for 20 min. The absorption obviously decreased upon the addition of a small amount of water, showing the consumption of BNAH. These results indicate that water is essential for the reduction of **2** in the catalytic cycle. Then, the catalytic reduction of DDAO by BNAH in water-containing toluene-d_8 was monitored using ^{1}H NMR spectroscopy (Scheme 2, Figure 3). The consumption of DDAO and BNAH followed by the production of DDA was observed. The pseudo-first-order reaction rate constant k_{obs} (1.9×10^{-6} s^{-1}) was approximately 20 times faster than that of the reaction without the catalyst (9.0×10^{-8} s^{-1}), and the turnover number (TON) of the catalysis achieved to 46 with the complete consumption of DDAO.

Scheme 1. The OAT Reaction of DDAO and Regeneration of **1** from **2** by BNAH

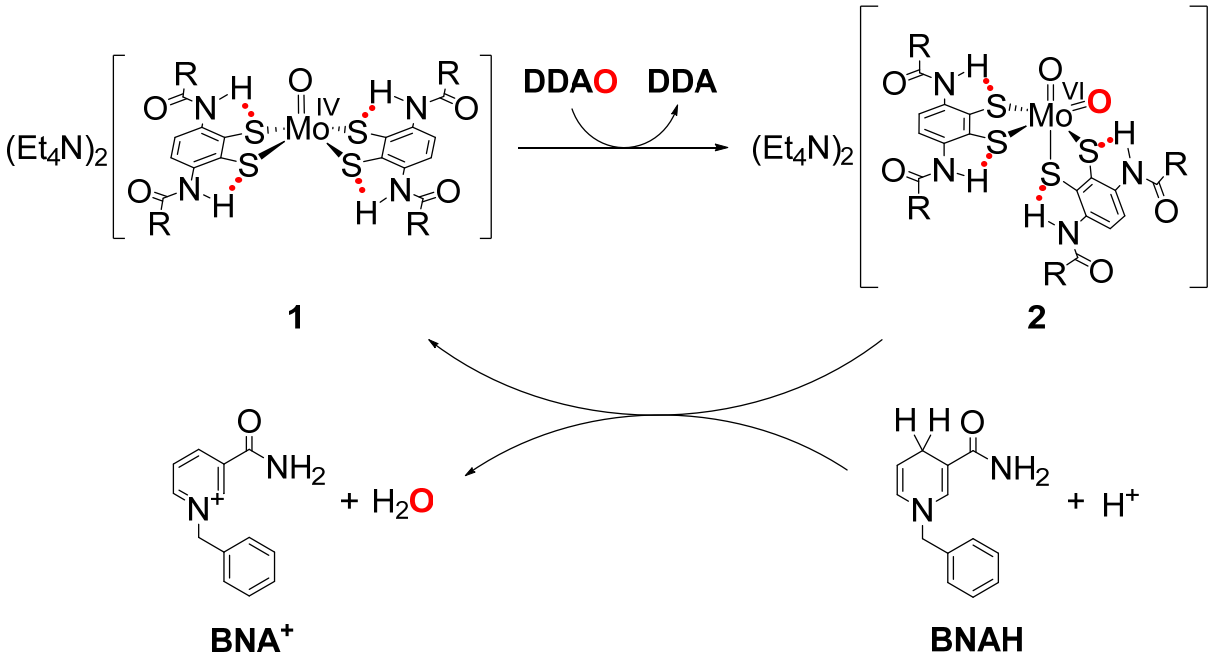

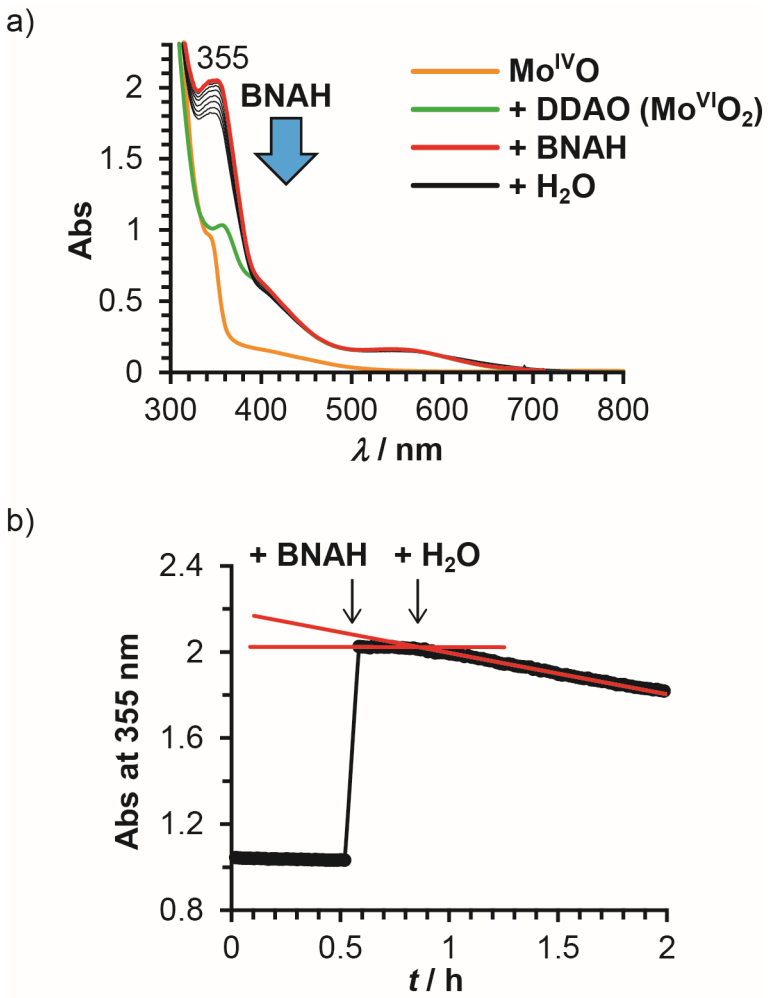

Figure 2. (a) UV-vis spectral change and (b) time-course of the reaction between **1**, DDAO, and BNAH in toluene/THF.

Scheme 2. Catalytic Reduction of DDAO by BNAH in Water-Containing Toluene-d_8

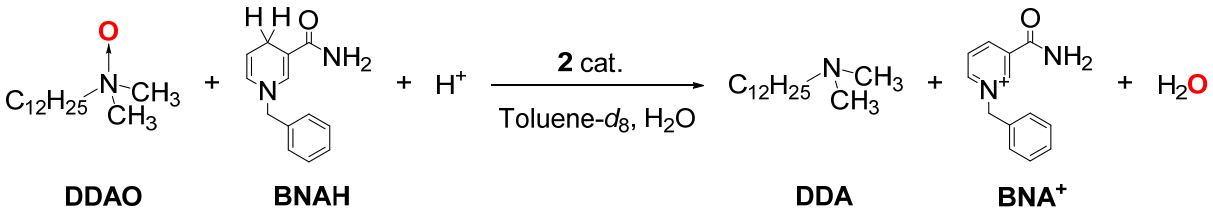

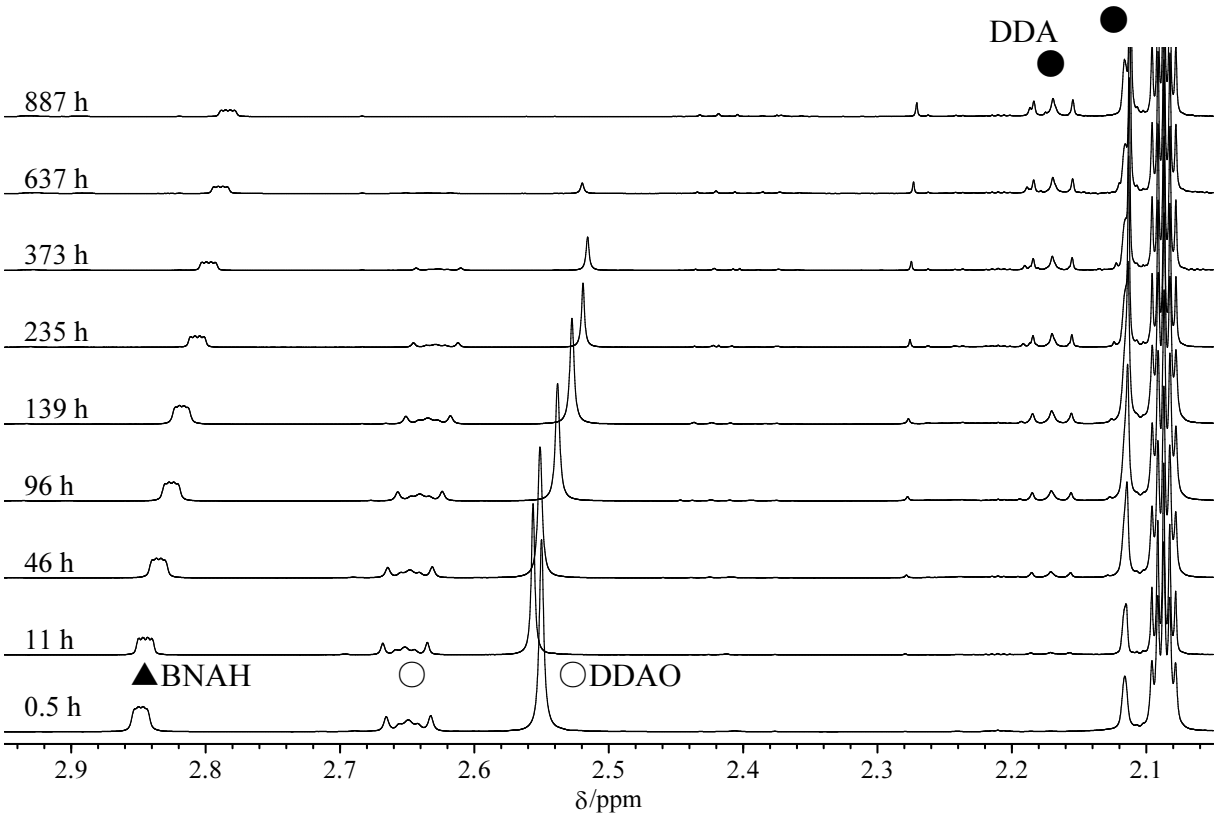

Figure 3. ^{1}H NMR spectral change in water-containing toluene-d_8 during the catalytic reduction of DDAO by BNAH with 2 mol% of **2** at 27 °C.

Synthetic approach toward a unimer-micellar type model complex. In order to construct the hydrophobic microenvironment in aqueous media, the author first attempted to introduce hydrophilic chains into the hydrophobic complex **1** as illustrated in Figure 4. Two types of the precursor of the amphiphilic dithiolate ligands were synthesized as shown in Scheme 3; however, the products could not be isolated ascribed to by-products in an *O*-alkylation reaction. The quantitative and selective *O*-alkylation on all phenol moieties in the reactant was very difficult owing to the competitive *N*- and *S*- alkylation reactions; and these by-products could not be removed even by the separation using preparative SEC column because of the similarity in solubility and molecular size.

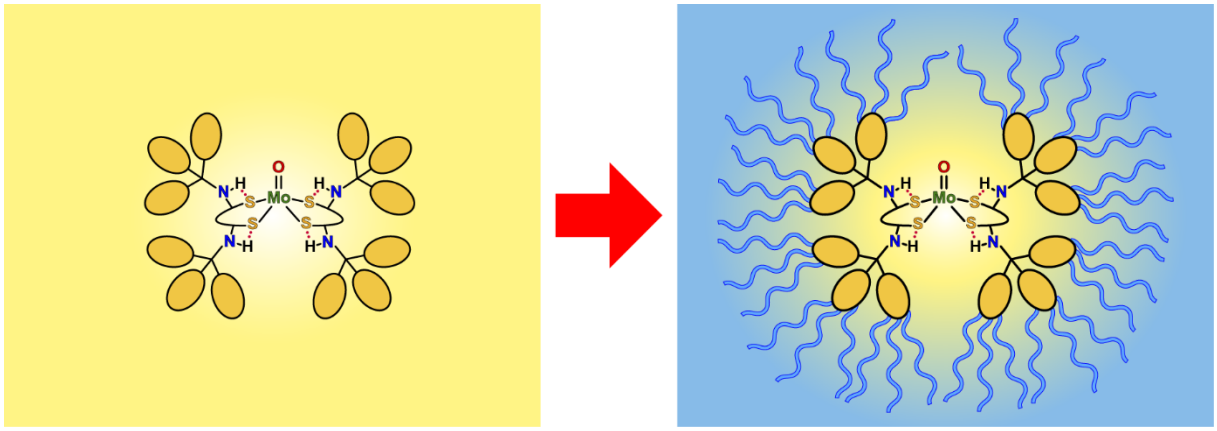

Figure 4. Schematic drawing of the introduction of hydrophilic chain (blue waving lines) into the hydrophobic groups (orange ovals) toward a unimer-micellar type complex.

Scheme 3. Synthetic Route of the Precursors of Amphiphilic Dithiolate Ligands (x = 1, 2)

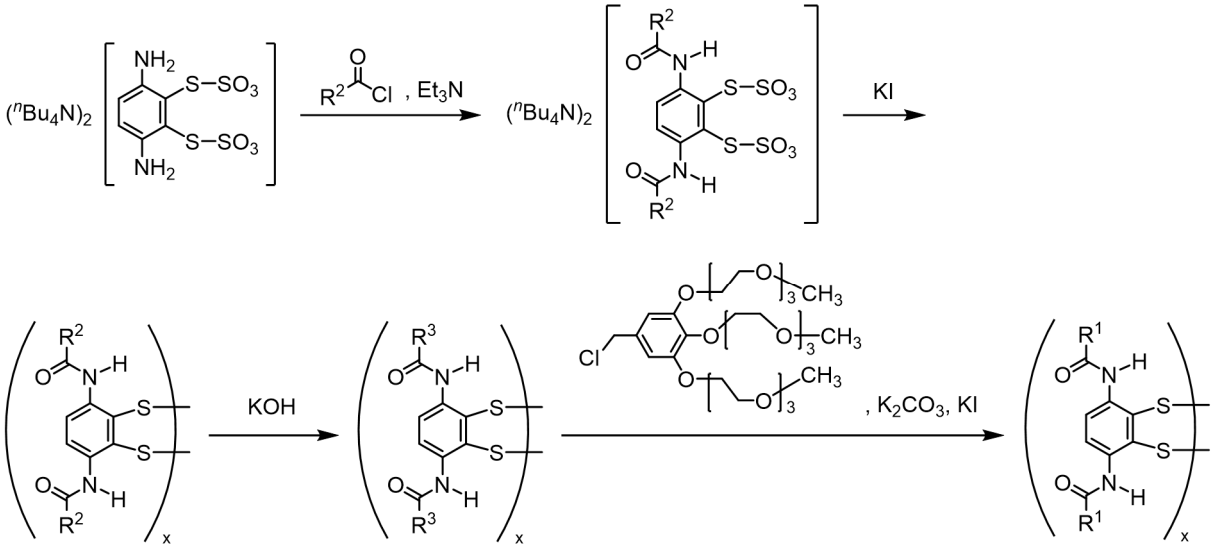

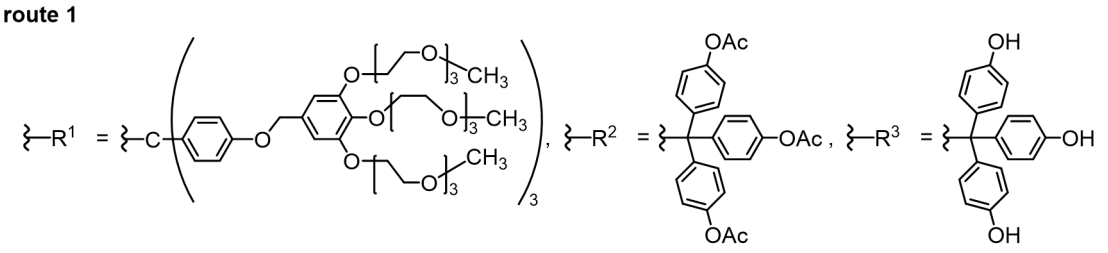

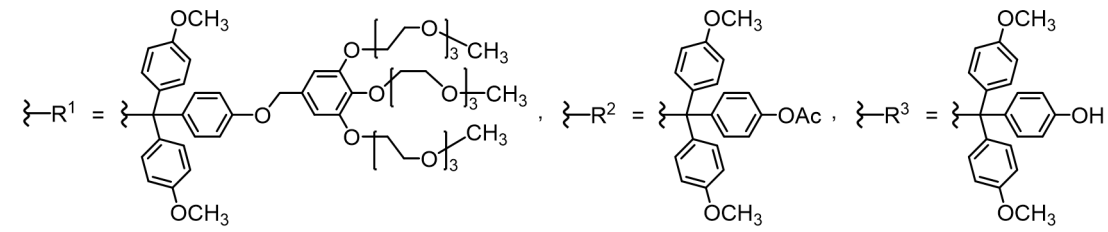

Catalysis in an aqueous micellar solution. Another way to dissolve the hydrophobic molecules into aqueous media is the formation of micelles. In the process of searching for a surfactant to solubilize the complex, Triton X-100, a liquid non-ionic surfactant,[33,34] could successfully form a transparent micellar solution of the complex **2**. Because the complex **2** was insoluble in water but readily soluble in toluene and Triton X-100, the complex must be located in the hydrophobic core of the micelles (Figure 5). The catalytic reduction of DDAO by BNAH in an aqueous micellar solution was monitored using UV-vis spectroscopy (Scheme 4, Figure 6). The pseudo-first-order rate constant of the catalytic reaction (k_{obs} = 36×10^{-6} s^{-1}) was about 10 times faster than that of the reaction without the complex (3.8×10^{-6} s^{-1}). When D_2O was used instead of H_2O, the reaction slowed down (KIE = k_H/k_D = 6.5), which indicates that water molecules (or protons) are involved in the rate-determining step and are crucial for the catalysis. A weak and broad absorption band was observed at 770 nm during the catalytic reaction (Figure 6), which suggests the presence of a monooxomolybdenum(V) species[28,35] generated by one-electron reduction as a side reaction. The absorption was not observed under nonaqueous conditions.

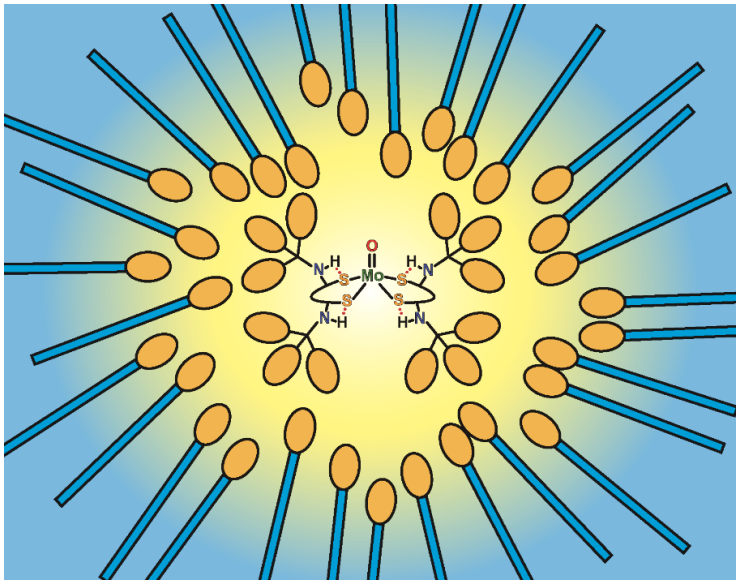

Figure 5. Schematic drawing of the complex in an aqueous micellar solution (orange oval: hydrophobic group, blue stick: hydrophilic group).

Scheme 4. Catalytic Reduction of DDAO by BNAH in an Aqueous Micellar Solution Using Triton X-100

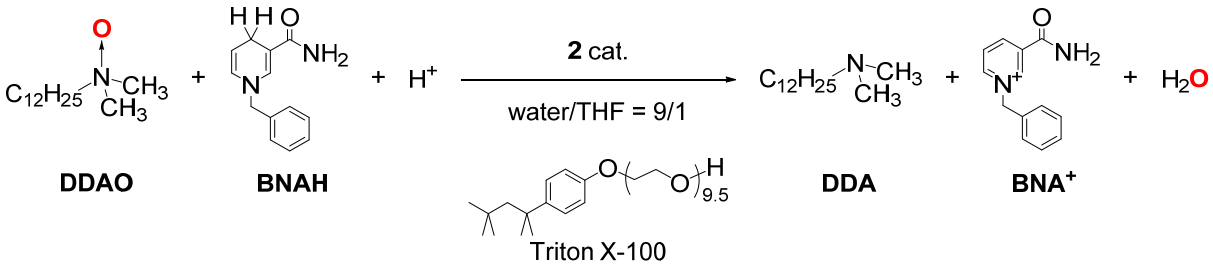

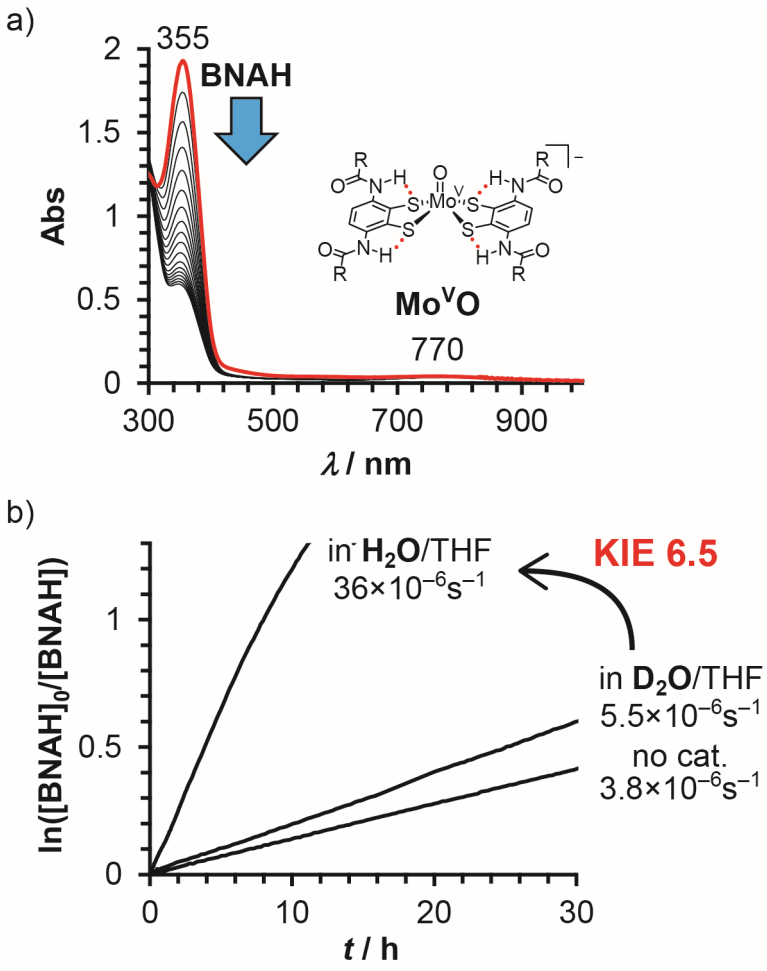

Figure 6. (a) UV-vis spectral change and (b) kinetic plot of the catalytic reduction of DDAO by BNAH in an aqueous micellar solution.

Discussion

The dioxomolybdenum(VI) complex **2** catalyze the oxygen-atom-transfer (OAT) reaction of amine *N*-oxide into water using NADH analog, BNAH in both toluene and aqueous media. In hydrophobic media, the OAT reaction could be directly observed using ^{1}H NMR spectroscopy, and the addition of only 2 mol% of the catalyst resulted in the dramatic acceleration of the reaction. Moreover, the stoichiometric reaction in nonaqueous media clearly showed the essential role of water molecules in the reduction step.

The non-ionic surfactant, Triton X-100, efficiently covered the complex containing bulky hydrophobic groups and made heterolytic microenvironment in water as shown in Figure 5. As a result of kinetic experiments, the reaction mechanism of the catalysis is considered as shown in Scheme 5. The large kinetic isotope effect (KIE) of the solvent indicated the protonation of dioxomolybdenum(VI) complex was involved in the rate-determining step. Furthermore, the observation of molybdenum(V) species suggested the presence of one-electron reduction process, which is reminiscent of the proposed catalytic cycle of TMAOR where the one-electron redaction associates with protonation of the terminal oxo ligand (Figure 1).[1]

Scheme 5. Proposed Mechanism of the Catalysis

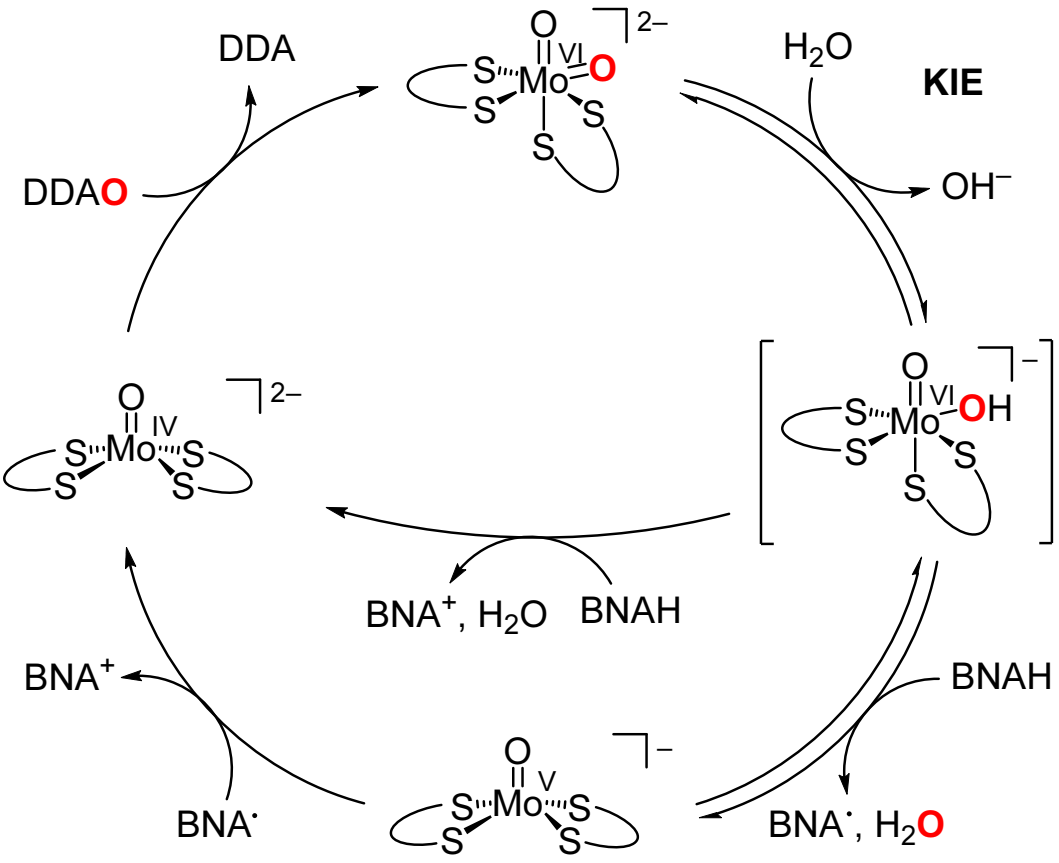

Conclusions

The author constructed a water-soluble molybdoenzyme model containing a hydrophobic microenvironment surrounded by an aqueous micellar solution. The model catalyzes the biomimetic reduction of amine *N*-oxide by an NADH analog in aqueous media. The hydrophobic microenvironment probably promotes the uptake of substrates from the outer aqueous media into the polar reactive site. The present catalytic system, which reduces the substrate followed by the production of water, is one of the most well-designed enzyme models.

Experimental

All procedures were performed under an argon atmosphere by the Schlenk technique. All solvents were dried and distilled under argon before use. Reagents were obtained commercially and used without further purification. $(4\text{-}HOC_6H_4)_3CCOOH$,[36] $(4\text{-}CH_3COOC_6H_4)(4\text{-}CH_3OC_6H_4)_3CCOOH$,[37] $(^nBu_4N)_2[3,6\text{-}(NH_2)_2C_6H_4\text{-}1,2\text{-}(SSO_3)_2]$,[38] $3,4,5\text{-}\{CH_3O(CH_2O)_3\}_3\text{-}C_6H_2CH_2Cl$,[39] and $(Et_4N)_2[Mo^{VI}O_2(1,2\text{-}S_2\text{-}3,6\text{-}\{(4\text{-}^tBuC_6H_4)_3CCONH\}_2C_6H_2)_2]$ (**2**)[38] were prepared by reported methods.

$(4\text{-}CH_3COOC_6H_4)_3CCOOH$. This compound was synthesized by a modified method reported in the literature.[40] To a mixed solution of $(4\text{-}HOC_6H_4)_3CCOOH$ (2.66 g, 7.9 mmol) in 1 M NaOH aq. (75 mL) and CH_2Cl_2 (75 mL) was added dropwise Ac_2O (5.9 g, 58 mmol). The aqueous layer turned from red to colorless, and yellowish white precipitates was generated. After stirring for 2 h, the mixture was acidified using 6 M HCl aq. (about 5 mL, pH 5) and extracted with AcOEt. The organic layer was washed with water and sat. NaCl aq., dried over $MgSO_4$, filtered, and evaporated under reduced pressure. The resulting yellowish white residue was recrystallized from AcOEt/methanol to give colorless blocks. Yield: 2.90 g, 79% (1st). The mother liquir was concentrated to dryness, washed by methanol, and recrystallized by hot methanol to give colorless plates. Yield: 0.775 g, 21%.

$(^nBu_4N)_2[3,6\text{-}\{(4\text{-}CH_3COOC_6H_4)_3CCONH\}_2C_6H_2\text{-}1,2\text{-}(SSO_3)_2]$. To a suspension of $(4\text{-}CH_3COOC_6H_4)_3CCOOH$ (1.70 g, 3.69 mmol) in CH_2Cl_2 (18 mL) were successively added $(COCl)_2$ (0.7 mL, 8.2 mmol) and a drop of DMF. The reaction mixture was stirred for 1.5 h to afford a colorless solution. After removal of volatile materials, CH_2Cl_2 (5 mL) was added to the resulting $(4\text{-}CH_3COOC_6H_4)_3CCOCl$ to afford a colorless solution. To a mixed solution of $(^nBu_4N)_2[3,6\text{-}(NH_2)_2C_6H_4\text{-}1,2\text{-}(SSO_3)_2]$ (1.41 g, 1.72 mmol) and Et_3N (0.8 mL, 5.74 mmol) in CH_2Cl_2 (10 mL) was added dropwise the solution of $(4\text{-}CH_3COOC_6H_4)_3CCOCl$ in CH_2Cl_2.

After addition of a catalytic amount of DMAP and Et_3N (0.8 mL, 5.74 mmol), the reaction mixture was stirred for 40 h. After removal of volatile materials, THF was added to the yellow residue, and the mixture was filtered and concentrated to dryness. The resulting colorless needles were recrystallized from acetonitrile/Et_2O. Yield: 1.21 g, 41%.

(1,2-S_3-3,6-{(4-$CH_3COOC_6H_4$)$_3$CCONH}$_2$$C_6H_2$)$_3$. To a mixture of (^{n}Bu$_4$N)$_2$[3,6-{(4-$CH_3COOC_6H_4$)$_3$CCONH}$_2$$C_6H_2$-1,2-($SSO_3$)$_2$] (759 mg, 446 μmol) and KI (74.6 mg, 450 μmol) was added AcOH (1.2 mL), and the reaction mixture was stirred for 1.5 h at 100 °C to afford a yellow suspension. The precipitates were filtered off, washed with methanol for several times, and dried under reduced pressure to afford slightly yellow powder. Yield: 268 mg, 55%.

(1,2-S_3-3,6-{(4-HOC_6H_4)$_3$CCONH}$_2$$C_6H_2$)$_3$. To a solution of (1,2-$S_3$-3,6-{(4-$HOC_6H_4$)$_3$CCONH}$_2$$C_6H_2$)$_3$ (250 mg, 78.7 μmol) in THF (10 mL) was added dropwise a solution of KOH (0.85 g, 15 mmol) in water (15 mL), and the reaction mixture was stirred for 2 h at r.t. to afford a purple solution. After acidified by 1-M HCl aq. (15 mL), the mixture was extracted with AcOEt, washed with 2% HCl aq, dried over $MgSO_4$, and evaporated under reduced pressure to afford yellowish-orange powder. Yield: 190 mg, quant.

{1,2-S_2-3,6-({4-(3,4,5-{$CH_3O(CH_2O)_3$}$_3$$C_6H_2CH_2O$)$C_6H_4$}$_3$CCONH)$_2$$C_6H_2$}$_x$ (x = 1, 2). To a solution of 3,4,5-{$CH_3O(CH_2O)_3$}$_3$$C_6H_2CH_2Cl$ (498 mg, 812 μmol) in DMF (40 mL) were added (1,2-S_3-3,6-{(4-HOC_6H_4)$_3$CCONH}$_2$$C_6H_2$)$_3$ (101 mg, 41.8 μmol), K_2CO_3 (318 mg, 2.30 mmol), and KI (26.0 mg, 157 μmol), and the reaction mixture was stirred for 40 h at 80 °C to afford a yellowish-green suspension. After removing the volatile materials, and the residue was extracted with CH_2Cl_2, washed with 4% $NaHCO_3$ aq. and sat. NaCl aq., dried over Na_2SO_4, and evaporated under reduced pressure to afford brown oil. Yield: 519 mg.

(^{n}Bu$_4$N)$_2$[3,6-{(4-$CH_3COOC_6H_4$)(4-$CH_3OC_6H_4$)$_3$CCONH}$_2$$C_6H_2$-1,2-($SSO_3$)$_2$]. To a solution of (4-$CH_3COOC_6H_4$)(4-$CH_3OC_6H_4$)$_3$CCOOH (2.05 g, 5.04 mmol) in CH_2Cl_2 (20 mL) were added $(COCl)_2$ (0.95 mL, 11 mmol) and a catalic amount of DMF at 0 °C. After stirring

for 2 h at r.t., the volatile materials were removed under reduced pressure to afford light-yellow residue. A solution of the resulting acyl chloride (5.04 mmol) in DCE (10 mL) was added dropwise at 0 °C to a solution of (^{n}Bu$_4$N)$_2$[3,6-(NH$_2$)$_2$C$_6$H$_2$-1,2-(SSO$_3$)$_2$] (2.04 g, 2.51 mmol) and Et$_3$N (1 mL, 7 mmol) in DCE (15 mL). The reaction mixture was stirred at 80 °C for 74 h to afford a yellowish-brown solution, and the volatile materials were removed under reduced pressure. The resulting residue was washed with water and water/methanol and extracted with AcOEt. After removal of the solvent, the resulting residue was washed with acetone/*n*-hexane for several times and dried under reduced pressure to afford pale-yellow powder. Yield: 1.78 g, 44%.

(**1,2-S$_2$-3,6-{(4-CH$_3$COOC$_6$H$_4$)(4-CH$_3$OC$_6$H$_4$)$_3$CCONH}$_2$C$_6$H$_2$)$_x$ (x = 1, 2).** To a mixture of (^{n}Bu$_4$N)$_2$[3,6-{(4-CH$_3$COOC$_6$H$_4$)(4-CH$_3$OC$_6$H$_4$)$_3$CCONH}$_2$C$_6$H$_2$-1,2-(SSO$_3$)$_2$] (1.63 g, 1.03 mmol) and KI (177 mg, 1.02 mmol) was added AcOH (3 mL), and the reaction mixture was stirred for 2.5 h at 100 °C to afford a yellowish-brown suspension. After adding water and AcOEt, the organic layer was extracted with AcOEt, washed with water, 4% NaHCO$_3$ aq., sat. NaCl aq., 2% HCl aq., and sat. NaCl aq., successively, dried over Na$_2$SO$_4$, evaporated, and reprecipitated from acetone/methanol to afford yellowish-brown powder. After dissolving the product in DMF, the resulting yellowish-orange solution was stirred for 24 h at 100 °C. After removing the solvent, the resulting orange residue was washed with methanol to afford yellow powder. The crude product was purified by column chromatography (AcOEt/*n*-hexane (v/v) = 2/1) and reprecipitated from AcOEt/methanol to afford yellow powder. Yield: 468 mg, 48%.

(**1,2-S$_2$-3,6-{(4-HOC$_6$H$_4$)(4-CH$_3$OC$_6$H$_4$)$_3$CCONH}$_2$C$_6$H$_2$)$_x$.** To a solution of (1,2-S$_2$-3,6-{(4-CH$_3$COOC$_6$H$_4$)(4-CH$_3$OC$_6$H$_4$)$_3$CCONH}$_2$C$_6$H$_2$)$_x$ (42.4 mg, 44.8 μmol) in acetonitrile (~1 mL) was added dropwise an aqueous solution of KOH (1 M, 1 mL), and the reaction mixture was stirred for 1.5 h at r.t. After acidifying the mixture with 1 M HCl aq., the product was

extracted with AcOEt, washed with 1 M HCl aq., sat. NaCl aq., $NaHCO_3$ aq., sat. NaCl aq., successively, dried over Na_2SO_4, and evaporated to afford a brown oil. Yield: 39.6 mg, quant.

{1,2-S_2-3,6-({4-(3,4,5-{$CH_3O(CH_2O)_3$}$_3C_6H_2CH_2O$)C_6H_4}{4-$CH_3OC_6H_4$}$_2$CCONH)$_2$-C_6H_2}$_x$. To a solution of (1,2-S_2-3,6-{(4-$CH_3COOC_6H_4$)(4-$CH_3OC_6H_4$)$_3$CCONH}$_2C_6H_2$)$_x$ (36.6 mg, 42.4 μmol) in DMF (2 mL) with heating was added K_2CO_3 (128 mg, 929 μmol) to afford a reddish-orange suspension. After adding dropwise a solution of 3,4,5-{$CH_3O(CH_2O)_3$}$_3C_6H_2CH_2Cl$ (66.7 mg, 109 μmol) in DMF (2 mL), the reaction mixture was stirred for 4 h at 65 °C and evaporated. After adding water and CH_2Cl_2, the organic layer was extracted with CH_2Cl_2, washed with 4% $NaHCO_3$ aq., sat. NaCl aq., successively, dried over Na_2SO_4, and evaporated to afford a brown oil. The crude product was purified by preparative SEC ($CHCl_3$) and evaporated to afford a yellowish-brown oil. Yield: 52.0 mg.

Stoichiometric reaction between 1 and DDAO and the subsequent reduction by BNAH in toluene/THF. The procedure was similar to that described above for Me_3NO in toluene, except for the use of DDAO (30 mM, 20 μL) in THF. After the complete formation of **2** was confirmed, a solution of BNAH (30 mM, 20 μL) in THF was added. After 20 min., H_2O (10 μL, 180 mM) was added, and the time course of the reaction was monitored by using the absorption maximum of BNAH.

Catalysis in toluene-d_8. A solution of **2** (0.51 mg, 0.21 μmol) in toluene-d_8 (0.1 mL) was added to a mixed solution of DDAO (0.80 mg, 3.5 μmol) and BNAH (0.74 mg, 3.5 μmol) in toluene-d_8 (0.6 mL)/H_2O (0.2 μL, 11 μmol) at –78 °C. The reaction at 27 °C was monitored by using ^{1}H NMR spectroscopy.

Preparation of a micellar solution of 2. To a solution of **2** (1.55 mg, 0.63 μmol) in THF (0.3 mL) was added a 0.1-M THF solution of Triton X-100 (0.9 mL, 90 μmol). The resulting reddish-brown solution was concentrated under reduced pressure, and water (1.8 mL) was added to afford a 0.35-mM aqueous micellar solution of **2**.

Catalysis in a micellar solution. A reaction system containing **2**, DDAO, and BNAH was monitored in the region 280–1000 nm. The measurements were carried out in a 1-mm UV cell at 27 °C. After the thermal equilibrium, a 90-mM aqueous solution of DDAO (10 μL, 0.9 μmol) and a 30-mM THF solution of BNAH (30 μL, 0.9 μmol) were added to a 0.35-mM aqueous micellar solution of **2** (0.26 mL, 0.09 μmol), and the cell contents were quickly mixed by shaking. The absorption at 355 nm (BNAH) was monitored at 27 °C

Physical measurements. ^{1}H NMR spectra were obtained with JEOL ECA-500 spectrometer in toluene-d_8 at 30 °C. UV-visible absorption spectra were recorded using a SHIMADZU UV-3100PC spectrometer.

References

(1) Hille, R.; Hall, J.; Basu, P. *Chem. Rev.* **2014**, *114*, 3963-4038.

(2) Iobbi-Nivol, C.; Haser, R.; Méjean, V.; Czjzek, M. Trimethylamine N-Oxide Reductase. In *Encyclopedia of Inorganic and Bioinorganic Chemistry*; John Wiley & Sons, Ltd: 2011.

(3) McCrindle, S. L.; Kappler, U.; McEwan, A. G. Microbial Dimethylsulfoxide and Trimethylamine-N-Oxide Respiration. In *Adv. Microb. Physiol.*; Robert, K. P., Ed.; Academic Press: 2005; Vol. Volume 50, p 147-198.

(4) Czjzek, M.; Dos Santos, J.-P.; Pommier, J.; Giordano, G.; Méjean, V.; Haser, R. *J. Mol. Biol.* **1998**, *284*, 435-447.

(5) Cox, J. C.; Madigan, M. T.; Favinger, J. L.; Gest, H. *Arch. Biochem. Biophys.* **1980**, *204*, 10-17.

(6) Pollock, V. V.; Barber, M. J. *J. Biol. Chem.* **1997**, *272*, 3355-3362.

(7) Nelson, K. J.; Rajagopalan, K. V. *Biochemistry* **2004**, *43*, 11226-11237.

(8) Temple, C. A.; George, G. N.; Hilton, J. C.; George, M. J.; Prince, R. C.; Barber, M. J.; Rajagopalan, K. V. *Biochemistry* **2000**, *39*, 4046-4052.

(9) Mondal, S.; Basu, P. *Inorg. Chem.* **2001**, *40*, 192-193.

(10) Smith, D. K.; Diederich, F. *Chem. Eur. J.* **1998**, *4*, 1353-1361.

(11) Gorman, C. B.; Smith, J. C. *Acc. Chem. Res.* **2001**, *34*, 60-71.

(12) Vögtle, F.; Gestermann, S.; Hesse, R.; Schwierz, H.; Windisch, B. *Prog. Polym. Sci.* **2000**, *25*, 987-1041.

(13) Cardona, C. M.; Mendoza, S.; Kaifer, A. E. *Chem. Soc. Rev.* **2000**, *29*, 37-42.

(14) Basu, P.; Nemykin, V. N.; Sengar, R. S. *Inorg. Chem.* **2003**, *42*, 7489-7501.

(15) McNaughton, R. L.; Mondal, S.; Nemykin, V. N.; Basu, P.; Kirk, M. L. *Inorg. Chem.* **2005**, *44*, 8216-8222.

(16) Holm, R. H.; Solomon, E. I.; Majumdar, A.; Tenderholt, A. *Coord. Chem. Rev.* **2011**, *255*, 993-1015.

(17) Hine, F. J.; Taylor, A. J.; Garner, C. D. *Coord. Chem. Rev.* **2010**, *254*, 1570-1579.

(18) Ng, V. W. L.; Taylor, M. K.; Young, C. G. *Inorg. Chem.* **2012**, *51*, 3202-3211.

(19) Majumdar, A.; Sarkar, S. *Coord. Chem. Rev.* **2011**, *255*, 1039-1054.

(20) Sugimoto, H.; Tatemoto, S.; Suyama, K.; Miyake, H.; Mtei, R. P.; Itoh, S.; Kirk, M. L. *Inorg. Chem.* **2010**, *49*, 5368-5370.

(21) Basu, P.; Burgmayer, S. J. N. *Coord. Chem. Rev.* **2011**, *255*, 1016-1038.

(22) Schultz, B. E.; Hille, R.; Holm, R. H. *J. Am. Chem. Soc.* **1995**, *117*, 827-828.

(23) Berg, J. M.; Holm, R. H. *J. Am. Chem. Soc.* **1985**, *107*, 925-932.

(24) Harlan, E. W.; Berg, J. M.; Holm, R. H. *J. Am. Chem. Soc.* **1986**, *108*, 6992-7000.

(25) Döring, A.; Fischer, C.; Schulzke, C. *Z. Anorg. Allg. Chem.* **2013**, *639*, 1552-1558.

(26) Whiteoak, C. J.; Britovsek, G. J. P.; Gibson, V. C.; White, A. J. P. *Dalton Trans.* **2009**, 2337-2344.

(27) Ueyama, N.; Oku, H.; Kondo, M.; Okamura, T.; Yoshinaga, N.; Nakamura, A. *Inorg. Chem.* **1996**, *35*, 643-650.

(28) Ueyama, N.; Yoshinaga, N.; Okamura, T.; Zaima, H.; Nakamura, A. *J. Mol. Catal.* **1991**, *64*, 247-256.

(29) Baba, K.; Okamura, T.; Suzuki, C.; Yamamoto, H.; Yamamoto, T.; Ohama, M.; Ueyama, N. *Inorg. Chem.* **2006**, *45*, 894-901.

(30) Baba, K.; Okamura, T.; Yamamoto, H.; Yamamoto, T.; Ohama, M.; Ueyama, N. *Chem. Lett.* **2005**, *34*, 44-45.

(31) Das, S. K.; Chaudhury, P. K.; Biswas, D.; Sarkar, S. *J. Am. Chem. Soc.* **1994**, *116*, 9061-9070.

(32) Sugimoto, H.; Tarumizu, M.; Miyake, H.; Tsukube, H. *Eur. J. Inorg. Chem.* **2006**, 4494-4497.

(33) Nakata, M.; Ueyama, N.; Fuji, M.; Nakamura, A.; Wada, K.; Matsubara, H. *Biochim. Biophys. Acta* **1984**, *788*, 306-312.

(34) Okamura, T.; Taniuchi, K.; Ueyama, N.; Nakamura, A. *Polym. J.* **1999**, *31*, 651-657.

(35) Boyde, S.; Ellis, S. R.; Garner, C. D.; Clegg, W. *J. Chem. Soc., Chem. Commun.* **1986**, 1541-1543.

(36) Palchaudhuri, R.; Hergenrother, P. J. *Bioorg. Med. Chem. Lett.* **2008**, *18*, 5888-5891.

(37) Bistrzycki, A.; Jabloński, S. *Helv. Chim. Acta* **1932**, *15*, 890-906.

(38) Hasenaka, Y.; Okamura, T.; Tatsumi, M.; Inazumi, N.; Onitsuka, K. *Dalton Trans.* **2014**, *43*, 15491-15502.

(39) Oar, M. A.; Serin, J. M.; Dichtel, W. R.; Fréchet, J. M. J.; Ohulchanskyy, T. Y.; Prasad, P. N. *Chem. Mater.* **2005**, *17*, 2267-2275.

(40) Nesterenko, V.; Putt, K. S.; Hergenrother, P. J. *J. Am. Chem. Soc.* **2003**, *125*, 14672-14673.

Chapter V

Summary

The aim of this thesis is to reveal the role of hydrophobic microenvironment surrounding the active site of molybdoenzymes.

In Chapter II, the toluene-soluble anionic monomolybdenum(IV) and dioxomomolybdenum(VI) complexes containing very bulky and hydrophobic moieties have been synthesized and fully characterized. The encapsulation of counterions were observed even in solution state, and the approach of polar Me_3NO was more efficient in hydrophobic environment formed by bulky hydrophobic groups and nonpolar solvents, which resulted in the dramatic acceleration of the oxygen-atom-transfer (OAT) reaction.

Chapter III has described the importance of local hydrophobicity around the active center. The silylation of the terminal oxo ligand enhanced the reactivity of the complex; in other words, the resulting desoxomolybdenum(IV) complex promoted the OAT reaction of the biological substrate, DMSO. X-ray structural analysis, spectroscopic measurements, and kinetics of the OAT reaction of Me_3NO indicate that the modification of the complex was done keeping the coordination structure and the hydrophobic pocket surrounded by bulky hydrophobic groups of the monooxomolybdenum(IV) complex. The comparable reaction rates to reduce DMSO in polar and nonpolar solvents indicates that the hydrophobic microenvironment and transient distorted structure play a dominant role in the uptake and activation of the neutral small molecule like DMSO.

Finally, in Chapter IV, the author has described the model system containing the hydrophobic microenvironment in aqueous media. Catalytic reduction of amine *N*-oxide by

NADH analog was achieved in an aqueous micellar solution. The hydrophobic pocket of the fundamental complex to uptake the substrates successfully constructed the heterolytic environment in water.

The author has demonstrated the toluene-soluble molybdenum complexes having very bulky and hydrophobic moieties. The polar active center and counterions are successfully covered by bulky substituents, and the effective approach of Me_3NO was achieved in hydrophobic environment supported by nonpolar media. The simple but very effective modification of the complex, i.e. the silylation of the terminal oxo ligand, resulted in the enhancement of reactivity for DMSO even in polar media. The result indicates the formation of the hydrophobic pocket for the binding and activation of the substrate. Finally, the author has demonstrated the micellization of the complex, which reconstructed the hydrophobic microenvironment in aqueous media.

In conclusion, the hydrophobic microenvironment formed by protein surrounding the active center of molybdoenzymes has been successfully modeled by the enzyme model complex containing bulky and hydrophobic groups. The concept of reconstructing the active site of metalloenzymes with the hydrophobic microenvironment will provide new insights for enzyme modeling.

List of Publications

1. Yuki Hasenaka, Taka-aki. Okamura, Miki Tatsumi, Naoya Inazumi, and Kiyotaka Onitsuka: Behavior of anionic molybdenum(IV, VI) and tungsten(IV, VI) complexes containing bulky hydrophobic dithiolate ligands and intramolecular NH···S hydrogen bonds in nonpolar solvents, *Dalton Trans.*, 2014, **43**, 15491-15502. (**Chapter II**)

2. Yuki Hasenaka, Taka-aki. Okamura, and Kiyotaka Onitsuka: Efficient uptake of dimethyl sulfoxide by desoxomolybdenum(IV) dithiolate complex containing bulky hydrophobic groups, submitted to *Dalton Trans.* (**Chapter III**)

3. Yuki Hasenaka, Taka-aki. Okamura, and Kiyotaka Onitsuka: Modeling of Hydrophobic Microenvironment of Water-Soluble Molybdoenzymes in Aqueous Micellar Solution, to be submitted. (**Chapter IV**)